POLITECNICO DI MILANO
DEPARTMENT OF MECHANICAL ENGINEERING
DOCTORAL PROGRAMME IN MECHANICAL ENGINEERING

VIBROACOUSTIC MODELING OF SANDWICH FOAM CORE PANELS

Doctoral Dissertation of:
Simona Moschini

Supervisor:
Prof. Alfredo Cigada

Tutor:
Prof. Massimiliano Gobbi

The Chair of the Doctoral Program:
Prof. Bianca Maria Colosimo

2014 - XXVI Cycle

Abstract

Lightweight structures became widespread along the years in several industrial frameworks. Being characterized by a pretty rich basket of design parameters lightweight structures can be tailored exactly to the specific requirement. As main drawback, this class of structures tend to vibrate easily inducing undesired noise. Better performances can be obtained considering sandwich panels with foam core. The metallic skins, usually in Aluminium, provide bending resistance while the core material and structure can be selected to obtain the desired vibration damping and noise reduction performance. Therefore, a reliable vibroacoustic numerical model becomes a powerful designing tool. The aim of the current research is to develop an integrated numerical/experimental procedure to predict the vibroacoustic performances of a sandwich foam core panel. The innovative feature of the proposed methodology is the integration among all the relevant aspects for vibroacoustic structural behavior evaluation: material parameter identification, vibroacoustic numerical modelling and experimental validation of the modelling strategy. In literature, research works are typically focused either in material characterization or in numerical modeling. Conversely, the current research work considers the whole workflow required for a reliable vibroacoustic prediction. Each of the abovementioned aspects has been studied and designed. A dedicated experimental activity has been designed and carried out to obtain the material parameters required for the numerical model implementation. The panel core is a viscoelastic material that requires a specific identification procedure. The structural dynamic response has been evaluated through a Finite Element model while the coupled vibroacoustic problem has been tackled via a combined Finite Element - Boundary Element model. The model prediction capability has been assessed in terms of either vibration damping or sound transmission reduction performance. Dealing with lightweight structures makes the experimental activity more challenging, especially in terms of dynamic characterization. As a result few literature works present dynamic models of lightweight structures together with experimental validation. In the current research work instead the numerical/experimental comparison has been considered of fundamental importance for the assessment of the modeling strategy reliability.

Index

Chapter 1 1

1. Introduction 1
Composite materials 3

2. Building certifications 5
3. Research Objectives 6

4. Dissertation Outline 7

Chapter 2 9

1. Sound and Vibration 9
2. Sound radiation by vibrating planar structures 14
2.1. Waves in fluids and solids 14

2.1.1. Sound waves and solid structures 15

2.2. Critical and coincidence frequency 16

2.3. Coincidence effects in layered structures 19

3. Porous core sandwich panels: relevant characteristics 20
3.1. Polymeric foams: stress - strain relationship 20

3.1. Sound propagation in porous materials 36

3.1.2. Rigid frame porous materials 36

3.1.3. Elastic frame porous material 38

4. Sound transmission 40
4.1. Transmission Loss 40

5. Vibroacoustic modeling techniques 44
5.1. Dynamic modeling 44

5.2. Numerical analysis of sound fields 51

5.2.2. Deterministic methods 51

5.2.3. Mid - frequency methods 57

5.2.4. Statistical methods 58

5.3 Equivalent modeling 58

Chapter 3 61

1. Vibroacoustical numerical modeling 61
2. Structural model 64
2.1. Dynamic behavior modeling 65
2.1.1. Finite Element Modeling of skins 69
2.1.2. Finite Element Modeling of the core 79
3. Coupled problem modeling 83
3.1. Acoustic problem modeling 84
3.2. Coupling of structural and acoustic models 89
4. Sound Transmission Loss prediction for higher frequencies 92

Chapter 4 99

1. Experimental investigation role in vibroacoustics 99
2. Panel materials characterization 102
3. Dynamic identification procedure 111
3.1. Test case: Sandwich panel with foam core 112
3.1.1. Suspended panel modal analysis 113
3.1.2. Clamped panel modal analysis 123
3.1.2.1. Investigation of the adhesive layer dynamic effect 129
3.2. Test case: Sandwich panel with foam core – A4 size 132
4. Vibroacoustic behavior identification 138

Chapter 5 151

1. Numerical and experimental data correlation relevance 151
2. Dynamic model validation 152
2.1. Model predictive capability assessment 157
3. Vibroacoustic modeling 160
4. Acoustic behavior prediction at higher frequencies 163

Chapter 6 167

1. Conclusions 167
References 171
List of Symbols 176
Acronyms 181
List of figures 182
List of Tables 186

CHAPTER 1

Chapter 1 gives the framework of the current dissertation. Specific attention is paid to the importance of the selected topic and to the motivations at the basis of the work. The structure of the thesis is described as well.

1. Introduction

During the last years energy efficiency become one of the most challenging topics. The global warming has been an issue for the international community since the beginning of the 90s. In 1992 the Rio de Janeiro Summit, to which 154 nations took part, drafted the United Nations Framework Convention on Climate Change (UNFCCC). The main goal of the UNFCCC was to reduce the greenhouse gases (GHG) emission and to stabilize their level by the year 2000, though without any formal duty for the signing nations. The next important step was the Kyoto Protocol in 1997. It states the will of reducing the GHG emissions of the 8% in the years 2008-2012. Focusing on the European Union (EU), the 15 nations that committed to reduce their emissions according to the Kyoto Protocol statement are well on their path.In 2011, the latest year for which comprehensive data are available, EU-15 emissions stood 14.9% below their level in Member States' chosen base years (Figure 1).

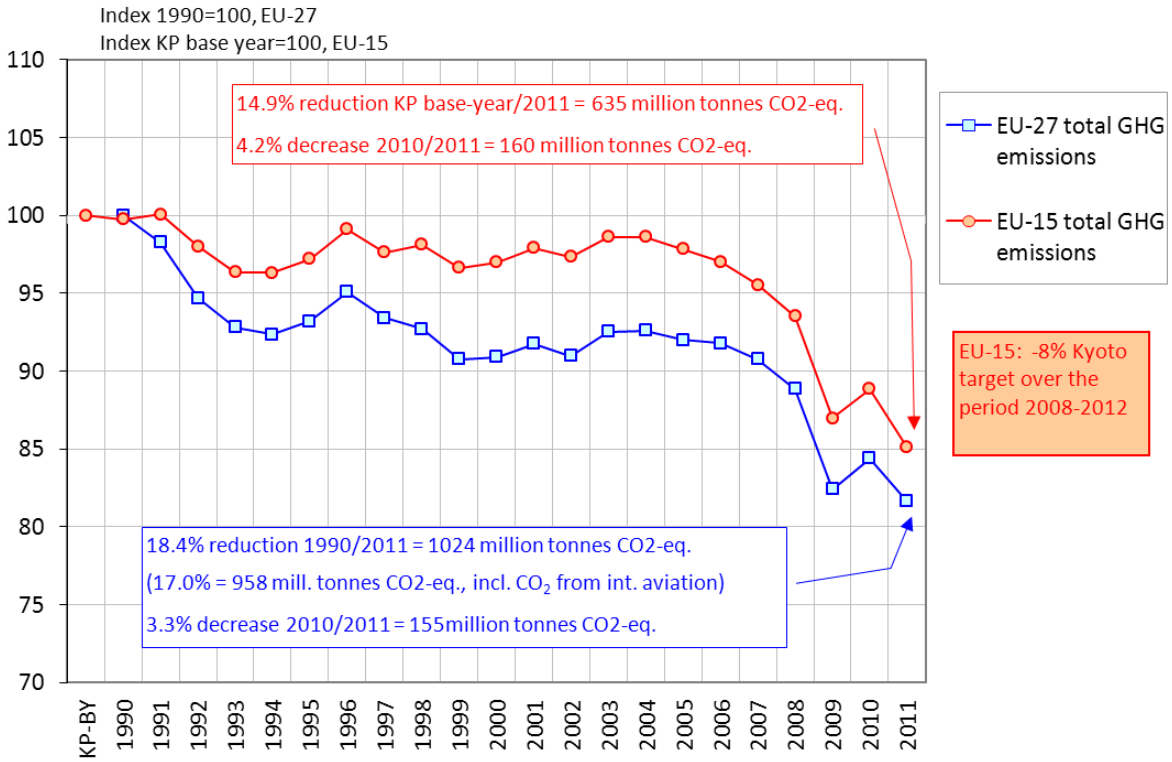

Figure 1 GHG emissions reduction Kyoto Protocol base-year /2011 (source: European Environment Agency).

The next target for EU is 2020. The EU has made a unilateral commitment setting three key objectives:

- A 20% reduction in EU greenhouse gas emissions from 1990 levels;
- Raising the share of EU energy consumption produced from renewable resources to 20%;
- A 20% improvement in the EU's energy efficiency.

Energy efficiency enhancement will then play a core role in 2020 horizon. The two strategic areas are transportation and housing. In EU, nearly 40% of final energy consumption is in houses, public and private offices, shops and other buildings [1]. As Figure 2shows, in residential homes, two thirds of this is for space heating.

Figure 2 - Energy consumption in residential homes (source: European Commission).

A straightforward way to improve building energy efficiency is to reduce heating dissipation. This result is achieved by interposing layer of low thermal conductivity material between the exterior and the interior wall or under the building roof. The same can be done for the construction of the building front doors. An ideal solution is represented by structures that can give both structural and thermal resistance avoiding overload. This necessity results in an additional application field for composite materials, typically used in aerospace and automotive industry.

Composite materials

Composite materials have been subject of intensive interest since the beginning of XX century. The goal for composite development has been to achieve a combination of properties not achievable by any of the elementary materials. They are basically made by a material, the *matrix*, that is reinforced by a second one, called *reinforcement*. The matrix is a homogeneous phase, it controls the shape of the material, transfers load to the reinforcement and protects it, giving cohesion to the whole part. Conversely, the reinforcement givesstiffness and mechanical resistance to the material, bearing the bigger part of the load. Typical reinforcements are fibers (short or long) and particles (Figure 3). Orienting long fibers along the load direction gives the possibility to exploit at best the composite characteristics. Using short fibers randomly oriented results in a globally isotropic material. Layers of composites material, called plies, are then usually bonded together to made a composite macro-material. Polyester materials are widely used as matrix in commercial products, due to their low cost. Polymeric resins are instead used for applications that require high mechanical performances.

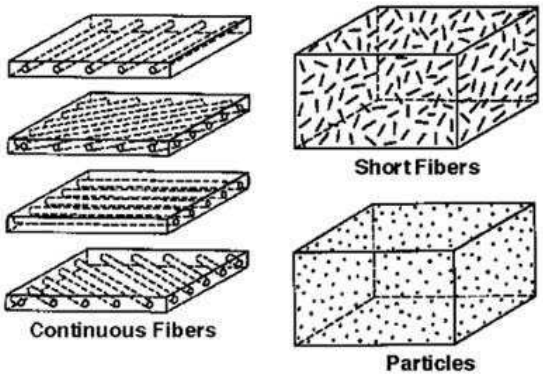

Figure 3 - Schematic example of composite materials.

A special class of composite material, the one widely used in building construction, is structural sandwich. The structural sandwich normally consists of two facings, called skins, of relatively thin, hard, durable material which are bonded to a relatively thick core of lightweight and less stiff material, named core (Figure 4). Different materials can be used for the facings (metals, plywood, hardboard...) and for the core (foam, wood, honeycomb...). The typical adhesives are synthetic resins, such as epoxy and phenol formaldehyde.

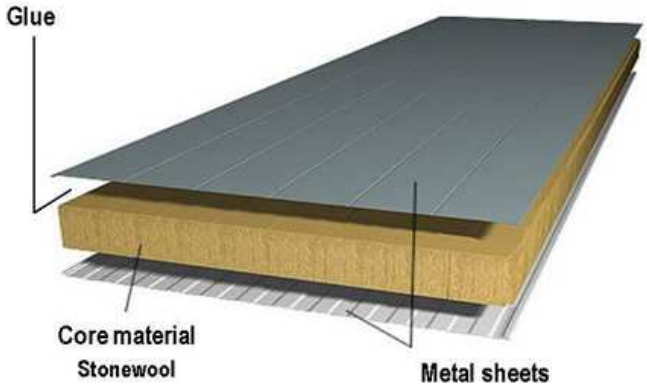

Figure 4 - Schematic example of sandwich panel.

Building sandwiches are asked to perform a number of functions beyond strength and stiffness. The exterior facing must withstand sunlight, rain and snow, wind pressure and abrasion thus specific coatings or paintings are often applied. The interior facing must instead withstand the normal wear of the interior of a building. A central role is played by the core characteristics that should provide the for instance whole thermal insulation capability of the panel.

2. Building certifications

The EU directives lead towards a nearly - zero impact building configuration. This can be achieved moving to renewable energy sources, like solar panels, and designing the building with particular attention to orientation and balance between open and closed surfaces. For instance, a huge window south oriented can provide light and warmth without energy consumption. Beside the design strategies, also the global mentality should be oriented toward an "energy saving" concept. A Class A house can be expensive and the benefits may not be evident in the short period. As well as we are used to see with household appliances, higher initial investment may lead to real saving considering the whole building lifetime. The idea behind the certification process is enabling the client to make more informed decisions. Different parameters are taken into account for building energy certification as: extension, number and kind of windows, heating system kind and insulation type and quality.

The choice of the insulation materials plays a fundamental role for a second certification procedure. The acoustic performance certification has become mandatory in Italy in 2011 [2]. This certification takes in account the noise transmission either from outdoor to indoor or from one room to the other. The strategies to insulate from noise are exactly the same than to reduce heat dissipation. An acoustic transmission problem can be depicted like in Figure 5.

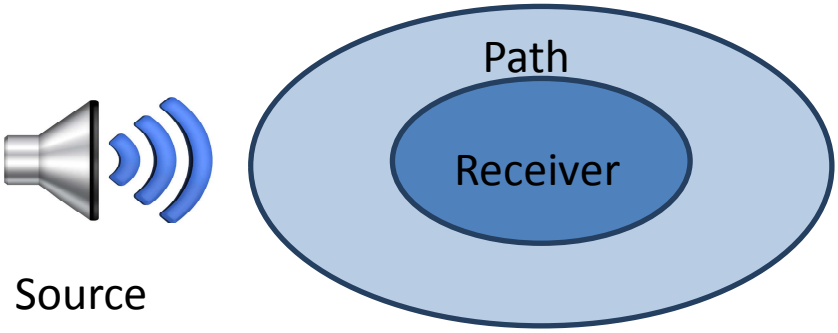

Figure 5 - Acoustic problem.

A central role is played by the path the sound wave travels between the noise source and the environment to protect. Thus the interposal of a layer of suitable material comes again to the fore (Figure 6).

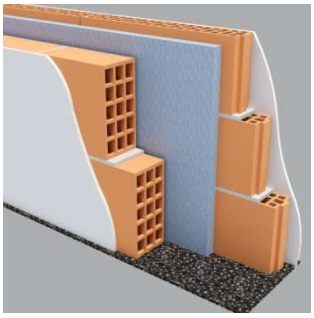

Figure 6 - Sound insulation strategy - example.

Moreover, noise pollution is often not due to a real sound source but by wall or surface vibrations and their reflection on adjacent surfaces. This is a frequent problem in industrial framework dealing with big machineries or, for instances, huge fridges. There is a strong connection between noise and vibration thus noise insulation cannot neglect, from a general point of view, vibration transmission reduction. The vibration attenuation is again achievable by modifying the vibration path with layers of suitable materials. The peculiar structure of sandwich panels makes them suitable to perform many varied function. It is possible to combine a potential infinite number of materials obtaining panels exactly tailored to a specific application. The appealing idea of a multifunctional panel becomes achievable by tuning and optimizing the design parameter that characterizes sandwich panels. Despite these appealing characteristics lightweight structures have the main drawback of poor noise and vibration mitigation performances. A full understanding of the noise and vibration performances becomes a key factor as well as the availability of a helpful designing tool.

3. Research Objectives

The goal of the present dissertation is to develop a combined numerical/experimental methodology able to predict the global vibroacoustic response of a sandwich panel. The panel behaviour is defined in terms of dynamic response to incoming broadband vibration and sound transmission loss in the acoustic frequency range. The final aim is to obtain a reliable model to be used for panel design purposes. Given the application field, different panel solutions can be evaluated and tailored to optimize the structural sandwich according to the specific situation. Particular attention has been paid to accurately structure a complete procedure: starting from material properties identification to the extraction of the

predicted vibroacoustic properties. The steps of the whole chain have been designed. Firstly, material properties have been characterized through a dedicated experimental campaign. The modeling block, made by a Finite Element (FE) model and a coupled Finite Element - Boundary Element (BE) model, has been designed and tuned to lead to reliable results. The numerical model has been developed using a commercial code. Avoiding the development of a specific routine using a programming language makes it a wider exploitable tool. Finally, an important part of the work is related to the model validation.

An extended and dedicated experimental activity is needed to define the model reliability. Standard and non standard experimental techniques have been applied to characterize different aspects of the panel vibroacoustic performance such as damping factor, natural frequencies and Insertion Loss. The effectiveness of the proposed modeling strategy has been further investigated checking the modelpredictive capability. The numerical model validated on a given panel has been used to simulate the dynamic response of a panel characterized by a different planar extension. The latter has been experimentally investigated to assess the validity of the obtained results. The experimental campaign pointed out the challenges related to dealing with lightweight structure. Load effect of sensors and excitation as well as test boundary condition definition have been carefully studied. As side objective of the present work, an experimental evaluation of the dynamic role of the adhesive layer has been carried out.

4. Dissertation Outline

This thesis builds on the field vibroacoustic modeling and specifically addresses the problem related to the numerical modeling of sandwich foam core panels. The thesis is organized in six chapters, of which the first is represented by the current introduction and the last contains the conclusions. A chapter-by-chapter brief outline is presented hereafter.

Chapter 2 introduces the topic of vibroacoustics and describes all the relevant aspects helping to understand the significance of the topic itself. An overview on numerical modeling techniques is provided highlighting how dynamic and acoustic modeling can be coupled. The current work deals mainly with structural sandwich panel having foam core. In this framework a literature review of wave propagation in porous materials is provided as well as a basic description of viscoelastic material behavior.

Chapter 3 gives a brief overview on the adopted numerical methods together with an essential description of their mathematical basis. Particular attention has been paid to the viscoelastic behavior modeling. The potential and drawbacks of the most common models are presented. Keeping in mind the aim of the numerical modeling, the modeling choice are illustrated. Chapter 3 ends with the description of the equivalent model adopted to obtain results in a wider range of frequency.

Chapter 4 gives detailed description of the experimental activity that has been carried out to validate the proposed numerical strategy. The adopted techniques for data acquisition and post processing are detailed. The results are presented for either the dynamic or the vibroacoustic behavior identification. Particular attention has been paid to the characterization of the core material behavior and the related parameters.

Finally, Chapter 5 collects the obtained results. The chapter focuses on the comparison between the numerical and experimental results. Either the dynamic or the vibroacoustic numerical prediction are validated through the experimental results described in Chapter 4. Particular attention is paid to the assessment of the dynamic model predictive capability.

CHAPTER 2

Chapter 2 introduces the topic of vibroacoustics and describes all the relevant aspects helping to understand the significance of the topic itself.its significance. An overview on numerical modeling techniques is provided highlighting how dynamic and acoustic modeling can be coupled. The current work deals mainly with structural sandwich panel having foam core. In this framework a literature review of wave propagation in porous materials is provided as well as a basic description of viscoelastic material behavior.

1. Sound and Vibration

In everyday life it is common to experience various manifestations of the interaction between fluid and solid structures. Traffic noise heard through the windows or plumbing system noise are examples of undesirable aspects of this interaction (Figure 7). The same phenomenon may be exploited for good use: vibrations of musical instruments, microphone diaphragms and loudspeakers. The study of the physical interaction between sound and vibration is known as vibroacoustics. As a consequence of the vibroacoustic interaction large number of sound sources is nothing but the action of vibrating solid surfaces upon the surrounding fluid. The subject of sound radiation from vibrating surfaces has a great practical importance. It is a key factor for instance in loudspeaker and industrial machinery design, though with opposite aims. The former should be tuned to obtain a good radiation while the

latter must take into account the community noise limits fixed by standards and regulations.

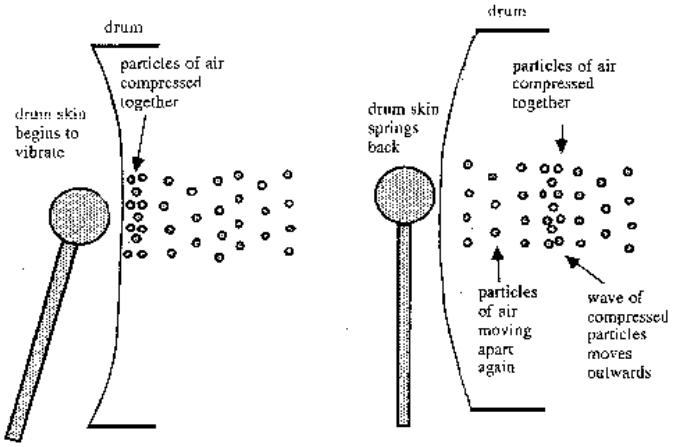

Figure 7 - Example of sound wave induced by structural vibration.

Many different structures can radiate sound but the mechanism is common to all of them. In the current dissertation, attention is confined to elastic structures that take the form of plates; for these thickness is much smaller than the dimensions defining the surface. Such structures tend to vibrate in a direction normal to the surface. This characteristic enables a mechanism of compressing and displacing of the surrounding fluid. As a result, similar structures are effectively able to radiate, transmit and respond to sound. A key point for understanding the fluid-structure interaction is the analysis of the forms and characteristics of the principal types of waves that can propagate through solids and fluids. The nature of the supporting media influences that of the propagating wave. On the other hand, the wave nature plays a role in determining the efficiency of the mutual interaction.

Given an incident sound source, only a part will be transmitted through the structure. Each impinging wave will be, in fact, partially reflected, partially absorbed and only the remaining part will be transmitted (Figure 8).

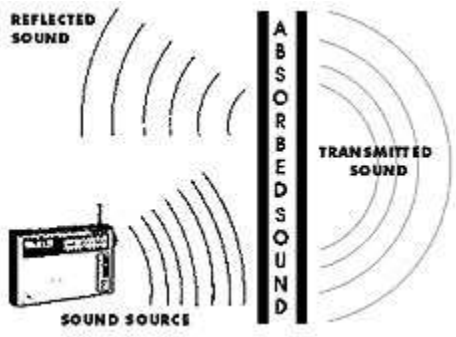

Figure 8 - Incident, absorbed, reflected and transmitted sound.

The reduction of the transmitted sound may be achieved acting on two distinct phenomena: the sound absorption and the sound emission due to vibration, thus the structural vibration reduction.

Aiming to design a structure effectively able to reduce the sound transmission, the historical rule of thumb "the heavier the better" is still valid. Increasing the mass of a structure leads to a better sound insulation. Anyway, in many application fields lightweight is a strict design constraint. Recent developments in material sciences along with the older concept of composite structures allow theovercoming of this difficulty.

The backbone of the current dissertation is depicted in Figure 9. Focusing on reducing sound transmission, sandwich structures are identified as a possible solution since they may satisfy the strictest lightweight design requirements.

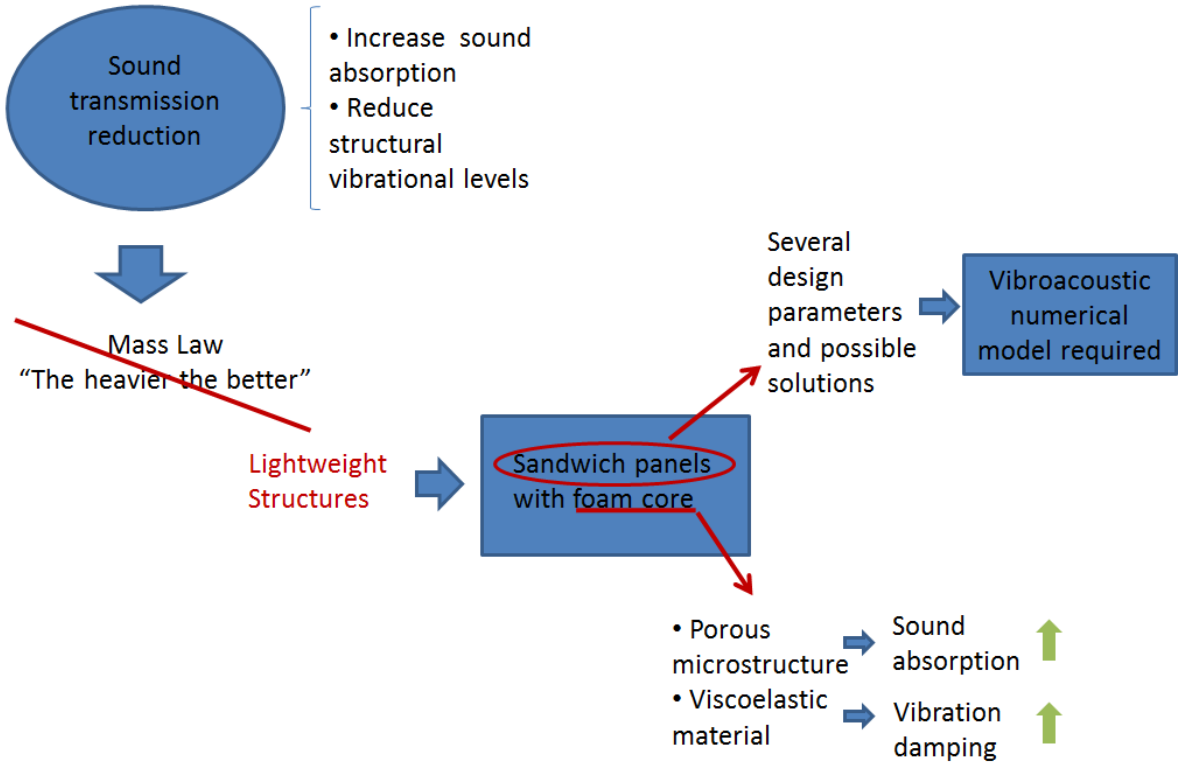

Figure 9 - Conceptual schema.

Lightweight structures usually exhibit poor noise and vibration reduction performances: they vibrate easily and with high vibration levels. However, composite structures allow the combination of different materials to exploit at best their characteristics. Among the others, an appealing solution for sound reduction is represented by sandwich structures with foam core. The structural resistance is given by the thin face sheets while an accurate choice of the core leads to interesting vibroacoustics properties.

Porous materials, like foams, are an excellent choice for sound absorbing purposes and can help insulation. Several mechanisms of absorption are at work. Among them two are of great importance: the viscous loss of air that is pumped through the cellular structure and the intrinsic damping in the material. The former is a direct consequence of the random microstructure that characterizes porous materials. The latter is related to the nature of the porous material. The material damping is generally low for metallic materials but it reaches high levels in polymer and foams.

This is due to the viscoelastic nature of the foam frame material. Viscoelasticity increases viscous losses and leads to hysteretic mechanical energy dissipations if the material is subjected to cyclic loads. As a result, viscoelastic materials efficiently reduce structural vibrational levels improving sound transmission reduction.

The sound transmission capability of a structure is typically characterized by the Sound Transmission Loss (TL) index. The analysis of the TL curve trend vs frequency allows one to identify the structural properties to be modified in order to optimize the structure performances. One of the most important phenomena related to fluid - structure interaction is coincidence. If the structural bending wavespeed and the free wavespeed in air, for a given incidence angle, correspond the structure acts as totally transparent to the impinging sound wave. The TL curve shows a deep dip at that frequency, testifying the structure tendency to become a perfect radiator.

The sound radiation and transmission properties are highly influenced by the structure cross sectionconfiguration and material. One of the major advantages of sandwich structures is that they can be tailoredexactly to specific requirements. The concept of multilayered structures releases many designconstraint enlarging the basket of available engineering solutions. This freedom highlightsthe need of a reliable numerical tool to evaluate the efficiency of different practical solutions. An accurate prediction of the structural dynamic response plays a key role in the study of the mutual interaction between structural vibration and sound propagation. The determination of the structural transfer function, for instance between the structural displacement and the force acting on the structure, allows the prediction of the response to any kind of excitation including the acoustic one. Subsequently, the pressure field in the fluid surrounding the structure can be evaluated by applying suitable numerical techniques.
Several analyticaltheories and numerical methods have been developed through the last part of this chapter is devoted to the review of the available modeling techniques to tackle the coupled vibroacoustic problem and to predict either vibration damping or sound transmission performances for the analyzed solutionyears, giving the designer the capabilityof choosing an efficient and effective modeling strategy to predict the vibroacoustic performances of a structure.

In the first part of this chapter the basics of wave propagation in solids and fluids are reviewed together with one of the most relevant aspects in sound structure interaction: the coincidence effect. Subsequently, attention is focused on the advantages of adopting sandwich structures with foam core with respect to homogeneous structures. In particular both the sound propagation modeling of porous materials and porous materials viscoelastic behavior are described. The

2. Sound radiation by vibrating planar structures

The study of the interaction between plate/type structures and the surrounding fluid is important for many engineering applications, particularly for structure borne sound analysis. Acoustic vibrations essentially involve the propagation of waves throughout the supporting media. The nature of the considered media influences the kind of waves that can propagate and not all the waves are relevant from a vibroacoustic point of view.

2.1. Waves in fluids and solids

The wave equation for the propagation of small acoustic disturbance through homogeneous, inviscid, isotropic, compressible fluid in its two dimensional form is known as the Helmholtz equation:

$$\frac{\partial^2 p}{\partial x^2}+\frac{\partial^2 p}{\partial y^2}=-\left(\frac{\omega}{c}\right)^2 p=-k^2 p \qquad (2.1)$$

Equation (2.1)[3] only involvesvariations in two orthogonal directions in association with a harmonic time dependence. The pressure is denoted by *p*, *c* is the frequency independent speed of sound related to the mean fluid pressure, the mean fluid density and the adiabatic bulk modulus of the fluid. *k* is the wavenumber and expresses the phase change for unit distance.

Equation (2.1) governs the wave propagation in fluids. In an unbounded solid instead different kinds of waves can propagate:

- longitudinal waves, that become quasi - longitudinal considering a solid unbounded only in the direction of the wave propagation,
- shear waves ,
- bending waves.

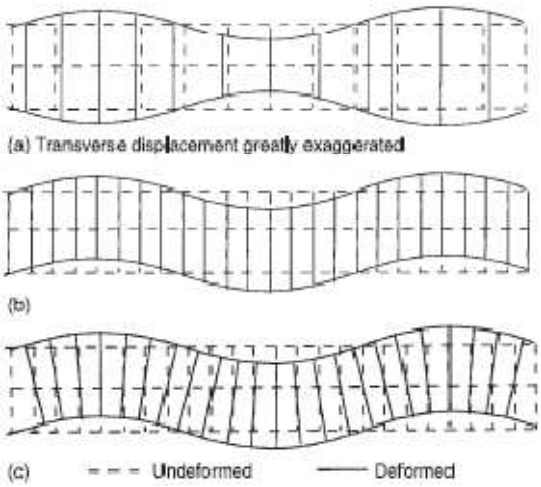

Figure 10 - Deformation patterns of different type of waves in flat plates and bars.

(a) quasi longitudinal wave, (b) shear wave (c) bending wave [3].

2.1.1. Sound waves and solid structures

Among the various type of waves that can propagate in bars, beams and plates bending waves are those of greatest importance in the process of fluid - structure interaction. The reason is that they involve displacement in a direction transverse to that of propagation that can interfere effectively with the adjacent fluid. In addition, the structure impedance able to carry bending waves may be of the same order of magnitude of that of the surrounding fluid, thus the energy exchange between the two systems is facilitated. As a result, the bending stiffness of the medium is a fundamental parameter from the vibroacoustic point of view. Generally speaking, the bending stiffness of a homogeneous structure is a constant value depending upon the geometrical and the material parameters. Thin structures vibrate easily than thicker ones being more efficient in sound radiation; loudspeakers membranes are in fact very thin.

Dealing with layered structures, the effective bending stiffness for free bending wave propagation results to be frequency dependent. At low frequencies the vibrational behavior of a sandwich panel is dominated by the overall section bending stiffness. The core acts as an ideal spacer distributing stresses between the outer layers and coupling the skins together, giving maximum bending stiffness. As the vibrational frequency increases, the bending stiffness decreases and it is controlled by the

propagation of shear waves in the core. At higher frequencies, the bending stiffness is asymptotic to a constant value approximately equal to the sum of the skins bending stiffness [4].

Bending waves are the main actors in the sound and vibration interaction process. If it were possible to construct plates favoring the propagation of shear waves instead of the bending ones, those plates would be great insulators. Unluckily, it is almost impossible to obtain homogeneous plates with high bending and low shear stiffness. The first research that pointed out the utility of sandwich panels with respect to homogeneous plates to increase the sound insulation was from Kurtze and Watters [5]. Bending of such a structure would require the extension/compression of the skins while shear requires shear of the core material and bending of the thin plates. Considering, for example, a plate consisting of soft but incompressible core sandwiched between two metal skins, such a structure can be considered stiffer in bending than in shear. As a result, it can be expected shear waves to propagate easily with respect tobending one and such a structure can be used for sound insulation purposes [5].

2.2. Critical and coincidence frequency

Bending waves in plates are the major responsible of sound radiation. However, radiation efficiency depends on the excitation, respectively mechanical or acoustic, and the inducedwave characteristics, acoustic or mechanical, respectively. The most important parameter is the ratio between the surface displacement wavelength, λ_B, and the corresponding acoustic wavelength λ. Considering an undamped, infinite plate mechanically forced to carry a plane bending wave of constant amplitude and propagation speed c_B, the plane radiated sound wave is characterized by a wavelength λ equal to:

$$\lambda = \lambda_B \sin \vartheta = \frac{c_B}{f} \sin \vartheta \qquad (2.2)$$

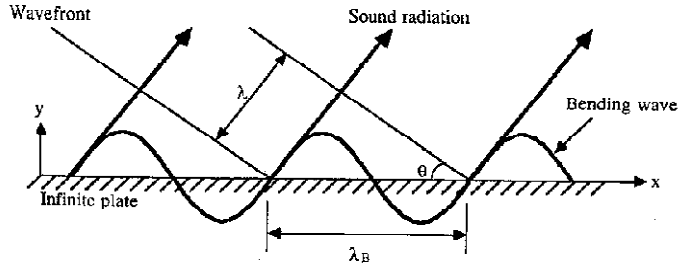

Figure 11- Sound radiation by an infinite plate [6].

As a consequence, sound radiation implies an acoustic wavelength equal or shorter than the bending wavelength (Figure 11). Both wavelengths are equal when the wavespeeds in both media are equals. This occurs at a particular frequency called *critical frequency* f_{cr}. Thus only above the critical frequency the free waves in a mechanically excited infinite plate can radiate sound efficiently [6].

The phenomenon of equality between acoustic and bending wavelenghts can be analyzed also considering acoustic excitation. At the critical frequency speed of the acoustic wave in air matches the speed of free bending wave. Under this condition, the structure acts as a perfect radiator. It can be shown [7] that for a thin plate the critical frequency can be analytically determined and is given by:

$$\omega_{cr}^2 = c^4 \rho_s / D \tag{2.3}$$

where c is the speed of sound of the medium, ρ_s is the plate mass per unit area and the bending stiffness is D. D is defined in terms of material Young modulus E, plate thickness h and material Poisson ratio ν:

$$D = \frac{Eh^3}{12\left(1-\nu^2\right)} \tag{2.4}$$

The vibration response of a panel to an acoustic field is the highest around the critical frequency. As depicted by Figure 11 ,the sound radiation characteristics are highly dependent on whether the excitation frequency is above or below the critical frequency. Aiming to design an efficient sound attenuating structure, the design parameter should be tuned so that the speed of the bending wave in the plate is lower than that of the speed of sound in free air. Otherwise, the fluid - structure interaction becomes efficient. Only for thin, heavy, isotropic plates the coincidence frequency assumes such a high value that is out from the frequency range of interest. [5]

A way to locate the value of the critical frequency is the study of dispersion curves. This means displaying the variation of the wavenumbers of the different wave kinds against the frequency and comparing it with the one of the wave propagation of the considered surrounding fluid.

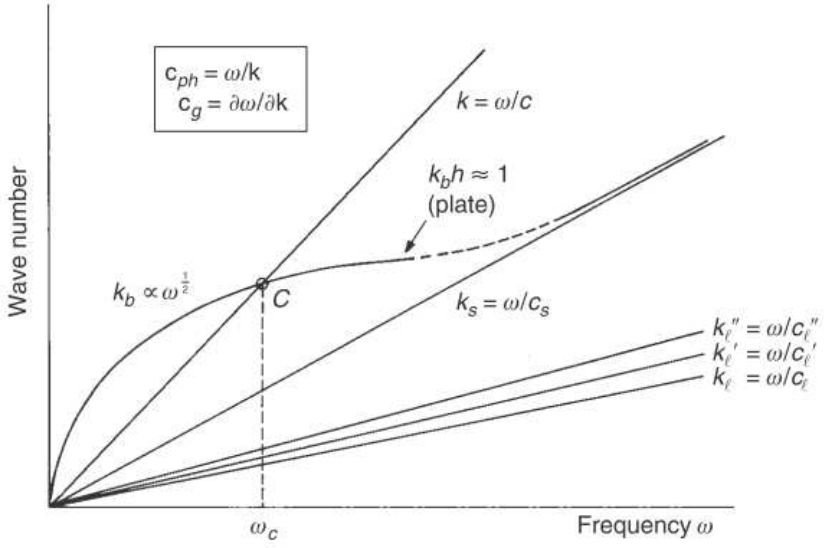

Figure 12- Dispersion curves [3].

In Figure 12 a generic plot of dispersion curves for various waveforms is reported. The wavenumbers associated to longitudinal waves (k_l), quasi longitudinal waves in bars ($k_l^{'}$) and plates ($k_l^{''}$) and with shear waves (k_s) are linearly frequency dependent, as well as the one related to the wave propagation in the surrounding fluid (k). Instead the bending waves wavenumber k_b is function of the square root of the frequency and intersects the air wavenumber exactly at the critical frequency [3]. The critical frequency is the equality of the free bending wavespeed and the speed of acoustic wave in air. This frequency is also termed lowest coincidence frequency [3]. If a structure is excited acoustically, the coincidence frequency is the correspondence of the forced bending wavespeed in the structure and the free bending wavespeed [7]. It can be shown that critical and coincidence frequencies are directly related [7].The concept of coincidence in flat panels has been developed at first by Cremer [8] who stated that at coincidence a plate excited to vibrate by sound waves acts as if it is totally transparent and the incident sound waves are freely transmitted.

2.3.Coincidence effects in layered structures

The core of a sandwich structure can be of every kind of material. A work of Ford, Lord and Walker [9] showed that the sound radiation from a sandwich panel having compressible core is dependent on bending and dilatational modes of vibration (respectively i and ii in Figure 13). Studies performed by Dym and Lang [10] pointed out how for symmetric panels symmetric (dilatational) and antisymmetric (bending) motions are uncoupled leading to a simpler problem analysis.

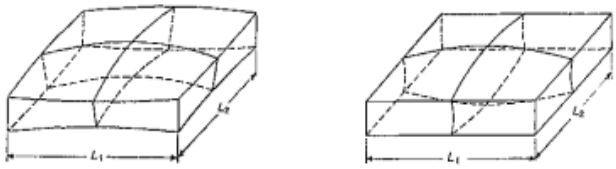

i ii

Figure 13 - Fundamental mode of vibration of a layered panel having compressible core: (i) Flexural and (ii) Dilatational [9].

Core compressibility causes transverse motion of the panel faces. This acts as a disturb for the surrounding fluid as well as the bending vibrations. According to [9], for low wavenumbers values the dilatational vibration mode can affect significantly the panel insulation properties. Three layered structures exhibit two values of impinging wave frequency that transform the layered structure in a perfect radiator:

- one related to the antisymmetric motion of the skins
- one related to their symmetric motion, so called double wall frequency

Sound radiation is higher near the coincidence frequency, due to the equality between forced bending wavespeed and free bending wavespeed. As described in paragraph 2.2, the same peak of sound radiation happens at the critical frequency or lowest coincidence frequency. Aiming to study a sandwich structure vibroacoustic behavior to optimize the performance, either for sound radiation or sound absorption, the knowledge of critical and coincidence frequencies values becomes of primary importance.

3. Porous core sandwich panels: relevant characteristics

Sandwich structures are characterized by a pretty rich basket of possible skin/core combination. This allows the tailoring of the structure exactly to the best required performance. Porous material, like mineral wool or polymeric foams, are an appealing option as core material. Their peculiar random microstructure gives them higher damping and specific acoustic characteristics. Focusing on polymeric foams, they are generally characterized by low shear modulus that enhances sound reduction performances (Figure 14).

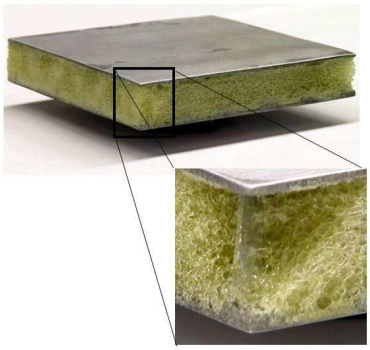

Figure 14 - Sandwich panel: stainless steel skins, polymeric foam core.

The vibration damping performances, higher with respect to bulk materials of the same thickness, are mainly due to the viscoelastic behavior. From a dynamic point of view the porous material can be considered as an "equivalent solid" since the wavelength of mechanical excitation is generally larger than the characteristic length of the porous media [11]. This hypothesis is no more satisfied in case of acoustic excitation. As a result, particular attention should be paid to porous material acoustic behavior.

3.1. Polymeric foams: stress - strain relationship

Due to its increased use in engineering application, many research have been devoted to different aspects of the foam behavior: from the chemical composition and structure to the microscale properties and from the microscale properties to the macroscale ones. Generally speaking, foam is a non-linear, viscoelastic, material whose static and dynamic behavior are different and sensitive to many variables, like the level of compression or amplitude/frequency of excitation.

A viscoelastic material combines the characteristics of purely elastic and purely viscous materials, i.e it has two asymptotic behaviors: (i) the elastic solid and (ii) the viscous liquid. The response to imposed strain of elastic, viscoelastic and viscous materials is qualitatively shown in Figure 15.

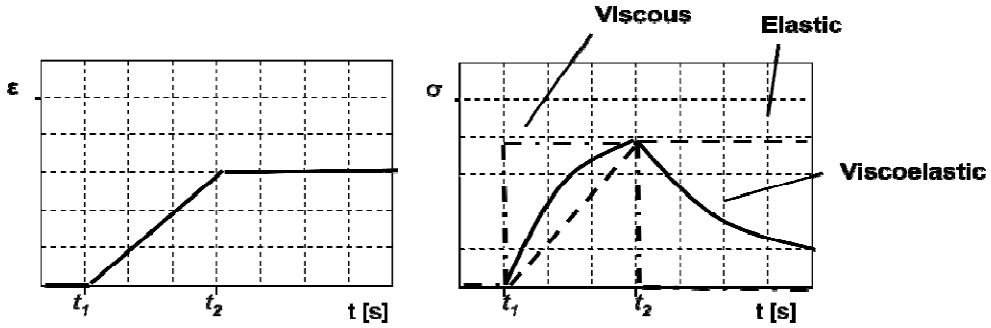

Figure 15 - Qualitative comparison among different material behavior.

The elastic solid has a defined shape and its stress-strain behavior is governed by the Hooke law that, for the case of uniaxial load is:

$$\sigma(t) = E\varepsilon(t) \tag{2.5}$$

The stress σ is immediately induced by the applied strain ε and they are related by E, the Young modulus. Once the load is removed the stress goes back to zero (Figure 15).

The viscous fluid, instead, is governed by the Newton law:

$$\sigma(t) = \eta \frac{\partial \varepsilon}{\partial t} \tag{2.6}$$

This means that the stress σ is related to the strain velocity through viscosity η. The main actor in this case is time. In fact, a high loading instantaneously applied may leave the material unchanged while small loading constantly applied in time may lead to irreversible strain due to internal creep.

A viscoelastic material presents an intermediate behavior between purely elastic and purely viscous materials. If subject to a time constant varying strain the resulting stress will not be neither directly proportional as for an elastic material nor constant as for a viscous material but slowly varying with a small amplification. Conversely, if subject to a constant strain the resulting stress would be constant for an elastic

material, zero for a purely viscous one and slowly decaying for a viscoelastic material (Figure 15).

The viscoelastic material behavior may be characterized in two ways:

- Time varying relaxation modulus or its dual, the time varying creep compliance
- Frequency dependent complex modulus

Relaxation is one of the most important consequences of the material viscoelastic nature. It expresses the decrease of loading under constant applied strain. The relaxation test is performed applying a constant strain to the specimen and measuring the resulting stress. The ratio between the stress and the imposed strain gives the relaxation modulus $E(t)$ as a function of time (Figure 16).

$$E(t) = \frac{\sigma(t)}{\varepsilon_0} \tag{2.7}$$

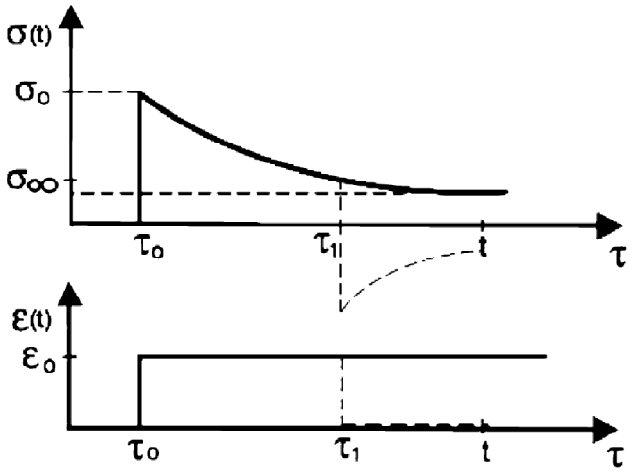

Figure 16 - Qualitative strain and stress trend during a relaxation test [12].

Creep is the relaxation dual phenomenon. As in the case of several elastic materials at high temperatures, creep is the increase of strain under constant loading. The creep test is performed applying a constant stress to the specimen and measuring

the resulting strain. The ratio between the strain and the imposed stress gives the creep compliance $J(t)$ as a function of time (Figure 17).

$$J(t) = \frac{\varepsilon(t)}{\sigma_0} \tag{2.8}$$

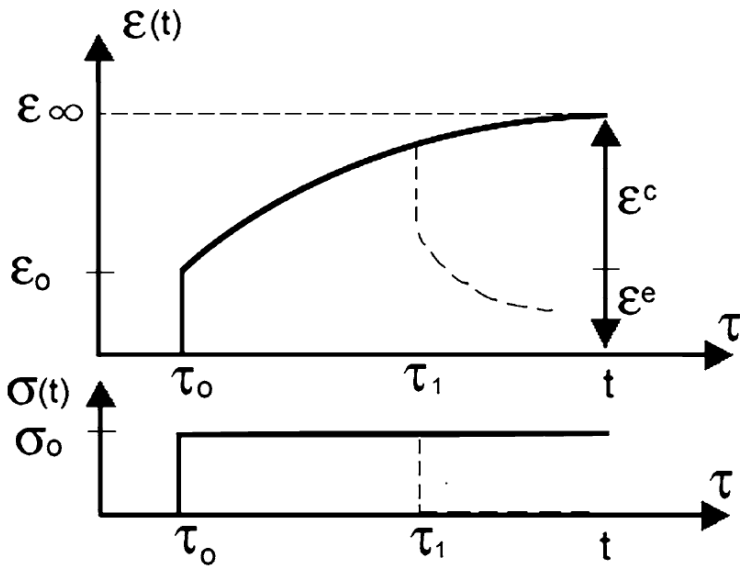

Figure 17 - Qualitative strain and stress trend during a creep test [12].

The viscoelastic material may be characterized also by the reaction to a sinusoidal strain like $\varepsilon_0 e^{i\omega t}$. The resulting stressis amplified and delayed with respect to the imposed strain due to the viscoelastic nature of the material. The delay is due the viscous losses of the material as a result of the internal friction.

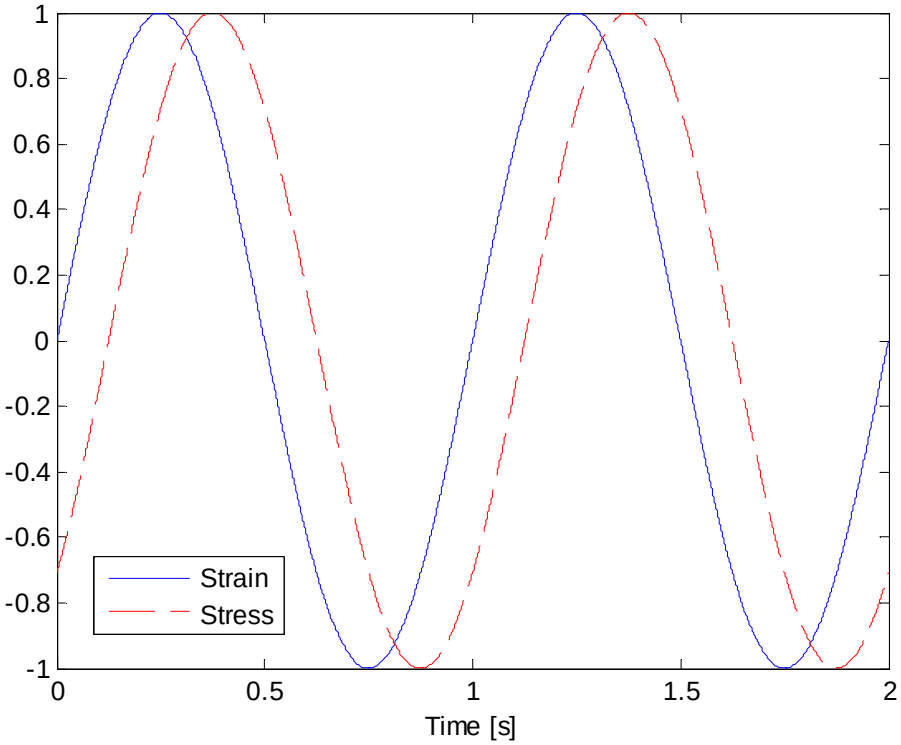

Figure 18–Qualitative strain and stress trend during dynamo mechanical test.

The stress -strain relation can be described by the following expression:

$$\sigma(t)e^{i\omega t} = \left(E^{'} + iE^{''}\right)\varepsilon_0 e^{i(\omega t-\delta)} \tag{2.9}$$

The component *E'* or *storage modulus*, is related to the strain in-phase component and to the elastic side of the material while the component *E''* or *loss modulus* is related to the viscous properties of the material and the 90° out of phase component of the strain. Storage and Loss modulus together are called *complex modulus*. The ratio of the loss modulus to the storage modulus expresses the phase delay of the stress with respect to the strain and is related to the material damping factor. All these quantities are frequency dependent. It is possible to define as well a complex compliance as frequency varying analogous of the creep compliance(2.8).

As creep compliance and relaxation modulus also relaxation modulus and complex modulus are different ways to express the material behavior. All linear viscoelastic material functions are mathematically equivalent and contain the same rheological information of the material. However, depending on the input excitation, the use of a certain material function can be more advantageous than another. If stress is

specified as input the creep compliance may be the preferred choice as well as the complex modulus if the problem deals with steady state harmonic input. Each material function has a specific testing protocol but, since they are all related to the same material, there are analytical relations enabling the conversion among those parameters. The conversion between creep compliance and relaxation modulus is based on the Laplace transform while the conversion between time and frequency dependent moduli exploits the Prony series or convolution integral properties [13, 14].

Considering, for instance, the conversion between relaxation and complex modulus the starting point is the Boltzmann superposition integral(2.10), that expresses a convolution.

$$\sigma(t) = \int_0^t E(t-\tau)\frac{d\varepsilon(\tau)}{d\tau}d\tau \tag{2.10}$$

The Boltzmann superposition integral can be applied until the material exhibits linear behavior. This is the case of viscoelastic materials subject to acoustic excitation. Small deformations are implied by the impinging pressure wave. As a result the material can be considered in the linear regime.

Equation (2.10) enables to predict the resulting stress, given the strain history, once the relaxation modulus is known. The relaxation modulus can be expressed as a constant value, the long term elastic modulus E_∞, and a time dependent one:

$$E(t) = E_\infty + \tilde{E}(t) \tag{2.11}$$

The constant value may be seen as the value to which the relaxation modulus settles itself at infinite time once the imposed strain is removed. Considering a sinusoidal strain and the relaxation modulus as defined in (2.11), (2.10) becomes:

$$\sigma(t) = E_\infty \int_{-\infty}^{t} \frac{d\left(\varepsilon_0 e^{i\omega\tau}\right)}{dt}d\tau + \int_{-\infty}^{t} \tilde{E}(t-\tau)\frac{d\left(\varepsilon_0 e^{i\omega\tau}\right)}{dt}d\tau \tag{2.12}$$

The lower integral limit has been set as minus infinite since the sinusoidal strain is a periodical signal. Then, solving the first integral and changing variable, from *(t - τ)* to *t'*, the following is obtained:

$$\sigma(t) = \varepsilon_0 e^{i\omega t}\left[E_\infty + i\omega\varepsilon_0 \int_0^\infty \tilde{E}(t')e^{i\omega t'}dt'\right] \tag{2.13}$$

Transforming the (2.13) using the polar representation of exponential function in the integral function it becomes:

$$\sigma(t) = \varepsilon_0 e^{i\omega t}\left[E_\infty + \omega\int_0^\infty \tilde{E}(t')\sin(\omega t')\,dt' + i\omega\int_0^\infty \tilde{E}(t')\cos(\omega t')\,dt'\right] \qquad (2.14)$$

Comparing now (2.14) and (2.9) it is possible to explicit the relation between complex and relaxation moduli [13]:

$$\begin{cases} E'(\omega) = E_\infty + \omega\int_0^\infty \tilde{E}(t')\sin(\omega t')\,dt' \\ E''(\omega) = \omega\int_0^\infty \tilde{E}(t')\cos(\omega t')\,dt' \end{cases} \qquad (2.15)$$

Viscoelastic materials mathematical modeling

Different mathematical models for the viscoelastic behavior have been developed starting from the end of the XIX century. This kind of material is characterized by an intermediate behavior between purely elastic and purely viscous material. It is then justified the choice of a combination of springs to represent the elastic part and dashpots to represent the viscous one (Figure 19). These models have been developed in the rheology framework, i.e. the study of the flow of the matter.

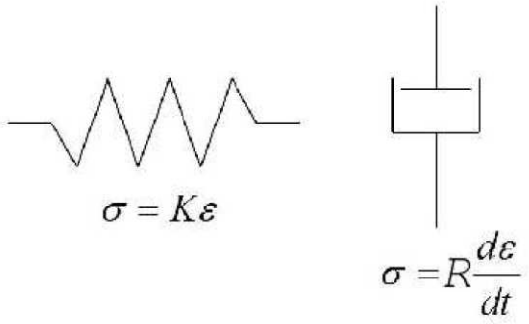

Figure 19 - Basic elements for rheological models.

The spring and dashpot parameters, respectively K and R, are not directly the material constant. It is though therefore possible to derive them from the material experimental data through data fitting procedures.

The more simpleviscoelastic models are based on the series or parallel connection of springs and dashpots [13]:

- Maxwell model
- Kelvin Voigt model

Maxwell model

Maxwell model has been one of the first developed one. It is made of a spring and a dashpot connected in series (Figure 20).

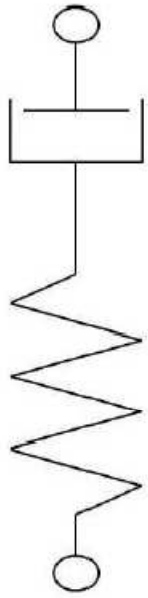

Figure 20 - Maxwell model.

If a load F is applied, both element, spring and dashpot, undergo the same stresstension σ . The time derivative of the final strain is given by the summation of the time derivatives of the strain of the two elements:

$$\dot{\varepsilon} = \frac{\dot{\sigma}}{K} + \frac{\sigma}{R} \tag{2.16}$$

Among the different experimental strategies to investigate the viscoelastic behavior stress relaxation and creep test play a key role. The simulation of such test conditions is useful to analyze the coherence of a mathematical model, like Maxwell's, with a real hypothetic viscoelastic material behavior. Viscoelastic behavior

is generally complex and the modeling choice should be very accurate in order to ensure reliable results.

- *Creep test condition simulation*

Considering the creep test, a constant stress σ_0 should be applied to the system. According to (2.16) the resulting strain will be:

$$\dot{\varepsilon} = \frac{\sigma_0}{R} \Rightarrow \varepsilon = \frac{\sigma_0}{K} + \frac{\sigma_0}{R} t \tag{2.17}$$

The creep compliance, defined as the ratio of the strain to the imposed stress, can be written as:

$$J(t) = \frac{1}{K}\left(1 + \frac{t}{\tau}\right) \text{ with } \tau = R/K \tag{2.18}$$

- *Relaxation test condition simulation*

The relaxation test implies the application of a constant strain to the specimen thus:

$$\frac{\dot{\sigma}}{K} + \frac{\sigma}{R} = 0 \Rightarrow \sigma(t) = K\varepsilon_0 e^{-\frac{t}{\tau}} \tag{2.19}$$

The relaxation modulus, defined as the ratio of the resulting stress to the imposed strain, can be written then as:

$$E(t) = Ke^{-\frac{t}{\tau}} \tag{2.20}$$

The trend of creep compliance and relaxation modulus for the Maxwell model is depicted in Figure 21.

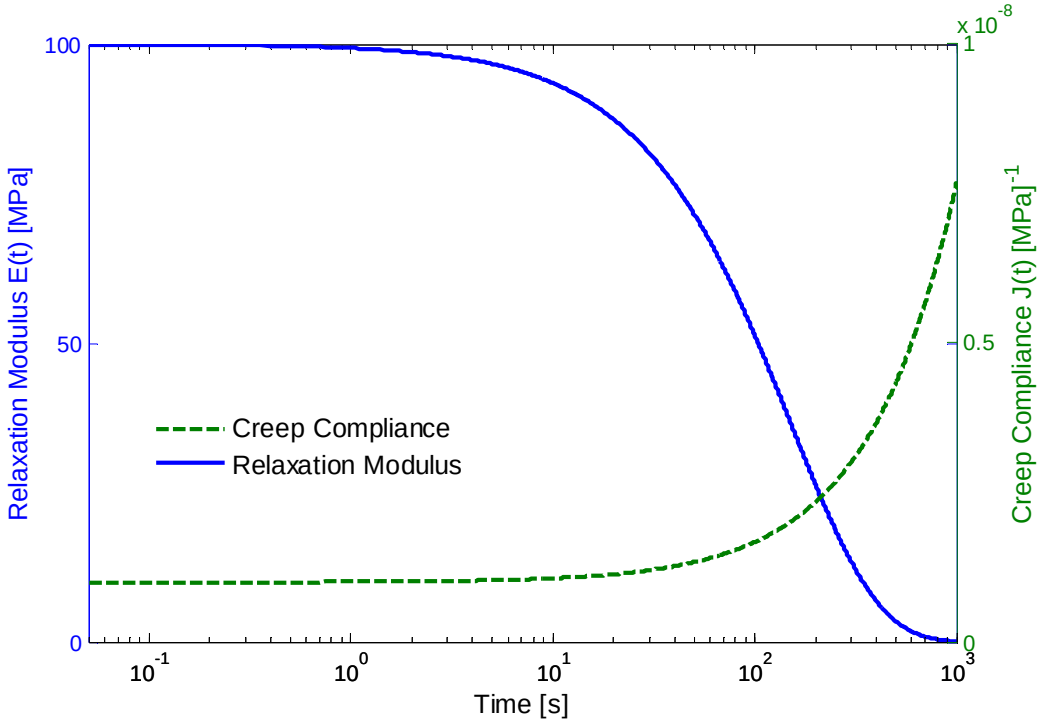

Figure 21 – Creep compliance and relaxation modulus for Maxwell model.

The trend of the relaxation modulus is not representative of the behavior of a real viscoelastic solid. In fact, for infinite time, the relaxation modulus tends to zero. This means that the resulting stress would be null at infinite time given a fixed value of deformation and that is not physically possible for a solid. The creep response is irrealistic since the primary creep prediction is a straight line, in contrast with what is observed experimentally [13]

Kelvin Voigt Model

A different rheological model is the Kelvin – Voigt one, made of a spring and a dashpot connected in parallel (Figure 22).

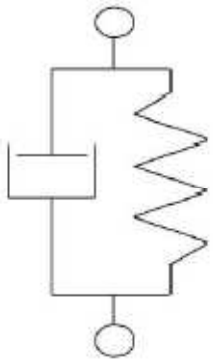

Figure 22 - Kelvin Voigt Model.

In this case both elements are subject to the same strain while the final stress is the sum of the stress acting on the spring and the dashpot.

$$\sigma = K\varepsilon + R\dot{\varepsilon} \tag{2.21}$$

- *Creep test condition simulation*

If a constant stress is applied to the Kelvin Voigt model, as in a creep test, the resulting deformation is:

$$\sigma_0 = K\varepsilon + R\dot{\varepsilon} \Rightarrow \varepsilon = \frac{\sigma_0}{K}\left(1 - e^{-\frac{t}{\tau}}\right) \tag{2.22}$$

The creep compliance, obtained as the ratio between the strain and the constant applied stress, is:

$$J = \frac{\varepsilon}{\sigma_0} = \frac{1}{K}\left(1 - e^{-\frac{t}{\tau}}\right) \tag{2.23}$$

- *Relaxation test condition simulation*

Applying a constant strain, as for the stress relaxation test, it is immediately possible to notice from (2.22) that only the spring element provides a response to the input. The stress in the dashpot vanishes immediately while the spring one remains constant without relaxing. The relaxation modulus is thus constant and equal to the value of the spring parameter K.

The trend of the relaxation modulus and the creep compliance is depicted in Figure 23. The Kelvin Voigt model is not able to correctly predict the stress relaxation

phenomenon, typical of viscoelastic materials. The creep compliance trend is instead more similar to the actual one of a viscoelastic material.

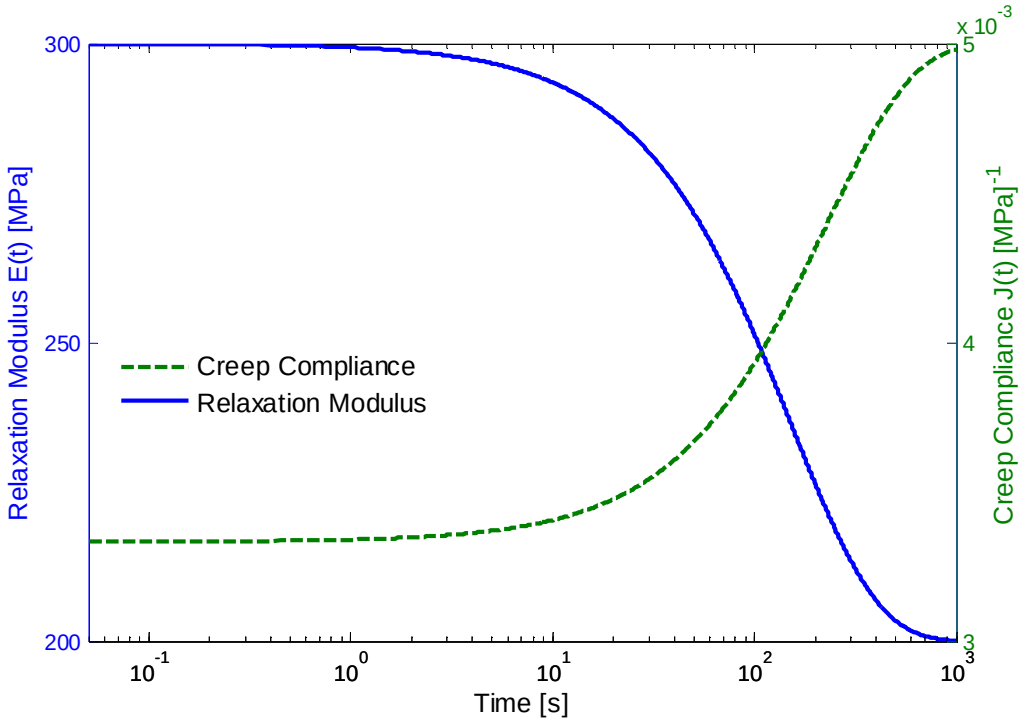

Figure 23 - Creep Compliance and Relaxation Modulus for Kelvin Voigt model.

More refined models have been developed in order to accurately model both creep and stress relaxation of a viscoelastic material. One of the simplest models that can represent in a more realistic way the viscoelastic behavior is is the Zener model or Standard Linear Solid (SLS) model.

Standard Linear Solid Model

The SLS model is made by a spring in parallel with a Maxwell model (Figure 24).

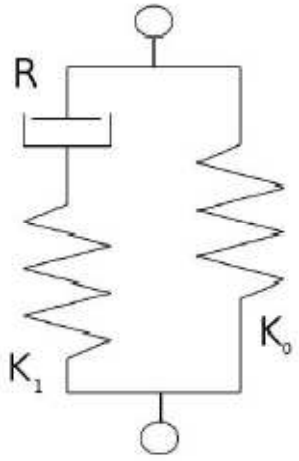

Figure 24 - Zener or SLS model.

The stress- strain relationship is given by:

$$\sigma + \frac{R}{K_1}\dot{\sigma} = K_0\varepsilon + R\left(1 + \frac{K_0}{K_1}\right)\dot{\varepsilon} \tag{2.24}$$

In order to analyze the validity of the SLS model to predict the behavior of a viscoelastic material, the condition of creep and stress relaxation tests are applied to the model.

- *Creep test condition simulation*

Applying constant stress, the resulting strain is:

$$\sigma_0 = K_0\varepsilon + R\left(1 + \frac{K_0}{K_1}\right)\dot{\varepsilon} \Rightarrow \varepsilon = -\sigma_0 \frac{K_1}{K_0\left(K_0 + K_1\right)} e^{-\kappa t} + \frac{1}{K_0} \tag{2.25}$$

with $\kappa = \frac{K_0}{K_0 + K_1}\frac{1}{\tau_1}$ and $\tau_1 = R/K_1$.

The creep compliance for the Zener model is given by:

$$J = -\frac{K_1}{K_0\left(K_0 + K_1\right)} e^{-\kappa t} + \frac{1}{K_0} \tag{2.26}$$

- *Relaxation test condition simulation*

Considering the stress relaxation test, thus constant strain, the resulting stress is:

$$\frac{R}{K_1}\dot{\sigma}+\sigma=K_0\varepsilon_0 \Rightarrow \sigma=\varepsilon_0\left(K_1e^{-\frac{t}{\tau_1}}+K_0\right) \tag{2.27}$$

The relaxation modulus, expressed as the ratio between the stress and the constant strain, is:

$$E=K_1e^{-\frac{t}{\tau_1}}+K_0 \tag{2.28}$$

The trend of the relaxation modulus and of the creep compliance is depicted in Figure 25. The SLS model is one of the simplest one able to combine both the meaningful behaviors of a viscoelastic material: the creep and the stress relaxation. The relaxation modulus doesn't tend to zero for infinite time allowing the presence of a finite value stress consequent to the constant imposed strain and the creep compliance is not monotonously increasing but it reaches a plateau as typical for viscoelastic materials.

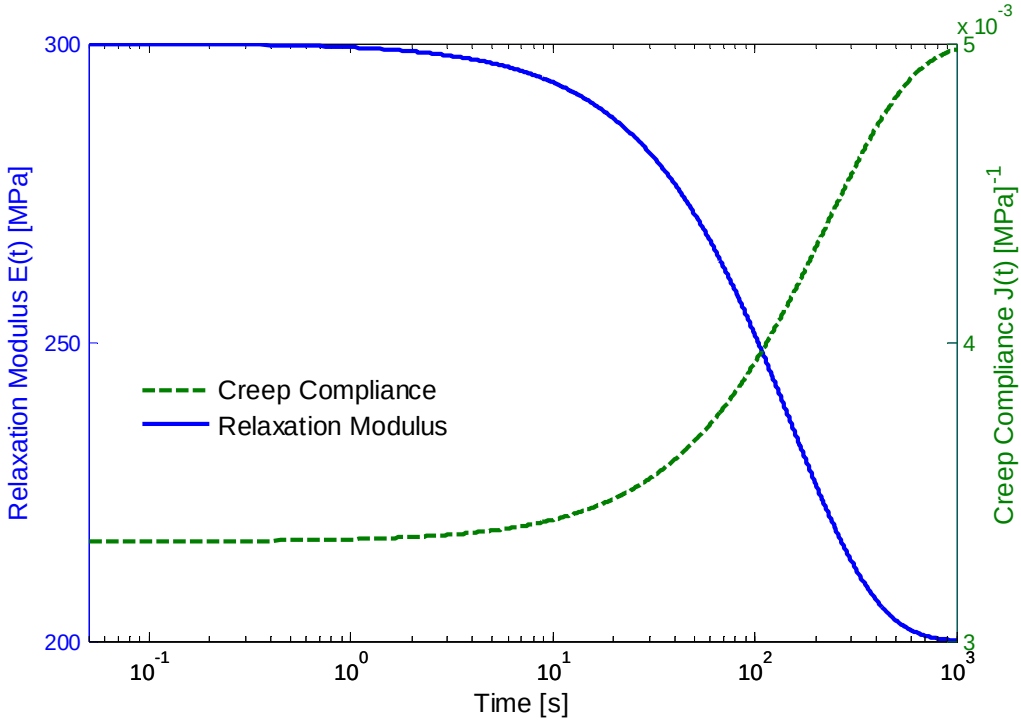

Figure 25 - Creep compliance and Relaxation modulus for SLS model.

Figure 25 shows qualitatively the trend of Creep Compliance and Relaxation Modulus obtained numerically with a SLS model. In Figure 3-13 the Creep Compliance and the Relaxation Modulus of a PMMA specimen are displayed. The trends of both quantities agree with the qualitative prediction of the SLS model. Therefore, the SLS model can be considered suitable to represent the behavior of a viscoelastic materal.

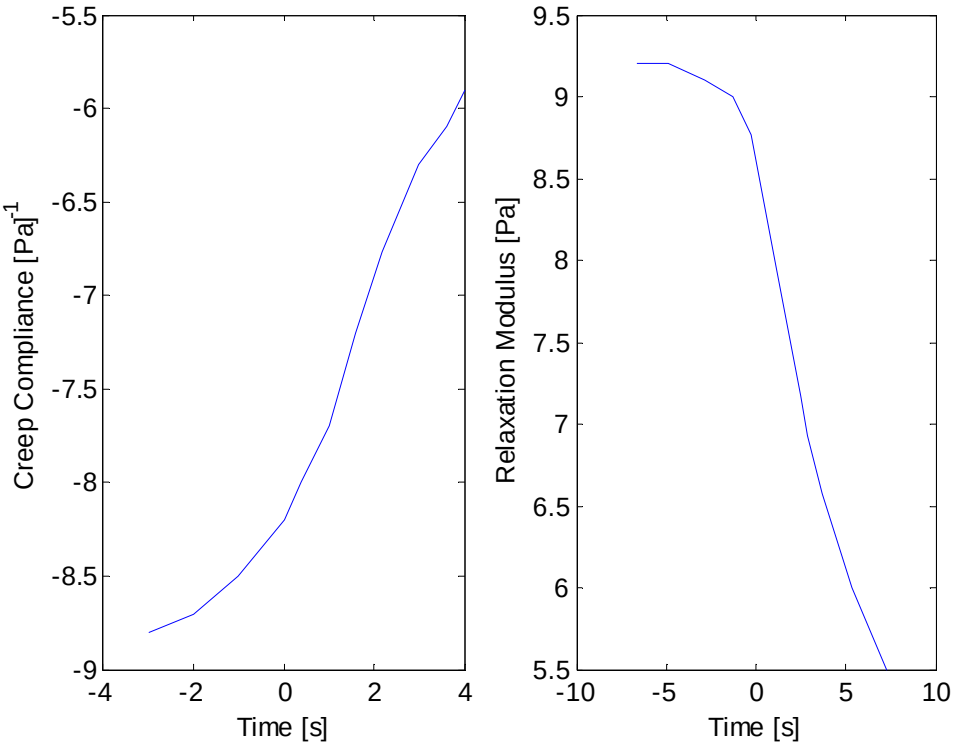

Figure 26 Bi - logarithmic plot of Shear creep compliance and Relaxation Modulus of PMMA at 110 ℃.

The viscoelastic material behavior is usually represented as a combination of springs and dashpots while the time domain material functions are expressed by a series of decaying exponentials [15]. It has been shown that the definition of the relaxation modulus using a Prony series, i.e. a series of decaying exponentials, improves the numerical code efficiency[14]. The definition of a mathematical model to define the viscoelastic material behavior is a fundamental step in the structural numerical model development.

3.1. Sound propagation in porous materials

The propagation of sound in porous media is a well knownresearch topic though the geometry of the pores in ordinary porous material is not so simple [16, 11]. Generally speaking the problem of sound propagation in porous materials can be faced in two ways:

1. *Porous material having rigid frame*

   This approach is optimal for porous materials directly subject to an acoustic field.The elastic part of the porous structure can be neglected, being relevant only for frequencies close to the resonances of the system.

2. *Porous material having elastic frame*

   This approach of considers the frame no more motionless with respect to the fluid but with a certain level of elasticity. The simulation of the frame elasticity is really important when studying a complex system for which the vibroacoustic behavior coupling is fundamental.

3.1.2. Rigid frame porous materials

Considering the frame as rigid implies that the acoustic behavior is affected only by the geometrical characteristics of the material and thus t by the obstacles that the acoustic wave meets on its path [17].The main condition for the validity of this approach is the long-wavelength condition [11]. The wavelength is much larger than the characteristics dimension of the pores and the saturating fluid can behave as an incompressible fluid at the microscopic scale. Aiming to model the acoustic behavior of porous material three approaches can be pursued: (i) Microstructural models, (ii) Empirical models, (iii) Phenomenological models

Microstructural models

The simplest analytical model of a porous material assumes that the solid constituent is rigid and that the behavior of the fluid constituent is equivalent to that of a homogeneous, isotropic fluid, taking into account effects of both viscosity and heat conduction. Many theories of acoustical wave propagation in porous media are derived from an initial conceptual model of a medium containing identical parallel

cylindrical capillary pores running normal to the surface the frame of which is assumed to be rigid [16].

Figure 27 - Porous material as assembly of parallel tubes.

The first attempt to describe sound propagation in cylindrical tubes (Figure 27) is the Kirchhoff and Lord Rayleigh one [11, 17, 16]. The theory provides a general description of sound propagation in a small circular cross-section tube, including visco us and thermal effects. However, this theoryresults to be too complicated for many practical applications. Next steps were made by Monna and Scott [16]. The former considered that the air in such a structure behaves as if it were an homogeneous isotropic fluid. As a consequence the air motion can be described exactly by the same differential equation that describes the propagation of sound in unconfined air, except for the contribution of an additional damping term related to particle velocity. The latter found a way to determine the propagation constant and the complex density that characterizes how a plane wave propagates in the material. A simplified model has been worked out by Zwikker and Kosten [16] for the case of circular cross section. The abovementioned authors have shown that the viscous and thermal effect can be included considering a complex density and complex compressibility. The validity of this model has been proved in the range of acoustical frequencies for pore radius from 10^{-3} cm to some cm [17] but it's no longer suitable in case of pores with a wide cross section variation or in case of not straight pores. Further developments were made by Biot, Stinson and Johnson [18, 17], introducing a dynamic shape factor to allow for any form of pore section between the extremes of parallel walled slit and circular capillarity. The dynamic shape factor allows to take into account not straight pores, including as well viscous effect. However, in the case of common porous materials, an analytical description that takes in account the complete geometry of the microstructure is almost impossible due to material complexity.

Empirical Models

Empirical models are widely used for fibrous materials. They allow the calculation of the acoustic impedance and the propagation constant considering one or more

material parameter. These models are based on dedicated experimental tests so that they have limited validity. The Delany and Bazley model [17] is still one of the most commonly adopted due to its simplicity. As a drawbackthis model requires the knowledge of the flow resistivity from experimental data. Models have been developed, able to calculate the flow resistivity as a function of material density as the one of Bies and Hansen or Mechel and Ver [17, 19]. These models may be unaccurate if applied to materials with fiber diameter different from that studied from the abovementioned authors. Several studies have been made to extend this class of models to foams, like Dunn - Davern model [17] or Wu Qunli [17]. Due to the complex structure of foams, however, monoparametric models as the overmentioned one may lead to severe errors [17]. Mechel and Miki [17] introduced empirical models with two and three parameters in order to improve the capability of empirical models also for porous materials.

Phenomenological Models

This class of models distinguishes among viscous friction, inertia and heat transfer phenomena introducing the concepts of dynamic density and compressibility for a fluid that is considered equivalent to the analyzed porous material. From a qualitative point of view the sound propagation is dominated from viscous forces at low frequencies and inertia at high frequencies. The air in the pores is expanding and contracting in a isothermal manner at low frequencies and in an adiabatic way at higher frequencies due to particle velocity [16, 17]. The most important model for porous material is the Johnson-Champoux- Allard model [17, 11]. It relates the equivalent quantities dynamic density and compressibility to five physical parameters of the material: flow resistivity, porosity, tortuosity, viscous and thermal characteristic length. This model shows high reliability for materials that present high porosity while for low porosity materials the model proposed by Attenborough [17] is to prefer although it requires the challenging experimental determination of some parameters.

3.1.3. Elastic frame porous material

Whenever the porous material is set between two elastic plates (Figure 28) the frame, i.e. the porous material, vibration is induced by the vibration of the plates itself. As a consequence, the air and the frame move simultaneously.

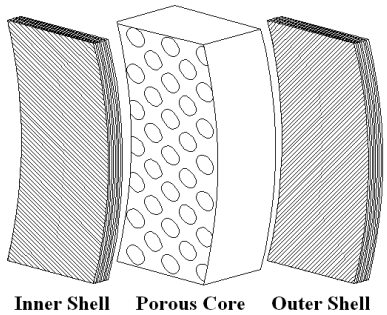

Figure 28- Porous material set between two elastic shells.

The earliest attempt to describe this phenomenon has been made by Kosten et al.[16, 20] that at first noticed that both media takes part to vibration. The most well known model for wave propagation in porous media having an elastic frame is provided by the Biot theory [18]. Generally speaking, in the Biot theory the deformations of the structure are related to wave propagation and are supposed to be similar to those of an elastic solid, i.e. in a representative volume there is no dispersion of the velocity in the solid part in contrast to the velocity in the air [11]. Although appearing fifty years ago, this theory is still the reference one. It is based on the derivation of the stress - strain relations from the potential energy of deformation in a Lagrangian model [11]. It allows one to consider the propagation of elastic waves in the material structure distinguishing between transversal and longitudinal compression waves, or so called slow and fast waves. A fine description of Biot theory has been developed by Allard [11] based on the coupling of the displacement of the frame and the fluid, so called u-u formulation. In this formulation the stress tensors of both fluid and frame are related to both displacement considering mass coefficients.Taking into account the fact that the flow through the pores may not be uniform, the interaction between inertia forces of fluid and solid phase is expressed through a coefficient function of the tortuosity of the material. A damping term is considered to take in account viscous interaction forces between frame and fluid [17]. The u-u formulation is widely exploited in numerical modeling of wave propagation in porous materials having elastic frame though it can lead to high computational cost. To overcome these difficulties, Atalla [21] proposed a mixed u-p formulation in which the coupling is no longer considered between displacement of frame and fluid but between frame displacement and fluid pressure. Basically, in this formulation, it is assumed that the porous material properties are homogeneous and that the displacement of the fluid can be expressed in terms of fluid pressure in pores [17]. The basic hypotheses of the Biot theory are: isotropic, quasi-homogeneous medium; uniform porosity; impervious pore walls and pore size concentrated around an average value [16]. The pore size is assumed to be much

smaller than the wavelength of interest. As a consequence of the last assumption the validity of this theory is restricted to the case in which the travelling wave wavelength is obviously larger than the characteristics dimension of the volume of homogenization [22]. Further developments of the initial theory of Biot [18] that implies laminar flow and no friction has been made by Biot himself to include anisotropy, viscoelasticity and solid dissipation [23]. A recent extensionto the case where the medium frame is made of not compressible material was made by Dazel [11].

4. Sound transmission

The sound transmission and/or radiation by finite panels excited by incident, diffuse sound waves is made up of two components, respectively a *resonant* and *non resonant* response. The former is due to the resonance of the modes having their frequency within the excitation frequency range. The latter arises from the waves that are forced to propagate in the partition at a speed imposed by the speed of sound in air and by the incidence angle. The non resonant waves tend to transmit most of the sound at frequencies below the critical frequency, i.e. the correspondence between the structural free bending wavespeed and the acoustic wavespeed in air. The resonant frequencies below the critical frequency have very low radiation efficiency and bending wave lengths smaller than the incident wave one. Thus they are very poor sound transmitters. Below the critical frequency the mass of the panel controls the sound transmission since there is no appreciable effect of the structural modes resonance. Above the critical frequency, instead, resonant modes are most responsible for the sound transmission.

Different indicators have been defined to experimentally characterize the sound transmission. Among the others, Transmission Loss (TL) is of great importance and common use.

4.1. Transmission Loss

The TL is an index used to quantify the sound transmission capabilityof a partition

$$TL(f) = 10\log\frac{\Pi_{incident}}{\Pi_{transmitted}} \tag{2.29}$$

The calculation of TL following (2.29) means the logarithmic ratio between incident and transmitted sound power. TL value is frequency dependent and varies between two asymptotic behaviors: a perfectly reflective material having infinite TL and an opening being characterized by TL equal to zero.

The sound power flowing through a surface Π is defined as the dot product between sound intensity integrated over the surface $\{I(t)\}$ and the considered surface area A. The sound intensity expresses the magnitude and direction of the instantaneous sound power per unit area.

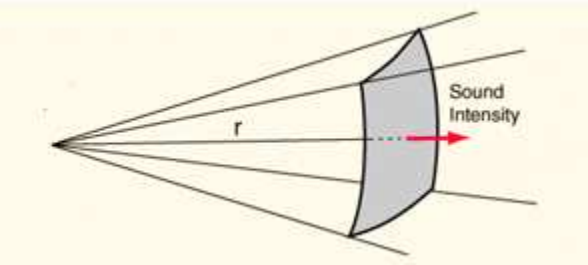

Figure 29 - Sound Intensity, schematic interpretation.

The instantaneous sound intensity is given by the product of the instantaneous particle velocity $\{v(t)\}$ and the instantaneous sound pressure p:

$$\{I(t)\} = p(t)\{v(t)\} \tag{2.30}$$

The TL, as expressed in (2.29), is generally frequency dependent. The characteristic Transmission Loss of a bounded homogeneous panel is showed in Figure 30:

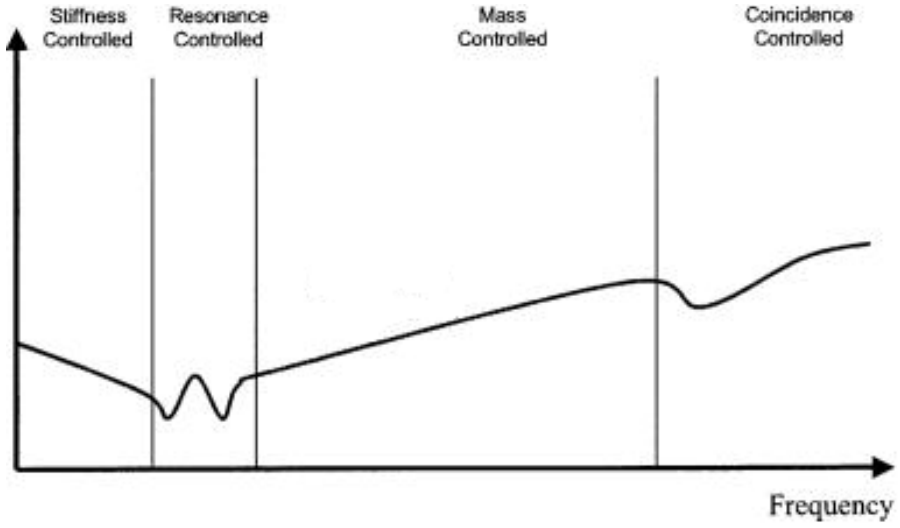

Figure 30 - Typical TL trend of a bounded homogeneous single panel.

Four regions can be identified [6]:

Stiffness controlled

At frequencies well below the first natural frequency, the stiffness of the panel dominates its sound transmission characteristics. In this region there is a -6 dB/octave slope of TL.

Resonance controlled

Increasing the frequency the modal behavior of the panel influences its sound transmission properties. Dips appear in the TL curve in correspondence of the resonance frequencies of the structure. The importance of resonant modes is higher for mechanically excited panels. In such a case, addition of suitable damping material increases the TL. If the panel is acoustically excited, the forced bending wave at the excitation frequency dominates the sound transmission and the resonant modes are of relative importance.

Mass controlled

Above the first natural frequencies but below the critical frequency the panel mass per unit area ρ_s controls the sound transmission. This region is characterized by a 6 dB/octave slope. The same increase is given by doubling the mass. Damping and

stiffness are irrelevant on the sound transmission and the TL is said to follow the Mass Law. For an impinging sound wave of given incidence ϑ, travelling in a medium of density ρ with speed c, the sound transmission loss can be evaluated as:

$$TL_{\text{mass law}}(f,\vartheta) = 20\log\left(\frac{2\pi f \rho_s}{2\rho c}\cos(\vartheta)\right) \tag{2.31}$$

Coincidence controlled

At regions in proximity to the critical frequency there is a sharp drop in the sound transmission loss curve. Below coincidence the disturbance induced by the structural bending wave in the surrounding fluid is local. The flexural wavelength is smaller than the acoustic one hence no sound waves are radiated and only a near field exists [6]. Above coincidence frequency the bending wavelength is greater than the acoustic one and the radiation becomes efficient. At coincidence the acoustical and the forced structural wavelengths are equal and the panel becomes completely transparent to sound transmission. For infinite, homogeneous plates, the coincidence frequency for a given incidence angle ϑ can be evaluated in terms of plate structural parameters:

$$f_c = \frac{c^2}{2\pi \sin\vartheta}\sqrt{\frac{\rho_s}{D}} \tag{2.32}$$

The coincidence frequency is a function of the incidence angle [7]. The coincidence minimum frequency called *critical frequency* occurs for grazing incidence. Above critical frequency damping, stiffness and mass contribute to sound radiation.

Below coincidence frequency resonant modes have very poor radiation properties but particular attention should be paid to the presence of discontinuities. Adjacent plate region cancel each other leaving only uncancelled volume velocities in regions close to structural constraint (Figure 31).

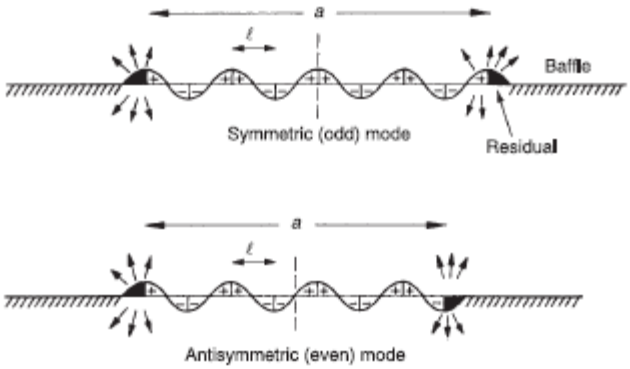

Figure 31 - Interregion cancellation and edge effect [3].

Even modes radiate less than odd modes since the remaining volume velocity zones are antisymmetric (Figure 31).

5. Vibroacoustic modeling techniques

The main advantage of using sandwich structures is given by their adaptation feature. In fact, they are characterized by a rich basket of designing parameter and options that allows the structure to be tailored to the specific application case and field. For instance, given the application field and the frequency range of interest it is possible to combine core and skin materials and microstructure to obtain the structure best performance. A key role in the design phase is thus played by the numerical modeling tools. A reliable model allows the investigation of different panel parameters combination and to evaluate the global panel performance. In the vibroacoustic framework, the numerical model should be able to predict both dynamic and acoustic behavior as well as the coupling of them.

5.1. Dynamic modeling

Mechanically excited structures radiate sound mainly at frequencies corresponding to their structural resonances. In this condition the structure becomes a perfect radiator. In addition, resonances amplify incoming vibrations. As a result, a detailed knowledge of the so called structure modal behavior, i.e. resonances frequencies and mode shapes, plays a fundamental role in the design step. Aiming to reduce the vibration transmission and the consequent sound radiation, thedesigner has to tune

structural parameters to reduce the number of resonant modes within the excitation frequency range. The availability of a reliable dynamic model for predicting the structure behavior becomes then a fundamental point [24].

One of the most powerful tools in engineering is the Finite Element Method (FEM). This discretization method is based on the idea that a structure can be approximated by replacing it with an assemblage of discrete elements (Figure 32).The displacement field within each element and on its boundaries is expressed as function of the nodes of the elements, using unique suitable interpolating functions called "shape functions".

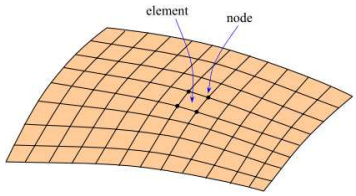

Figure 32 - Continuum discretized with FE.

Thanks to the elasticity theory, the displacement functions uniquely define the state of strain within each element. Exploiting the constitutive law of the structure material it is possible to define the stress state of each element as function of strain. In this way a continuum problem is reduced to a finite number of unknows, the nodes displacement. The same unknowns are variables in the structure dynamic equation to obtain the characteristic mode shapes. The natural frequencies are derived from the material parameters and structure geometry.

Multilayered plates and shell structures (Figure 33) require appropriate modeling to handle the complicating effects that arises from their intrinsic in plane and out of plane anisotropy.

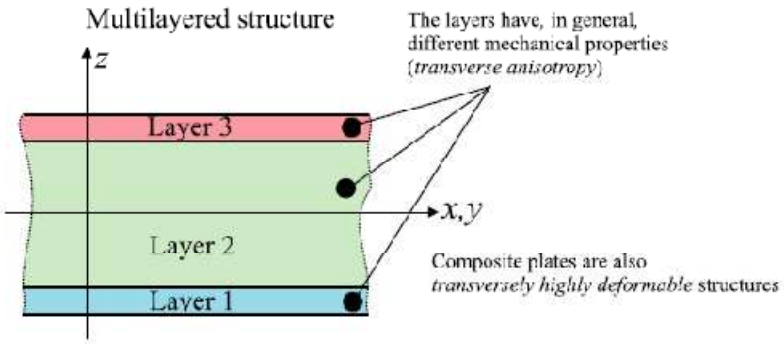

Figure 33 - Sketch of a multilayered structure [25].

The literature of the second half of the last century displays a large number of analytical and numerical 2D contributions to layered structures. The available theories may be subdivided in three main groups:

(i) *Equivalent Solid Layer (ESL) Approach*

This group of theories arises from the basic Kirchhoff plate theory. The composite structure is considered as an integral equivalent layer. ESL gives sufficiently accurate global laminate response but they are inadequate if stresses at ply level are required. In addition, they may lead to inaccurate results in case of high anisotropy or localized loads.

(ii) *Layer Wise (LW) Approach*

The composite structure is thought as an aggregate of independent layers. This approach, mandatory for a full 3D description of the stress – strain state in laminates introduces anyhow some errors. The description of the cross sectional deformation of each layer may be inaccurate and normally the continuity of transverse shear stresses among layers is not satisfied a priori. However these errors are much less than the one introduced by ESL theories, originating upon the construction of a kinematic model of the entire packet of layers [26].

(iii) *ZigZag Theory*

This approach aims to overcome some inaccuracy of the ESL approach avoiding the high computational cost of LW one. The basic concept behind this theory is that the equilibrium between adjacent layers implies the out of plane stresses to be equal at the interface. These stresses can be thought of as a combination of strain multiplied by some coefficient that is material dependent. Each layer may be of a different material thus different strains are

required to ensure equilibrium. The strains are related to the derivative of the displacement hence the displacement field exhibits different slopes along the structure cross section. Thus continuity of the stresses leads to discontinuity of the displacement first derivative. This effect is called “zigzag form of the displacement” [27].

ESL theories: overview

The first developed equivalent single layer theory is the Kirchhoff Love [28]. This theory lies on the Classical Lamination Theory (CLT). The so called *thin plate* theory is based on the assumptions of Kirchhoff in late XIX century [29]. Basically, it is possible to represent the state of deformation based on the displacements of the middle surface and a rotation of the normal. As a result, transverse shear and normal strains are considered to be negligible with respect to other strains. Thes assumption is legitimate only in the case of thickness negligible with respects to other dimensions. This may not be the case for sandwich materials in which the deformation involves often shear stresses in the core.

Starting from CLT First order shear deformation theories (FSDT) have been developed to include shear strains. FSDT provide a balance between computational efficiency and accuracy for the global structural behavior of thin and moderately thick plates. These theories have been widely employed to analyze free vibrations of composite laminated plates and are simply the extension of the so-called Reissner-Mindlinn model to layered structures [30]. A simple but significant improvement of this theory was carried out by Vlasov [30] permitting the fulfillment of the homogeneous conditions for the transverse shear stresses in correspondence to the top and bottom shell/plate surface. Anyhow, Equivalent solid layer models (ESLM) can undergo difficulties in analyzing thick multilayered plates. This class of models leads to a very poor description of the transverse normal stresses that cannot be neglected in those kind of plates. Reissner's mixed approach [30] has been used in some ESLM, see as example [30], but have shown deficiency in treating arbitrarily laminated plates [30].

This last issue has been faced structuring Higher order theory (HOT). HOT includes both transverse shear and normal strains, as the Hildebrand, Reissner and Thomas theory [30]. The comparison between the displacement field considered in FSDT and HOT is shown in Figure 34.

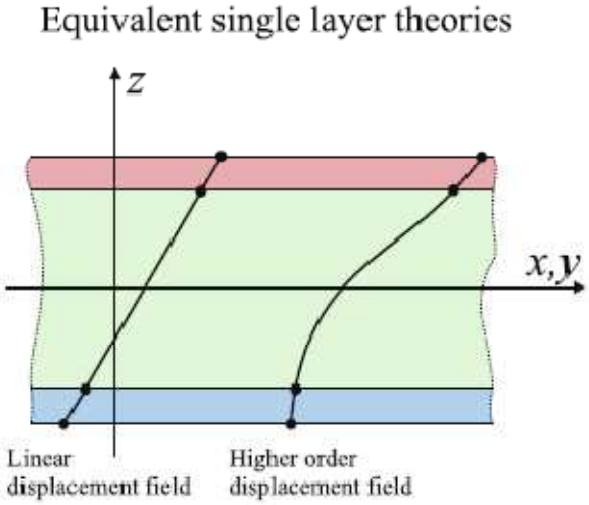

Figure 34 - Displacement field: FSDT vs HOT [31].

ESLM may lead to inaccurate results if the analyzed structure presents significant variation in thickness and/or properties among skins and core. Determining the effective properties of the whole sandwich structure becomes indeed very challenging. As experienced in early three dimensional elasticity analysis [30] the variation of mechanical properties in the thickness direction of layered structures, leads to the so-called zigzag form of displacement field. ZigZag displacement field and interlaminar continuity for the transverse stressed has been summarized in the term C^0_z *requirement* i.e. displacement and transverse stress field must be C^0 continuous function in the *z* direction. Among the ESL theories only the HOT theories allow partial fulfillment of the C^0_z *requirement* [30].

Layer Wise theories: overview

ESLM approach remains insensitive to individual layers. If a detailed response of the individual layers is required or there is a significant variation of the displacement among layers the kinematics of each single layer should be described. Layer Wise Models (LWM) come then to the fore. The LWM assume separate displacement field expansions within each material layer, providing indeed a correct representation of the strain fields in discrete layer laminates and allowing accurate ply-level stresses to be determined. The accuracy is greater than ESLM but the computational cost is also increased. Many LWM simply arise from the application of CLT or FSDT to each single layer. Generalizations of those approaches were proposed where displacement variables are expressed in terms of Lagrangian polynomial. Normally,

in LWM do not take in account a priori transverse stresses continuity between adjacent layers [31]. The displacement field considered in LWM is depicted in Figure 35:

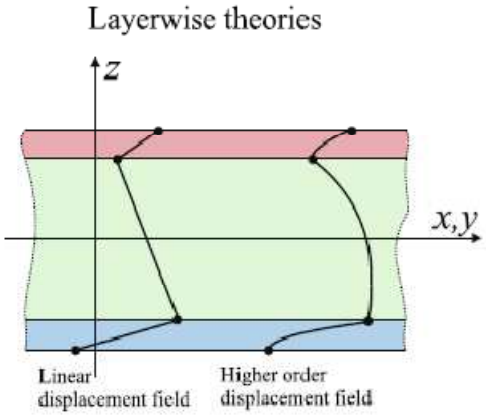

Figure 35 - LWM displacement field [31].

ZigZag theories: overview

Both approaches ESL and LW do not fulfill the C^0_z *requirement*a priori. This can be achieved applying the ZigZag theories. The basic idea behind this theory is to assume a certain displacement and/or stress model in each layer then to use compatibility and equilibrium conditions at the interface to reduce the number of unknown variables. ESL approaches can be developed introducing a ZigZag displacement function ZZF, like the one developed by Murakami [32]. The resulting displacement field is sketched in Figure 36. The simplicity of ESL approach is then improved by considering the ZigZag effect without introducing the LWM high computational cost.

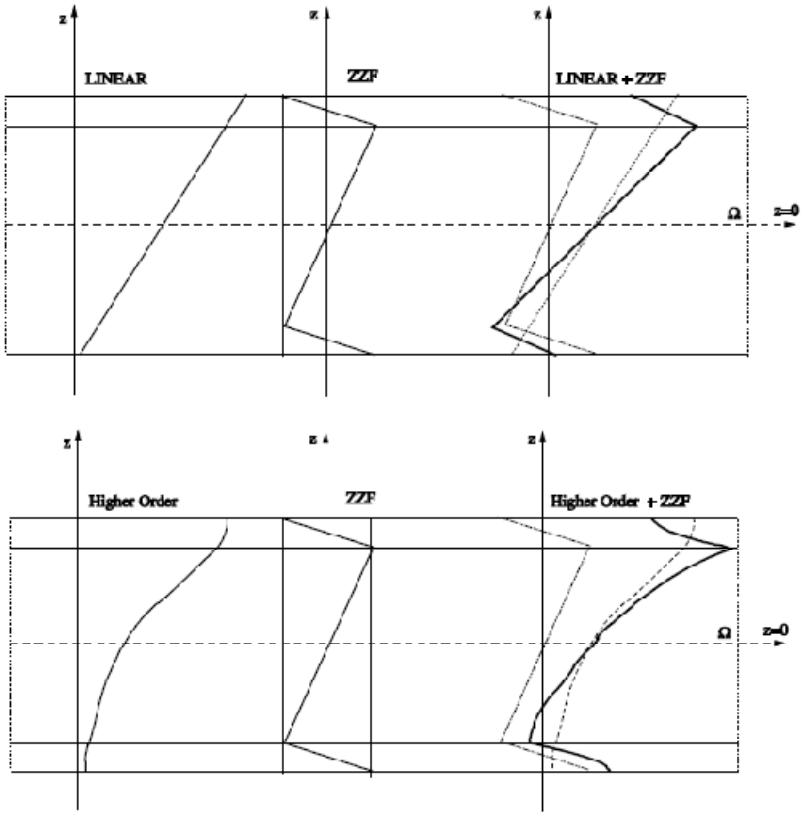

Figure 36 - ZZF and ESL approach combination [32].

Generally speaking it is possible to distinguish among three independent ZigZag approaches: (i) Lekhnitskii - Ren approach (ii) Ambartsumian - Whitney - Rath - Das approach and (iii) Reissner - Murakami - Carrera approach. A brief description of the methods is given in [30]. Approach (i) is based on the Lekhnitskii work [30] that proposed a method able to describe zigzag effects, both for in plane and through thickness displacements, and also interlaminar continuous transverse stress. Lekhnitskii applied the method to 3D problem of plane stress of a cantilever beam then Ren extended the work to orthotropic and anisotropic plates. Approach (ii) has been extended both to plates and to shells and has the peculiarities of preserving the same number of unknown variables as FSDT approaches. The Ambartsumian - Whitney - Rath - Das theory has been the milestone for dozens of simplified theories appeared over the last decades although for historical reasons most of these does not refer to the work of Ambartsumian or Whitney, Rath and Das but to the one of Cho and Parmeter [30]. The approach (iii) is based on a paper of Reissner in which a mixed formulation is presented considering displacement and transverse stress variables as independent [30].

5.2. Numerical analysis of sound fields

At present, the main numerical prediction techniques for acoustic behavior rely on element-based deterministic method, as well as the dynamic behavior modeling. The validity of this family of techniques is limited to the low frequency range. Moving towards higher frequencies the element size should decrease to minimize the dispersion error, i.e. the difference between the numerical and exact solution that increases with frequency. This leads to such large models that require almost unreasonable computational times. In addition, at high frequency the response of the system becomes very sensitive to changes in the system parameters that are generally known with a certain level of uncertainty. As a result, the system response predicted by a deterministic approach, that uses nominal parameter values, is no longer significant. To overcome these difficulties, probabilistic techniques such as Statistical Energy Analysis have been developed. The resulting model size is substantially smaller than the one obtained with element based. Anyhow, one of the basic assumption of statistical methods, i.e. high modal density, limits their application region to high frequencies. In between high and low frequency there is a mid frequency range for which specific methodology have been developed.

5.2.2. Deterministic methods

At present, most commonly used deterministic prediction techniques for sound radiation problems are Finite Elements Method (FEM) and Boundary Element Method (BEM)

Finite Elements Method

The Finite Elements Method is usually applied for the analysis of sound field in bounded or nearly bounded domains, i.e. a finite domain of fluid [3]. The basic concept of FEM in acoustics is exactly the same than in structural analysis. The domain is divided in contiguous elements substantially smaller than the highest frequency of interest. The original problem of determining the pressure field at any position in the fluid domain is reduced to determining the pressure values at some discrete position of the domain (Figure 37). Within each element the pressure is approximated as a polynomial expansion in terms of suitable shape functions. The main drawback is related to the problem size. In fact to obtain sufficient accuracy at least 10 elements per acoustic wavelength are required leading to very large model sizes. In addition, derived secondary field variables like fluid velocities or acoustic

intensities are characterized by lower accuracy than primary field variables, i.e acoustic pressure.

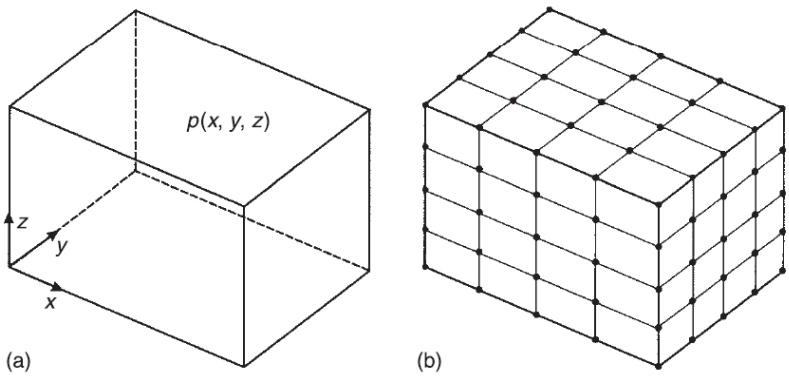

Figure 37 - (a) acoustic cavity (b) finite elements mesh [3].

An alternative to FEM is the Finite Difference Analysis (FDA)[3]. The fluid region is still divided in elements and field values are assigned to the elements nodes. In FDA the derivatives, in the partial difference equations that describe the problem, are represented by finite difference approximation. The result obtained for any given point involves values of the surrounding points. An initial set of field values is assumed and a systematic iteration provides a stable solution. The main drawbacks with respect to FEM are that FDA deals not so well with arbitrary volumes of fluid which boundaries does not conform the grid line pattern and is much more sensitive to local error of field representation [3].

Extension of FEM to unbounded domains

FEM is most practicable for bounded interior problems but there are different ways to extend it to exterior radiation problems. In this framework an artificial boundary surface is introduced at some distance from the original boundary. As a consequence the original unbounded domain is split in a bounded and unbounded region (Figure 38). The new bounded domain is now suitable for FE discretization and the artificial boundary should ensure that all acoustic waves propagate towards infinity and any wave is reflected (Sommerfeld radiation condition).

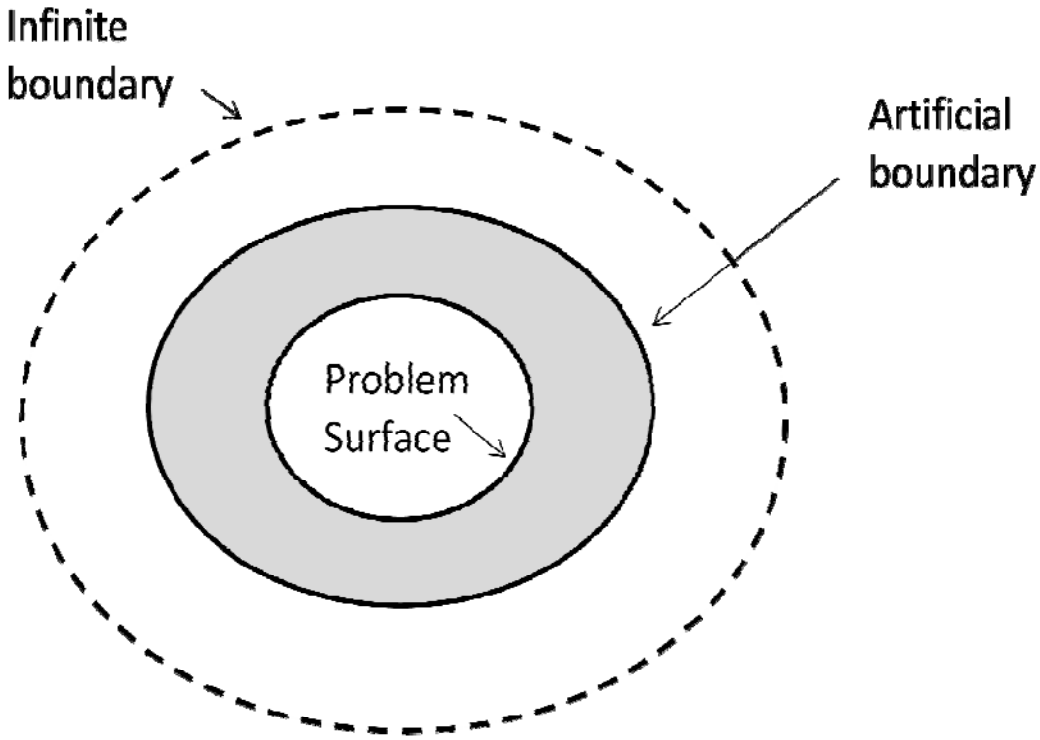

Figure 38 - FE model with artificial boundary.

Several approaches can be pursued to ensure this condition, among others:

- A coupling with a an approximated pressure field in the unbounded domain through the use of Infinite Elements. Each Infinite Element contains a part of the artificial boundary and it is infinitely extended away from it. The pressure within the Infinite Element is expressed in terms of shape function with a amplitude decay and wave like variation to model outgoing waves. The size of the new bounded volume is strongly related to the accuracy of the considered shape functions. Different kind of elements has been implemented [33].

- The definition of the specific acoustic impedance of freely propagating waves as impedance boundary condition. In order to make the non – reflectivity effective, it is necessary to put the artificial boundary at a very large distance from the initial problem boundary surface. Thus, the new formed boundary domain is still very large and it may yield to a computationally expensive FEM. To overcome these difficulties, Bayliss et al. [33] proposed a family of

higher order boundary condition that are able to limit the extension of the new bounded domain.

Boundary Element Method

A valuable modeling option when dealing with unbounded domains is represented by the boundary element method (BEM). This method approximates the Kirchhoff – Helmoltz equation by a summation over a number of small surface elements. The basic concept is to relate field variables in the continuum domain to boundary variables on the boundary surface of the domain. As in FEM, boundary variables are approximated by suitable functions locally defined over the set of small elements in which the boundary has been discretized. The original problem then goes back to a discrete set of equation in terms of sound pressure and velocities at the nodal position of the mesh.

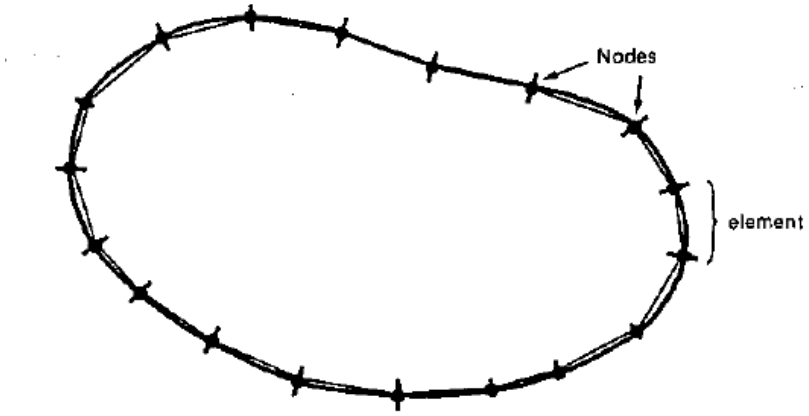

Figure 39 - Surface discretized with linear BE [34].

Two version of this method have been proposed:

- *Direct collocational BEM*

  Direct BEM can deal only problems with exterior/interior problems with closed boundaries. This approach relates the pressure at any point of the acoustic field to the pressure and normal velocity distribution on the boundary surface through the direct integral formulation. The problem of determining the boundary variable distribution is switched to a set of prescribed nodal shape function for pressure values and normal velocities. The direct integral formulation does not include spatial derivatives of boundary pressure or normal velocities thus the convergence is ensures also in presence of discontinuities among elements.

– *Indirect variational BEM*

  Indirect BEM is suitable for combined interior/exterior problems or acoustic problems with open boundary surface. In the same way of Direct BEM the boundary variables are approximated by a set of nodal shape functions. The pressure in any point of the acoustic domain is related to single and double layer potential on the boundary surface through the indirect boundary integral formulation. The single layer potential is defined as the difference in normal pressure gradient between both sides of the boundary surface. The double layer potential instead is the pressure difference between both sides of the boundary surface.

Compared to FEM, BEM offers several advantages: no accuracy loss for velocity prediction in comparison to pressure prediction, problem size substantially smaller since only the boundary of the problem is discretised and BEM can easily handle unbounded domains. As drawbacks it deals with complex, frequency dependent, fully populated matrices, it brings to a non symmetric problem, may lead to singularity when approaching the closed boundary, non uniqueness of the solution for exterior problems with closed boundary surfaces when the excitation frequency coincides with an eigenfrequency of an associated interior problem. Different techniques have been proposed to overcome this last problem [33].

Coupled vibroacoustic problem in the low frequency range

When dealing with coupled vibro -acoustic problems an acoustic and a structural problem must be solved. The mutual interaction between the fluid pressure and the structural deformation in order to define the acoustic performances of the considered structure should be analyzed.

One of the most efficient techniques, in the low frequency range, to model the coupled vibro acoustic problem is to apply the FEM to predict the structural response and the BEM to predict the acoustic one (Figure 40). Considering for instance a cavity in which the top face is not a rigid wall but a flexible plate the acoustic field in the cavity is influenced by the motion of the plate and the vibration of the plate is perturbed by the fluid pressure loading. Thus an acoustic BEM is used for modeling either the sound scattering/radiation in the exterior fluid domain or in the interior one while the structural FEM is used for modeling the displacements of the structure.

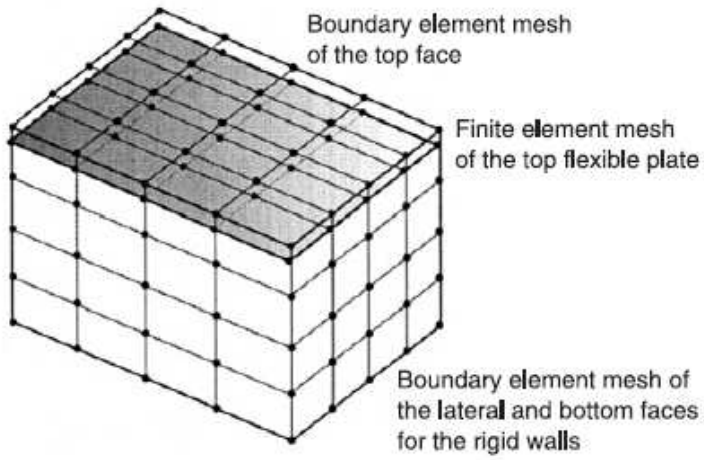

Figure 40 - Coupled FE BE model [3].

It is possible also to couple two FE models if the aim is to analyze a coupled vibroacoustic bounded problem (Figure 41).

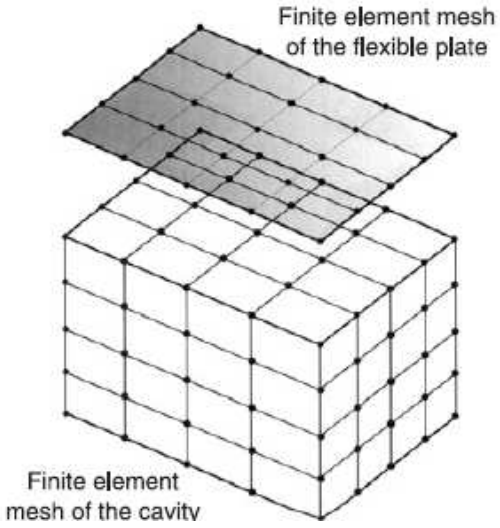

Figure 41 - Coupled FE FE model [3].

In this case, a FEM foresees a three dimensional mesh of the cavity and a two dimensional mesh of the plate. The acoustic mesh should be constructed in such a way that the upper face of the elements facing the plate matches its elements. As a consequence the transverse displacements of the plate elements produce volumetric acoustic excitation acting on the corresponding cavity element in the same way the vibration of the plate influences the cavity acoustic field.

The FE/FE model offers several advantages like: acoustic sparsely populated matrices, likely with a banded structure, symmetrical matrices if dealing with uncoupled problems, real and frequency independent stiffness and mass matrices thus natural frequencies can be obtained solving a standard eigenvalue problem, easily adaptable to inhomogeneous acoustic domain.

Comparing the coupled FE/BE to a coupled FE/FE the main issue is related to the computational aspect of the problem. The smaller size of the acoustic domain in a FE/BE model is not an advantage when dealing with interior problem due to the fully populated, complex and frequency dependent matrices. The computational efficiency may be improved using a frequency interpolation technique that avoids the construction of the matrices at each frequency step [33]. This may anyhow lead to an additional prediction error. In addition, considering coupled problems, the size of the structural FE model is usually comparable to the size of the acoustic one. Major advantages of a coupled FE/BE model are evident for coupled vibro – acoustic problems with an unbounded acoustic domain. The coupling between the two methods is expressed through the equality of the transverse structure velocity and the normal component of the fluid particle velocity over the surface of concurrent FE and BE elements.

5.2.3. Mid - frequency methods

In the world of numerical modeling there is a mid-frequency gap for which both deterministic and energy methods fail. Research on suitable mid - frequency prediction techniques divide them in three categories [35, 36]:

- Deterministic techniques with better computational performances if compared to FEM, so that the upper limiting frequency can be shifted towards higher frequencies. Different approaches have been developed, for example: (i) Replacement of the polynomial shape function with direct wavelike solution of the equation of motion (partition of unit FEM, discontinuous enrichment method and variational theory of complex rays, Trefftz methods like the wave based method) (ii) Equation of motion approximation by smoothing the short wavelength response in certain frequency bands (Complex envelope vectorization)
- Energy methods with relaxed assumption with respect to SEA, so that the lower limiting frequency can be shifted towards lower frequencies. Examples are the statistical modal distribution analysis and the energy distribution methods

- Hybrid approach in which deterministic and energy methods are combined. Applying this techniques each part of the problem is modeled using the suitable approach, FE or SEA, based on the own kind of behavior in the frequency range of interest. Examples are the spectral FEM in which special elements are developed and the Wave/FE approach.

5.2.4. Statistical methods

According to the Statistical Energy Analysis (SEA) the system is divided in a set of subsystems and the frequency range in a set of frequency bands. For each subsystem an energy balance should be written stating that the energy input should equal the transferred and dissipated energy. Dissipations are characterized by loss factors and transfer of energy by coupling factors among subsystems. SEA models are usually smaller than the models obtained using other techniques. Their use is legitimated by high modal density thus they are significant only in the high frequency range. Since the majority of the TL calculations have been based on a simplified equivalent layer model, according to Sokolinsky et al. [37], the use of this kind of model does not take in account thickness stretch vibration modes. SEA doesn't allow the prediction predict the symmetric coincident frequencies that are instead of great importance when dealing with sandwich structures.

2.3. Equivalent modeling

The main drawback of abovementioned numerical acoustics techniques is the limited frequency range that can be explored due to increasing computational cost and model uncertainties. So full models of moderately complex structures can be reliable up to few hundred Hz when it's possible that the frequency range of interests spans some kHz. The ultimate goal of the acoustic analysis is the prediction of the transmission loss of the panel in a wide frequency range. The description of the sound propagation in a multilayered medium involving elastic, porous and fluid layers can become very challenging. One of the most exploited methods to analyze a wide frequency range as the acoustical one is the Transfer Matrix Method.

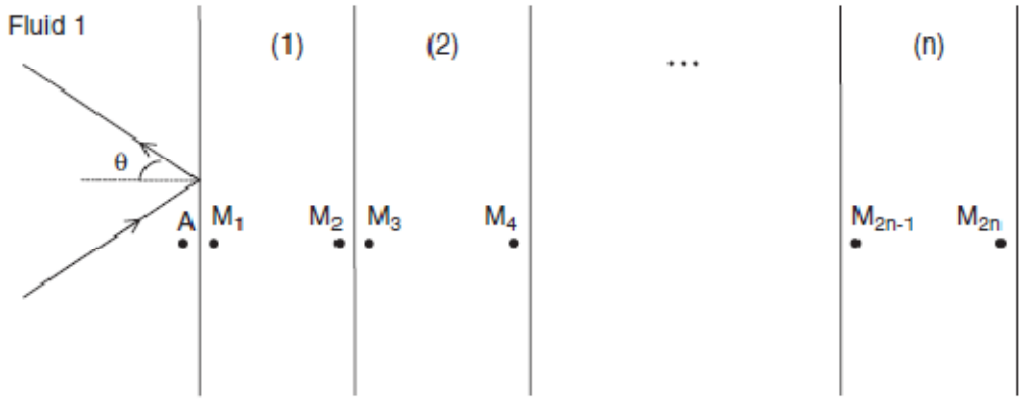

Figure 42 - Plane wave impinging on a multilayered domain [11].

A complete description of the method can be found in [11]. The TMM considers a bidimensional problem and defines the relations among pressure and stresses on both faces of he considered layer according to the layer nature (Figure 42). So, it defines a different transfer matrix considering a fluid, poroelastic or solid layer, taking in account the kind of wave that can propagate in the considered medium. Modified TMM has been proposed for investigating the frequency range above the decoupling frequency, i.e. the frequency domain in which the coupling between the solid and fluid phase is so weak that the frame can be considered motionless or to take in account the finite extent of small panels [11].

A different strategy that can be pursued, dealing with sandwich structures, is the study of the surface impedances. Examples can be found in [38]. The basic concept of this approach is that the dynamic behavior of a symmetric sandwich structure having identical face sheets and homogeneous core material can be easily described in terms of symmetric and antisymmetric impedances. The most important behavior of these impedances is related to the zeroes of impedance that corresponds to resonances of the composite panel, mainly related to the normal displacement of the skins. Moore and Lyon extended the approach of Ford et al [9] to symmetric panel configuration developing a formulation of the TL in terms of panel impedances thus allowing the prediction of the location of coincidence frequencies simply looking at when the impedances go to zero. A simplified expression of the TL as function of impedance neglecting the dilatational term in the expression of the core axial displacement, is proposed by Dym and Lang [10]. J.A. Moore and R.H. Lyon showed, starting from the analysis of the panel impedances, how at low frequencies symmetric motions are controlled by the stiffness so they do not propagate freely, even with zero impedance, while they do at higher frequencies in

correspondence of the double wall resonance, i.e. the mass of the skins in resonance against the stiffness of the core [38].

CHAPTER 3

Chapter 3 gives a brief overview on the adopted numerical methods together with an essential description of their mathematical basis. Particular attention has been paid to the viscoelastic behavior modeling. The potential and drawbacks of the most common models are presented. Keeping in mind the aim of the numerical modeling, the modeling choice are illustrated. Chapter 3 ends with the description of the equivalent model adopted to obtain results in a wider range of frequency.

1. Vibroacoustical numerical modeling

Numerical modeling plays an important role in engineering world. The availability of a reliable model allowsthe designer to perform two fundamental steps in the designing procedure: the design parameter tuning and the verification and validation of the proposed engineering solution. Sandwich structures offer an almost infinite variety of skin/core combinations and finding the best trade off among different technical requirements can be very challenging. An accurate numerical prediction of the structure performances may help to identify the optimal structure configuration.

Focusing on vibroacoustics, a correct modeling strategy of the structural response requiresconsidering all the relevant physical aspects involved in the phenomenon of sound - structure interaction. The flow chart of the proposed numerical modeling strategy is reported in Figure 43 .

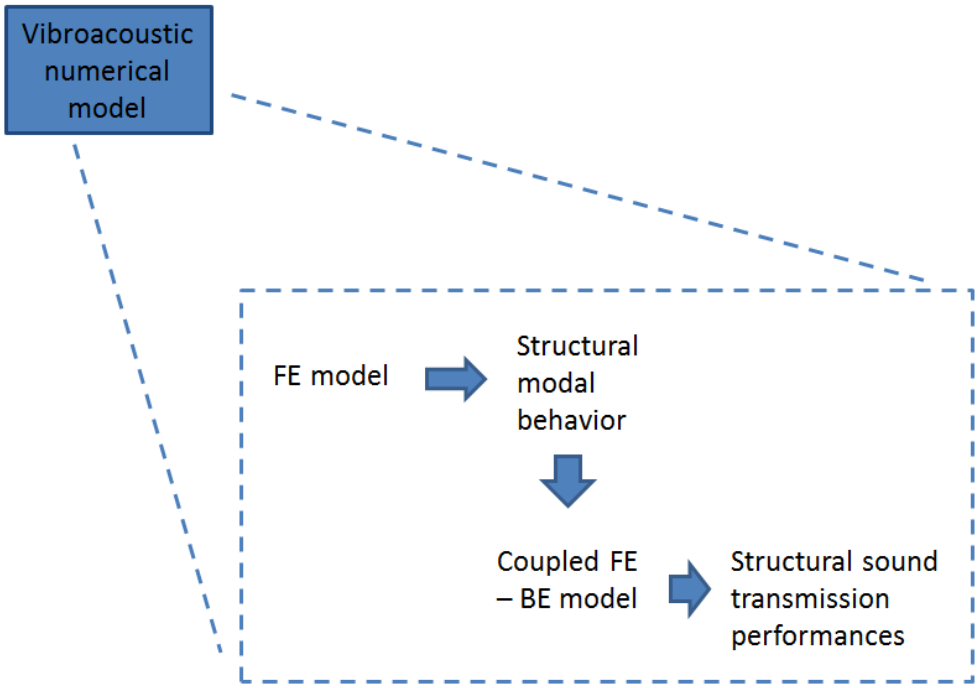

Figure 43 - Conceptual connection among modeling techniques.

The proposed numerical model has to take in account both dynamic and acoustic structural behavior. In fact, the interaction between sound and vibration is highlighted by the connection between the structural dynamic behavior and the sound transmission performances. The acoustic transmission through a structure is influenced by its forced and free response with different importance whether the excitation nature is mechanical or acoustical. If a structure is mechanically excited tends to radiate sound due to all the resonant modes comprised in the excitation frequency range [6]. Finite structures always exhibit natural frequencies and associated mode shapes. The natural frequencies are influenced by the structural material parameters, the boundary conditions and the geometry. These latter parameters also affect the associated mode shapes that are independent from the material properties. Generally speaking, the lower is the excited mode the less is the radiated sound. The efficiency with which a structure can radiate sound at a given vibration level is given by the radiation ratio σ. The radiation ratio of a structure is defined as the ratio of the acoustic power radiated by the vibrating structure Π_{struct} to the acoustic power that would be radiated by a circular piston having the same

surface area A and vibrating at the same r.m.s velocity $\langle v^2 \rangle$ surrounded by a medium characterized by density ρ and sound speed c:

$$\sigma = \frac{\Pi_{struct}}{\rho c \langle v^2 \rangle} \tag{3.1}$$

The radiation ratio provides a useful relation between structural response and radiated power. The surface vibration level, obtained theoretically or experimentally, is sufficient to determine the resulting structure sound radiation. Higher frequencies are typically characterized by higher radiation ratios. The radiation ratios of structural modes in fact generally increase with frequency. A limit situation can arise in which higher non resonant modes may radiate more sound than the lower resonant ones. However, the vibrational level of non resonant modes is reduced with respect to the resonant one [6]. As a result, the acoustic response of a mechanically driven structure is determined by the overlap of the excitation frequency range with the structural natural frequencies. The capability to predict the importance and relevance of this overlap is fundamental for the vibroacoustic performance evaluation of a structure.

A different situation arises when a structure is acoustically excited. The vibrational response of the structure and its consequent capability of radiating sound comprises two contributions: a resonant and a forced one. The former contribution is totally equivalent to that experienced for mechanically driven structures. The latter is instead related to the forced bending wave that is induced in the structure by the impinging sound wave. The forced response tends to transmit most of the sound but the evaluation of the structural vibroacoustic behavior cannot completely disregard the resonant modes contribution.

Aiming to identify the optimal solution for sound and vibrations insulation purposes, a double modeling problem should be faced. As a result, different modeling steps have to be considered. The first step should be devoted to the investigation of the dynamic structural behavior in terms of natural frequencies and mode shapes. The subsequent one should instead be addressed to the determination of the resulting pressure field in the surrounding fluid, taking into account the previously determined structural modal behavior.

The first part of the chapter is dedicated to the description of the adopted numerical technique to solve the structural problem. The central part describes the strategy to model the coupled vibroacoustic problem. A last part is devoted to the description of

an equivalent modeling strategy used to evaluate the acoustic performance on a wide range of frequency.

2. Structural model

The identification of the dynamic response is a key point for the analysis of the vibrational and vibroacoustic behavior. The sound radiation is indeed influenced by the response to mechanical excitation. The structural displacement induces the vibration of the surrounding fluid generating sound waves. Considering a mechanically driven structure, the amplitude fofthe resulting displacement strongly depends on the overlap of the excitation frequency range with that of the resonant structural modes. As a result, a model able to reproduce the transfer function between the incoming excitation and the resulting displacement becomes fundamental to evaluate the structure performance.

Finite element method (FEM) is a well established method in engineering. It is a numerical procedure widely applied in analyzing continua which modeling can be too cumbersome. The FEM discretizes the problem domain in a large but finite number of small elements (Figure 44)

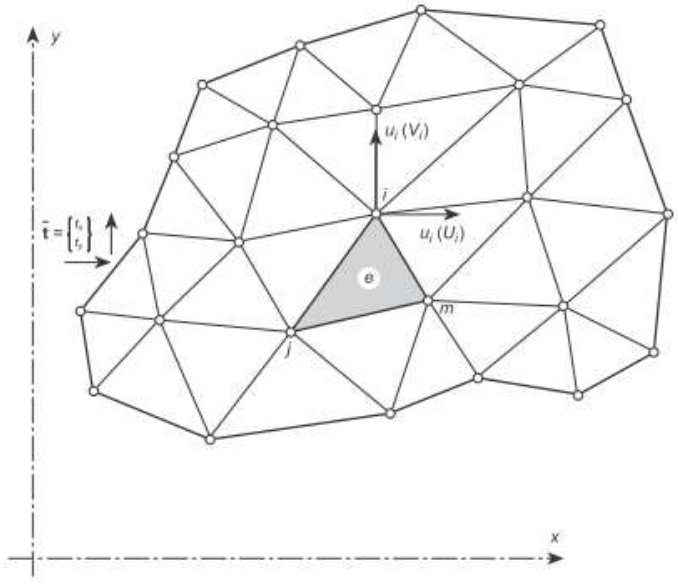

Figure 44 - Continuum divided into a set of elements [29].

The whole amount of unknowns, potentially infinite, is reduced to a finite number, the degrees of freedom (DOFs) of the element nodes. The displacement of any point inside the element can be expressed in terms of simple polynomial functions dependent on the nodes DOFs. The choice of the element type and dimensions depends on the physical problem under investigation and seriously influences the reliability and quality of the results.

2.1. Dynamic behavior modeling

The dynamic response of a generic structure is the result of the superposition of two components: the structure free vibration and the response to the excitationforce. A finite system vibrates freely in one or more specific pattern. Each of these patterns is called *mode shape* and it is associated to a specific constant frequency called *natural frequency*. Natural frequencies are related to the system properties such as inertia and stiffness while mode shapes are dependent on the geometry and the boundary conditions. The excitation of external forces induces forced vibrations in a structure. Forced vibrations occur at the excitation frequency, independently from the system natural frequencies.

The phenomenon of resonance arises from the coincidence between the excitation frequency and a natural frequency. When a structure is excited in resonance the resulting vibration is amplified and, as a consequence, the fluid structure interaction is powered. Aiming either to sound radiation enhancement or to sound transmission reduction as well as to vibration attenuation, the knowledge of the relative position of the excitation frequency band and natural frequencies is fundamental.

The equation that governs the dynamic response of a structure can be expressed in terms of the displacement $\{u\}$ [39]:

$$\mathbf{M}\{\ddot{u}\}+\mathbf{C}\{\dot{u}\}+\mathbf{K}\{u\}=\{R^{ext}\} \tag{3.2}$$

The resultant of external forces $\{R^{ext}\}$ in (3.2) includes applied loads, body forces and prescribed surface tractions.

Considering a FEM approach, the considered continuum is discretized in a set of elements defined by a certain number of nodes (Figure 44). The original problem variables are brought back to nodal degrees of freedom. Thus, the displacement at any point within each element $\{u\}$ is related to the element nodal variables vector

$\{a\}$ i.e. the element nodes DOFs, through the shape functions $\mathbf{N}$ (3.3) The shape functions are function of space only and nodal variables are function of time only.

$$\{u\} = \mathbf{N}\{a\} \tag{3.3}$$

Considering for instance the triangular element of Figure 45 the displacement $\{u\} = \{u, v\}$ of any point within the element can be expressed as function of the displacements of the nodes 1,2,3:

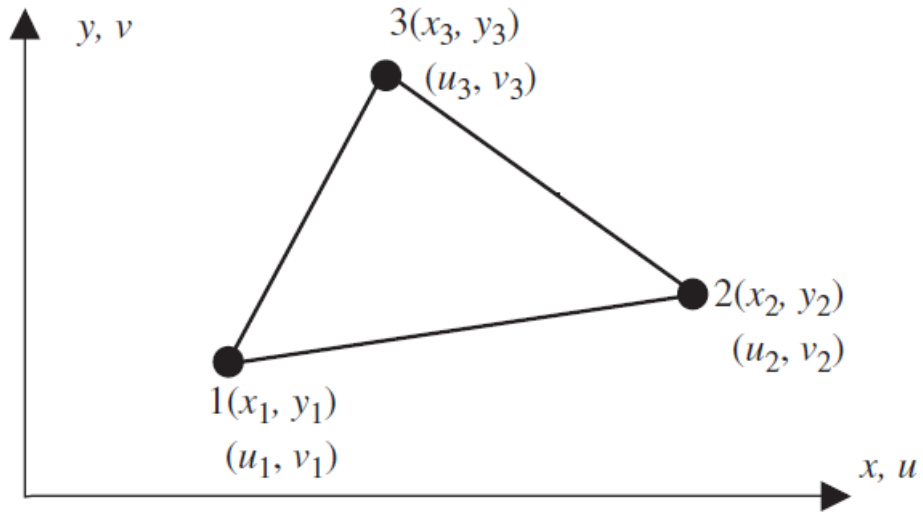

Figure 45 - Triangular element [40].

The matrices of mass $\mathbf{M}$, damping $\mathbf{C}$ and stiffness $\mathbf{K}$ in equation (3.2) are square matrix defined by assembling the mass, damping and stiffness matrices related to each single element. A detailed description of the standard assembling procedure can be found in [29]. The matrices are of the form:

$$\mathbf{M} = \begin{bmatrix} \mathbf{M}_{ii} & \mathbf{M}_{ij} & \cdots & \mathbf{M}_{in} \\ \vdots & \vdots & & \vdots \\ \mathbf{M}_{ni} & \cdots & \cdots & \mathbf{M}_{nn} \end{bmatrix} \quad \mathbf{C} = \begin{bmatrix} \mathbf{C}_{ii} & \mathbf{C}_{ij} & \cdots & \mathbf{C}_{in} \\ \vdots & \vdots & & \vdots \\ \mathbf{C}_{ni} & \cdots & \cdots & \mathbf{C}_{nn} \end{bmatrix} \quad \mathbf{K} = \begin{bmatrix} \mathbf{K}_{ii} & \mathbf{K}_{ij} & \cdots & \mathbf{K}_{in} \\ \vdots & \vdots & & \vdots \\ \mathbf{K}_{ni} & \cdots & \cdots & \mathbf{K}_{nn} \end{bmatrix} \tag{3.4}$$

Each submatrix is obtained assembling the corresponding submatrices of each element:

$$\mathbf{M}_{ij} = \sum_{e=1}^{m} \mathbf{M}_{ij,e} \quad \mathbf{C}_{ij} = \sum_{e=1}^{m} \mathbf{C}_{ij,e} \quad \mathbf{K}_{ij} = \sum_{e=1}^{m} \mathbf{K}_{ij,e} \tag{3.5}$$

Considering the mass and damping matrices, each element submatrix is function of material density ρ and of the material viscosity parameter η respectively:

$$\mathbf{M}_{ij,e} = \int_V \mathbf{N}_i \rho \mathbf{N}_j dV \quad \mathbf{C}_{ij,e} = \int_V \mathbf{N}_i \eta \mathbf{N}_j dV \tag{3.6}$$

The stiffness matrix $\mathbf{K}_{ij,e}$ is instead function of the material elastic properties and it is derived through the definition of the static elastic problem for the single element.

$$\mathbf{K}_{ij,e} = \int_V \mathbf{B}_i^T \mathbf{D} \mathbf{B}_j dV = \int_V \left(\mathbf{S}\mathbf{N}_i\right)^T \mathbf{D} \left(\mathbf{S}\mathbf{N}_j\right) dV \tag{3.7}$$

Matrix $\mathbf{D}$ is the elasticity matrix and it defines the stress-strain relationship. Matrix $\mathbf{S}$ expresses the relation among strains and displacement according to the solid mechanics theory. Both matrices are dependent on the hypothized stress state, for instance plane strain or plane stress. A more detailed definition of the stiffness matrices related to the investigated problem, i.e. structural dynamic analysis of a sandwich panel, is given in the following paragraphs.

Each term of the (3.2) has been defined and related to the respective structural parameters by equations (3.6) and (3.7). Following modal approach, the structural modal parameters, natural frequencies and mode shapes, are obtained solving a standard eigenvalue problem derived from the (3.2):

$$\left(\alpha^2 \mathbf{M} + \alpha \mathbf{C} + \mathbf{K}\right)\{\phi\} = 0 \tag{3.8}$$

where α is the eigenvalue, and $\{\phi\}$ are the eigenvectors. Eigenvalues are in general complex numbers while eigenvectors are real for real structures. From a physical point of view, the imaginary part of the eigenvalues can be interpreted as the system natural frequencies while the eigenvectors are related to mode shapes.

The evaluation of the structural dynamic performances in terms of structural response to the incoming excitation can be performed on the basis of the structure modal parameters. This strategy results to be particularly time efficient but does not allow the consideration of non linear effects. Conversely, the direct solution of the finite element approximation to equilibrium allows the consideration of non linear effects such as material frequency and temperature dependent parameters. In

particular, itconsiders in an accurate way the material viscoelasticity. The latter can be obtained through [41].

$$\mathbf{M}\{\ddot{u}\}+\{I\}-\{P\}=0 \tag{3.9}$$

At each time step, the equation (3.9) is solved in terms of acceleration of the nodal variables vector. The first term of the equation takes in account the d'Alembert forces. $\{I\}$and$\{P\}$ are the internal and external force vector respectively. In particular, the internal force vector is related to the stress state of the analyzed structure. A detailed mathematical description of the solution procedure can be found in [41].

The choice of the modeling strategy, i.e. the choice of the number and type of element, depends on the analyzed problem. Generally speaking, a static, stress strain analysis requires a finer mesh than a dynamic problem. The element dimension for a dynamic problem is strongly dependent on the maximum frequency of interest. As a rule of thumb, at least 10 elements are required for each wavelength. The element in-plane dimension l (Figure 46) can be evaluated as function of the maximum frequency of interest and the structure characteristics.

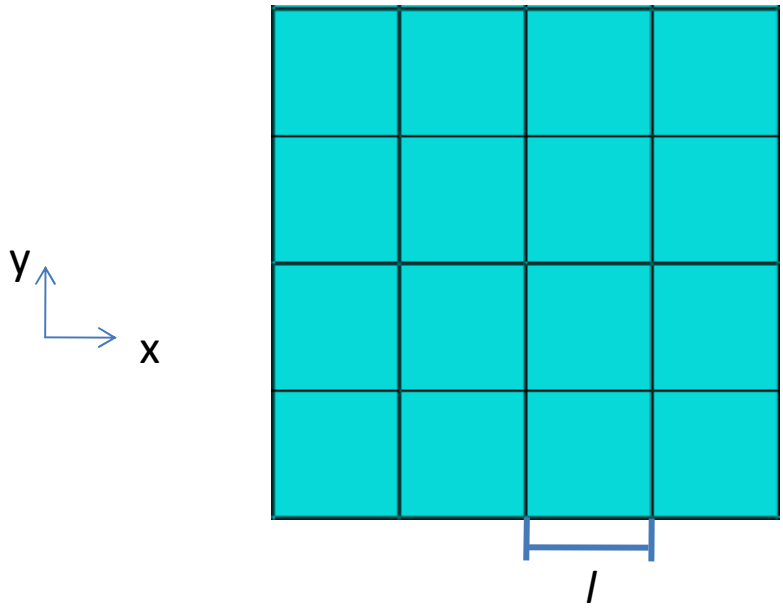

Figure 46 - FE discretization: element in plane dimension.

In case of plate dynamic analysis, the maximum in-plane element dimension is given in terms of material density ρ, plate thickness h and plate bending stiffness D (2.4)

$$l = \frac{\lambda}{12} = \frac{1}{12}\frac{2\pi}{\sqrt{\omega}\sqrt[4]{\frac{\rho h}{D}}} \tag{3.10}$$

The element dimension on the cross section is instead based on a trade off between the model accuracy and the computational cost. Generally speaking, a more refined mesh is required in case of discontinuities or concentrated loads.

The element type is determined by the structure geometry and its stress - strain problem type. A structure subjected to acoustic waves impinging on the surface undergoes mainly bending and plane strain state. In addition, the thickness difference among different layers of a sandwich structure implies a different modeling strategy to optimize the numerical efficiency and results accuracy., The core can be modeled as a 3D continuum but a full 3D approach for the face sheets may lead to ill conditioned equation due to the small thickness of the skins compared to other dimensions.

2.1.1. Finite Element Modeling of skins

The strain stress state and the small thickness compared to the in plane dimensions lead to the choice of shell elements for the skin modeling. Shell elements combine pure bending and membrane stresses (Figure 47) modeling accurately the structure behavior without increasing the computational cost, if compared to the number of solid elements necessary to obtain the same result accuracy.

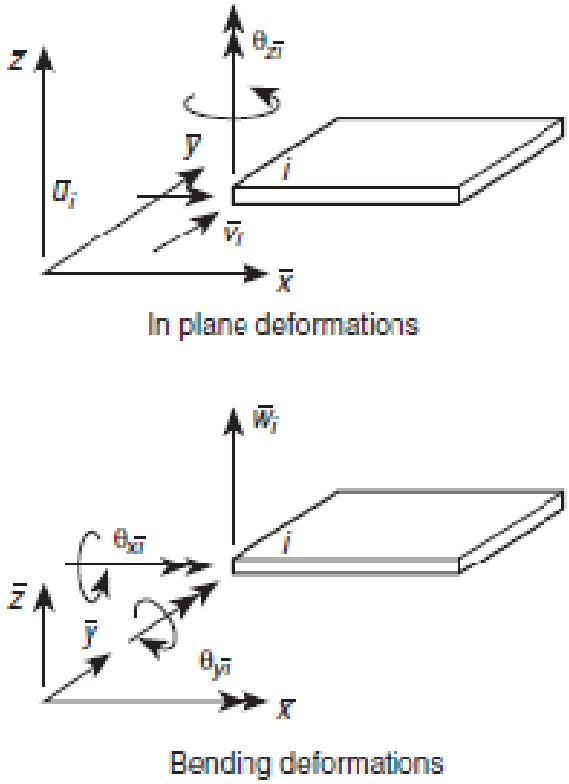

Figure 47 - Bending and in plane (membrane) deformations [29].

Plate bending condition modeling

The bending of plates and its extension to shells has been widely studied and it was one of the first cases to which the FEM was applied in the early sixties. Many structures, for instance airplane wings, can be idealized as plates. In various practical cases, the main load is applied in transverse direction and results in a bending action. Figure 48 displays the plate bending condition and defines the displacement directions.

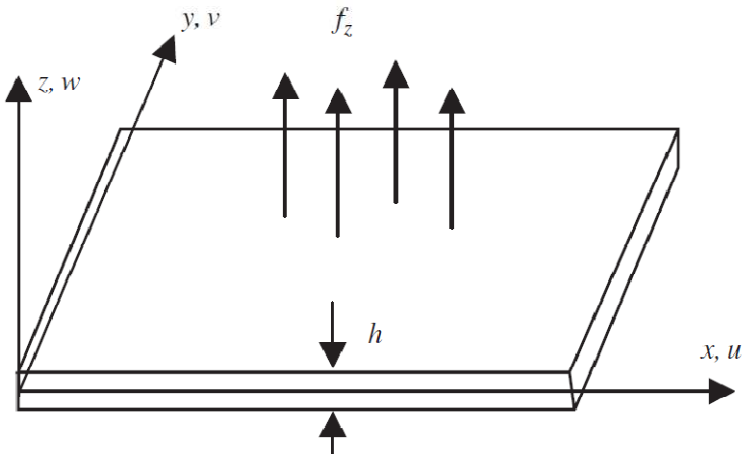

Figure 48- Plate subjected to transverse action resulting in bending deformation [40].

Two different approaches are available for plate bending stress strain state modeling:

- Mindlinn approach or thick plate theory
- Kirchhoff approach or thin plate theory

The main difference relies on shear stresses consideration. Analyzing thin plates is in fact possible to neglect the shear stresses. The Kirchhoff theory of thin plates can be considered as a particular case of Mindlinn theory for thick plates simply considering the shear modulus equal to infinite [29].

The definition of variables to mathematically state the plate bending problem is represented in Figure 49.

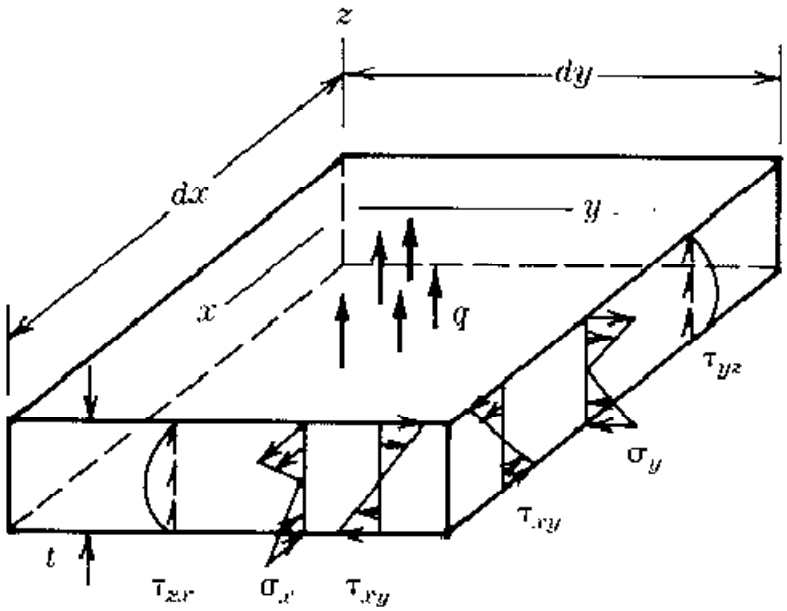

Figure 49 - Variables definition [39].

The concept of finite element modeling is to express the strain – stress state within each element in terms of nodal variables, i.e. element nodes rotation and translation, by means of suitable shape functions. From a mathematical point of view it is first necessary to state the stress – strain problem for plate bending and subsequently to discretize it.

A plate, like a straight beam, supports transverse load by bending actions. The Figure 49 displays the stresses on the cross section of an elastic homogeneous plate. Normal stresses σ_x and σ_y vary linearly with *z* and result from the bending moments M_x and M_y. Shear stress τ_{xy} is also linearly variable with z and it is related with the twisting moment M_{xy}. The normal stress σ_z is considered negligible with respect to the others. Transverse shear stresses τ_{yz} and τ_{zx} vary quadratically with the z direction. External load q may include both mass and surface forces. "Plate bending" usually means that there are no component of external loads parallel to the xy plane and that on the midsurface normal stresses σ_x and σ_y and shear stress τ_{xy} equal zero.

On the basis of solid mechanics theory to define a so called stiffness relationship relating the external loads to the nodal displacements. It is possible to show that strains ε and γ are related to displacement through differential operators [39], in particular:

$$\begin{Bmatrix} \varepsilon_x \\ \varepsilon_y \\ \gamma_{xy} \\ \gamma_{yz} \\ \gamma_{zx} \end{Bmatrix} = \begin{bmatrix} \frac{\partial}{\partial x} & 0 & 0 \\ 0 & \frac{\partial}{\partial y} & 0 \\ \frac{\partial}{\partial y} & \frac{\partial}{\partial x} & 0 \\ 0 & \frac{\partial}{\partial z} & \frac{\partial}{\partial y} \\ \frac{\partial}{\partial z} & 0 & \frac{\partial}{\partial x} \end{bmatrix} \begin{Bmatrix} u \\ v \\ w \end{Bmatrix} \tag{3.11}$$

$\{u, v, w\}$ are the displacement directed as in Figure 48. A qualitative graphical representation of (3.11) is displayed in Figure 50 and Figure 51. Figure 51 displays the relations for γ_{xy}, the representation of the relations for shear strains γ_{yz} and γ_{zx} can be obtained in analogous way.

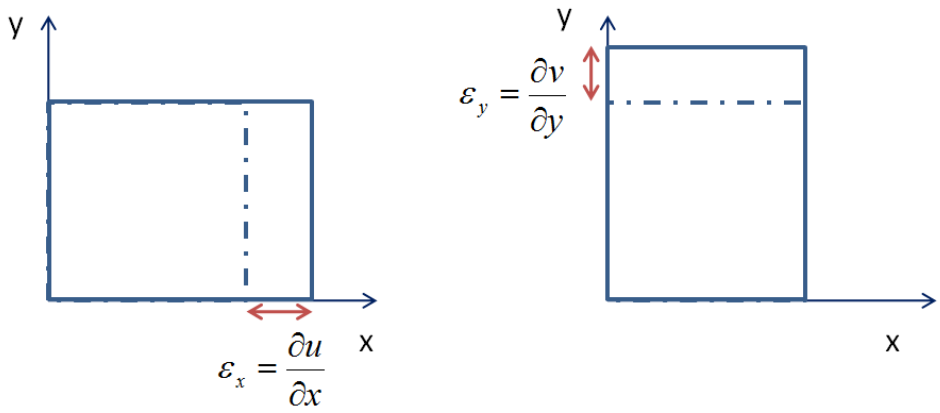

Figure 50 Relation among strains in x and y directions and displacements.

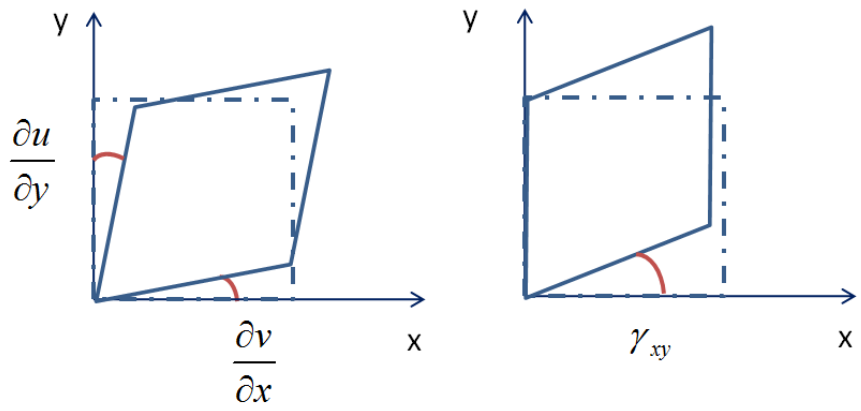

Figure 51 Relation among shear strain and displacements.

The displacement in the x and y direction, u and v respectively, can be expressed in terms of rotation of lines normal to the plate midsurface (Figure 52):

$$u = -z\theta_x$$
$$v = -z\theta_y \tag{3.12}$$

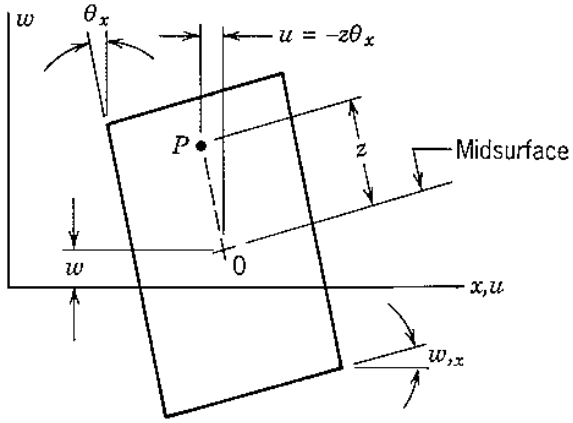

Figure 52 - Thick plate element after loading [39].

Combining (3.11) and (3.12), the expression for the deformation vector of thick plates is obtained as function of the rotation vector $\{\theta\}$ and of the out of plane displacement w:

$$\{\varepsilon\}=\begin{Bmatrix}\varepsilon_x\\ \varepsilon_y\\ \gamma_{xy}\end{Bmatrix}=-z\begin{bmatrix}\frac{\partial}{\partial x} & 0\\ 0 & \frac{\partial}{\partial y}\\ \frac{\partial}{\partial x} & \frac{\partial}{\partial y}\end{bmatrix}\{\theta\}=-z\mathbf{L}\{\theta\}$$
$$\{\gamma\}=\begin{Bmatrix}\gamma_{xz}\\ \gamma_{yz}\end{Bmatrix}=-\begin{Bmatrix}\theta_x\\ \theta_y\end{Bmatrix}+\begin{Bmatrix}\frac{\partial w}{\partial x}\\ \frac{\partial w}{\partial y}\end{Bmatrix}=-\{\theta\}+\nabla w \qquad (3.13)$$

The face sheets of structural sandwiches are typically very thin. As a result, it is possible to neglect transverse shear forces and resulting stresses and strains $\{\gamma\}$ [29]. The second equation of (3.13) becomes:

$$0=-\{\theta\}+\nabla w \qquad (3.14)$$

The moments acting on the structure can be related to the rotation vector introducing appropriate constitutive relations among stresses and strain through the elasticity matrix $\mathbf{D}^b$:

$$\{M\}=\begin{Bmatrix}M_x\\ M_y\\ M_{xy}\end{Bmatrix}=\mathbf{D}^b\mathbf{L}\{\theta\} \qquad (3.15)$$

In equation (3.15) the matrix $\mathbf{D}^b$ is function of plate thickness h and material parameters, Young modulus E and Poisson ratio ν:

$$\mathbf{D}^b=\frac{Eh^3}{12\left(1-\nu^2\right)}\begin{bmatrix}1 & \nu & 0\\ \nu & 1 & 0\\ 0 & 0 & \frac{1-\nu}{2}\end{bmatrix} \qquad (3.16)$$

The thin plate formulation for plate bending analysis can be stated in terms of displacement adding the equilibrium relations[29]:

$$\left(\mathbf{L}\nabla^T\right)\mathbf{D}^b\mathbf{L}\nabla w - q = \mathbf{0} \tag{3.17}$$

The thin plate approximation (3.17) expressed in terms of displacement is irreducible and a typical example of displacement formulation. Irreducible formulation does not allow the reduction of the number of dependent unknows by suitable algebraic operation, still leaving a solvable problem [29].

The displacement approach can be seen as a minimization of the total potential energy. It can be shown that in stable elastic situations the total potential energy is not only stationary but it is a minimum. The finite element process then seeks this minimum within the constraint of an assumed displacement pattern [29].

In the case of plate bending of thin plates the total potential energy is given by:

$$\Pi = \frac{1}{2}\int_\Sigma \left(\mathbf{L}\nabla\right)^T \mathbf{D}^b \left(\mathbf{L}\nabla\right) w d\Sigma - \int_\Sigma w^T q d\Sigma + \text{boundary terms} \tag{3.18}$$

The first term of (3.18) represents the bending energy and Σ is the considered domain.

Once the problem has been stated, it should be discretized to enable the definition of stress strain within each element in terms of nodal variables. Using either the Galerkin method and integration per parts or the virtual work principles the discretized equation can be obtained. The standard linear displacement approximation equation is expressed as follows:

$$\mathbf{K}^b\left\{a^b\right\} = \left\{f_{ext}^b\right\} \tag{3.19}$$

The vector $\left\{a^b\right\}$ includes the rotations and lateral displacement of the nodes and is related to the discretized displacement field through appropriate shape functions $\mathbf{N}$:

$$\left\{\overline{w}\right\} = \mathbf{N}\left\{a^b\right\} \tag{3.20}$$

The stiffness matrix components are obtained introducing the discretized displacement field in equation (3.18):

$$\mathbf{K}^b = \int_\Sigma \left(\left(\mathbf{L}\nabla\right)\mathbf{N}\right)^T \mathbf{D}^b \left(\mathbf{L}\nabla\right)\mathbf{N} d\Sigma \tag{3.21}$$

The vector $\left\{ f_{ext}^{b} \right\}$ in equation (3.19)is related to the external forces and the boundary terms.

$$\left\{ f_{ext}^{b} \right\} = \int_{\Sigma} \mathbf{N}^{T} q d\Sigma + \left\{ f_{b} \right\} \tag{3.22}$$

The boundary conditions that can be imposed are:

i. *traction boundary*: stress resultants, both moments and shear forces, are given prescribed values
ii. *fixed boundary*: displacements conjugate with the stress resultants are specified
iii. *mixed boundary conditions*: both tractions and displacements can be specified. A typical example is the simply supported edge.

In the case (i) $\left\{ f_{b} \right\}$ includes moments and shear actions prescribed on the boundary Γ, irrespectively of thick or thin plate condition:

$$\left\{ f_{b} \right\} = \int_{\Gamma} \left(\mathbf{N}_{n}^{T} \widetilde{M}_{n} + \mathbf{N}_{s}^{T} \widetilde{M}_{ns} + \mathbf{N}^{T} \tilde{S} \right) d\Gamma \tag{3.23}$$

where the terms $\widetilde{M}_{n}$, $\widetilde{M}_{ns}$ and $\tilde{S}$ are respectively the prescribed moments and shear while $\mathbf{N}_{n}$ and $\mathbf{N}_{s}$ are, for thin plates, the partial derivatives of the shape functions with respect to n and s directions in Figure 53.

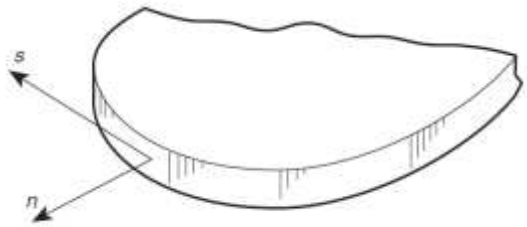

Figure 53 - Boundary tractions [29].

The whole static elastic problem is then reduced to an appropriate selection of the shape functions $\mathbf{N}$. The shape function is strongly related to the choice of element shape and order used to discretize the considered domain Σ. Two approaches are available to solve the previously stated problem: the method of weighted residuals (or Galerkin procedure), and the determination of the variational functionals for which stationarity is sought. As shown in [29] the two approaches are totally equivalent.

Plane stress condition modeling

The mode shapes associated with the plate natural frequencies induce a complex strain state in the plate. The plate in fact undergoes both in plane and out of plane strains. The out of plane action has been described in the previous section, discussing the plate bending modeling.

Considering only the in plane actions (plane stress condition) the state of strain can be described uniquely in terms of the u and v displacement of each node of the considered element defined in Figure 54.

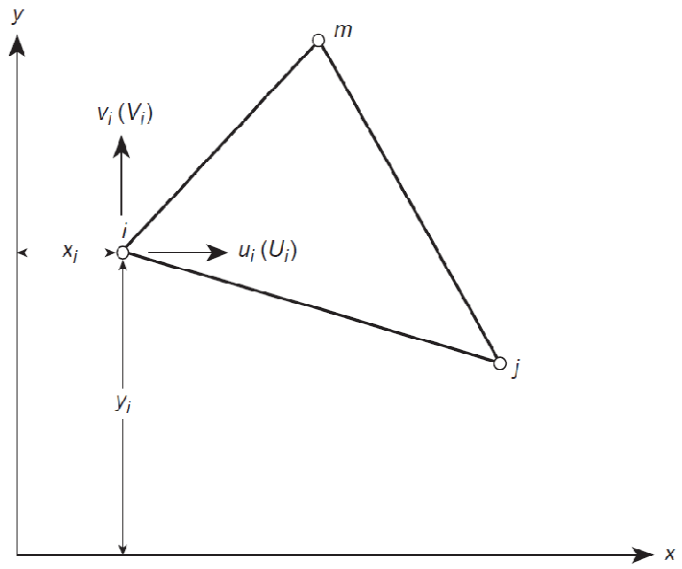

Figure 54 - An element in plane stress [29].

$$\{\varepsilon\} = \begin{Bmatrix} \varepsilon_x \\ \varepsilon_y \\ \gamma_{xy} \end{Bmatrix} = \begin{bmatrix} \frac{\partial}{\partial x} & 0 \\ 0 & \frac{\partial}{\partial y} \\ \frac{\partial}{\partial y} & \frac{\partial}{\partial x} \end{bmatrix} \begin{Bmatrix} u \\ v \end{Bmatrix} = \mathbf{S}\{u\} = \mathbf{S}\left(\mathbf{N}\{a^p\}\right) = \mathbf{B}\{a^p\} \qquad (3.24)$$

The vector $\{a^p\}$ includes the nodal displacements and $\mathbf{N}$ includes instead the shape functions that relate element displacements to the nodal ones.

Considering null the initial strain, the stresses can be expressed as follows:

$$\{\sigma\}=\begin{Bmatrix}\sigma_x\\ \sigma_y\\ \tau_{xy}\end{Bmatrix}=\frac{E}{1-\nu^2}\begin{bmatrix}1 & \nu & 0\\ \nu & 1 & 0\\ 0 & 0 & (1-\nu)/2\end{bmatrix}\{\varepsilon\}=\mathbf{D}^p\{\varepsilon\} \tag{3.25}$$

The minimization of the potential energy leads to the following stiffness matrix:

$$\mathbf{K}^p=\int_\Sigma \mathbf{B}^T\mathbf{D}^p\mathbf{B}d\Sigma \tag{3.26}$$

Leading to an expression similar to the one obtained for the plate bending, (3.19):

$$\mathbf{K}^p\{a^p\}=\{f_{ext}^p\} \tag{3.27}$$

Combining the expressions (3.19) and (3.27) the equation to define the behavior of a shell element can be obtained:

$$\mathbf{K}^e\{a\}=\begin{bmatrix}\mathbf{K}^p & \begin{matrix}0&0&0\\0&0&0\end{matrix}\\ \begin{matrix}0&0\\0&0\\0&0\end{matrix} & \mathbf{K}^b\end{bmatrix}\begin{Bmatrix}\{a^p\}\\ \{a^b\}\end{Bmatrix}=\begin{Bmatrix}\{f^p\}\\ \{f^b\}\end{Bmatrix}=\{f^e\} \tag{3.28}$$

The stiffness matrix of equation (3.28) is the one to be inserted in equation (3.2) to completely define the equation of motion for the structure face sheets.

2.1.2. Finite Element Modeling of the core

Dealing with multilayered structures all the layers undergo the same solicitation. Anyway, each layer may present different characteristics in terms of geometry and material parameters. Focusing on sandwich structures, usually they present three layers: two thin face sheets and a thick core. The different layers fulfill different functions. The thin face sheets give the main part of the structural resistance and bending stiffness to the structure. As a result, they easily can be dealt with the plate theory exposed in paragraph 2.1.1. The core is usually thicker than the skins and performs different non – structural functions, i.e. thermal insulation or vibration softening. From a structural point of view it carries the whole shear load acting on the structure. This last assumption together with the non negligible thickness with respect to in plane dimensions lead to a solid elements modeling. Following the

same approach previously adopted for the shell element it is possible to derive a formulation totally equivalent to the (3.28).

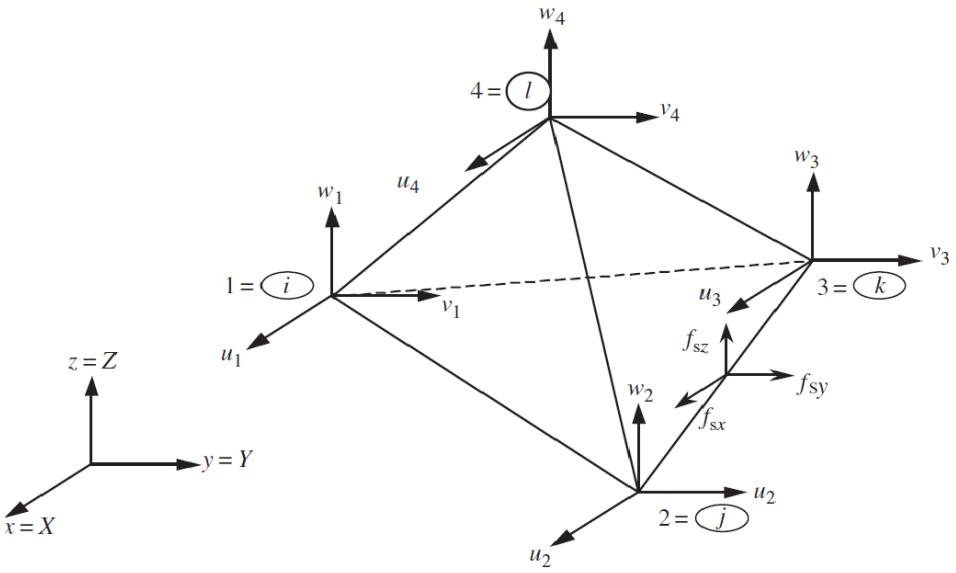

Figure 55 - Displacement definition for a solid thetraedrical element [40].

Considering full 3D strain – stress state condition, the strain vector $\{\varepsilon\}$ has six components and may be expressed as function of the three displacement of the element $\{u\}=\{u,v,w\}$ directed as the nodal one in Figure 55

$$\{\varepsilon\}=\begin{Bmatrix}\varepsilon_x\\ \varepsilon_y\\ \varepsilon_z\\ \gamma_{xy}\\ \gamma_{yz}\\ \gamma_{zx}\end{Bmatrix}=\begin{Bmatrix}\dfrac{\partial u}{\partial x}\\ \dfrac{\partial v}{\partial y}\\ \dfrac{\partial w}{\partial z}\\ \dfrac{\partial u}{\partial y}+\dfrac{\partial v}{\partial x}\\ \dfrac{\partial v}{\partial z}+\dfrac{\partial w}{\partial y}\\ \dfrac{\partial w}{\partial x}+\dfrac{\partial v}{\partial z}\end{Bmatrix}\{u\}=\mathbf{S}\{u\} \tag{3.29}$$

The element displacement field can then be discretized and expresses as function of nodal displacement vector $\{a_s\}$ through suitable shape functions $\mathbf{N}$, as well as in the (3.20) and (3.24):

$$\{u\} = \mathbf{N}\{a_s\} \tag{3.30}$$

The stiffness matrix for a solid element to be introduced in the (3.2) can be obtained using the same integral of the (3.26). Considering an isotropic material, the matrix $\mathbf{D}$,that relates strain and stresses, is expressed as follows:

$$\mathbf{D} = \frac{E}{(1+\nu)(1-2\nu)} \begin{bmatrix} 1-\nu & \nu & \nu & 0 & 0 & 0 \\ \nu & 1-\nu & \nu & 0 & 0 & 0 \\ \nu & \nu & 1-\nu & 0 & 0 & 0 \\ 0 & 0 & 0 & (1-2\nu)/2 & 0 & 0 \\ 0 & 0 & 0 & 0 & (1-2\nu)/2 & 0 \\ 0 & 0 & 0 & 0 & 0 & (1-2\nu)/2 \end{bmatrix} \tag{3.31}$$

The core of a sandwich structure addressed to vibroacoustic insulation is typically a porous material. Their peculiar random microstructure is the responsible of their vibroacoustic damping capability. On the other hand, random microstructure may imply inhomogeneity and from transverse isotropic to fully anisotropic behavior. In addition, the bulk material from which the porous material is derived typically exhibits a viscoelastic behavior. This characteristic increases the vibration softening capability of the material but leads to a more complex material modeling, due to the frequency dependence of the material parameters.

Viscoelastic material modeling

The simplest model able to represent in a sufficiently accurate way either the relaxation or the creep material behavior is the Standard Linear Solid Model (Chapter 2). However, in a real viscoelastic material the creep and relaxation phenomenon do not occur with a single characteristic time constant τ_1. Due to internal phenomena (for instance short polymer segments relax differently from the long one) the real relaxation modulus or creep compliance curves may show changes in the slope because the whole material doesn't react at the same moment to the imposed stress or strain. To take into account this, generalized models have been developed starting from the basic model previously described. In this

dissertation a generalized model based on Zener model has been considered for the capability of SLS to predict the material characteristic behavior.

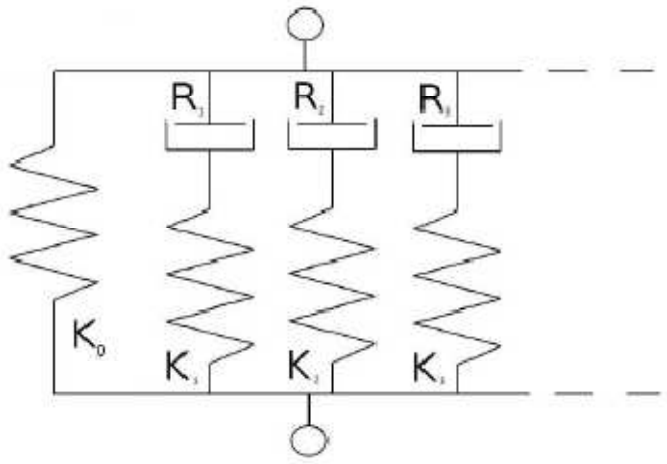

Figure 56 - Generalized Standard Linear Solid (GSLS) model.

The GSLS model (Figure 56) consists of *m* Maxwell elements connected in parallel and a single spring.

The relaxation modulus associated with this model configuration is:

$$E(t) = E_{\infty} + \sum_{i=1}^{m} E_i e^{-\frac{t}{\tau_i}} \tag{3.32}$$

The series expression in (3.32) is often referred as a Prony series. E_{∞} is the equilibrium or long term modulus, E_i and τ_i are respectively the relaxation moduli and the relaxation costants. All the parameters are positive constants. The computational efficiency of Prony series is double sided: (i) It can be proved that all the material function, i.e. relaxation modulus, creep compliance, complex modulus, are numerically inter-convertible using the same Prony series coefficient and (ii) the efficiency of numerical method of structural analysis using incremental stepped procedure, as the one used to extract the response of the structure to known inputs, is aided using Prony series representation of viscoelastic functions [14]. The material definition is based on Prony coefficient evaluation also in the considered FE software, Abaqus.

Generally speaking, viscoelastic material parameters are temperature and frequency dependent. An important parameter to characterize the material frequency behavior

is the complex modulus. Through a dedicated experimental campaign the foam complex modulus over the whole acoustic frequency range has been determined. Further details on the experimental setup and test conditions will be given in Chapter 4.

Each viscoelastic material function contains exactly the same quantity of information concerning the material behavior. As a result, complex modulus, complex compliance, relaxation modulus and creep compliance are all interconvertible. Park and Shapery showed in [14] how it is possible to derive from (3.32) the expression of the complex modulus Prony series through Laplace transform:

$$\begin{cases} E^{'}(\omega) = E_{\infty} + \sum_{i=1}^{m} \dfrac{\omega^2 \tau_i^2 E_i}{\omega^2 \tau_i^2 + 1} \\ E^{''}(\omega) = \sum_{i=1}^{m} \dfrac{\omega \tau_i E_i}{\omega^2 \tau_i^2 + 1} \end{cases} \tag{3.33}$$

The Prony series parameters, included the number *m* of Maxwell elements, can be determined through a data fitting procedure on the experimental data. Once the parameters of the (3.33) are obtained the material is fully defined for the finite element analysis.

3. Coupled problem modeling

It is experience of everyday life the existence of mutual interaction between sound and vibrations. This coupled effect can be modeled exploiting suitable numerical tools. The numerical model should provide information both on the effect of structural displacement on surrounding fluid and on the sound transmission capability of the considered structure.

Sound radiation from vibrating surface is influenced by different phenomenon if the structure is mechanically or acoustically driven. In the former case, the main part of sound is due to resonant modes. In the latter case, forced vibrations are the main responsible for sound radiation. Intuitively, if a forced wave exhibits the same wavelength of a free bending one the structure becomes a perfect radiator. Aiming to design a structure either for sound radiation or insulation purposes, the knowledge of the possible overlap between excitation and natural frequency range is a key point. The information about free structural vibrations are provided by the structural finite element model. Natural frequencies and related mode shapes are in fact obtained solving the eigenvalue problem of equation (3.8). Coupling these information with a

numerical procedure able to define uniquely the acoustic pressure field in the fluid domain that surrounds the structure, the vibroacoustic problem is fully defined.

3.1. Acoustic problem modeling

The steady state acoustic pressure p in a fluid domain Ω due to a time harmonic external source g of frequency $f = \omega/2\pi$ is governed by the second order Helmoltz equation:

$$\nabla^2 p(x,y,z) + k^2 p(x,y,z) = -j\rho_0 \omega g(x,y,z) \tag{3.34}$$

where $k = \omega / c$ is the acoustic wavenumber, c is the speed of sound and ρ_0 is the medium mass density. In case of vibroacoustic coupling the forcing term is related to structural transverse displacement.

A powerful numerical tool to solve the Helmoltz equation in bounded or unbounded fluid domains is the Boundary Element Method (BEM). The BEM is based on the boundary integral formulation of the problem. Different BEM approaches have been developed to deal with the various possible acoustic problems. The radiation and transmission of sound through partitions can be classified as a combined interior/exterior acoustic problem. This definition is strongly dependent on the experimental technique for theidentification the acoustic structural behavior. The adopted method and test rig will be explained in Chapter 4. The interior/exterior class of problems foresees the existence of two fluid domain: a bounded one that should satisfy the (3.34) and an unbounded one (Figure 57).

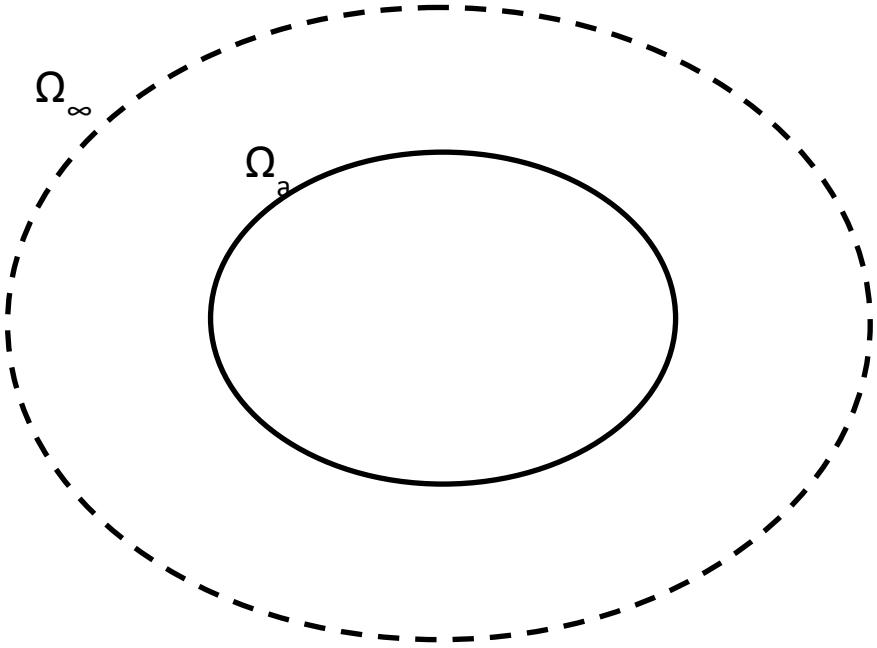

Figure 57 - Schematic representation of fluid domains for a combined interior/exterior problem.

The pressure field in the unbounded fluid domain must as well satisfy the (3.34) along with the Sommerfeld radiation condition at the boundary surface Ω_∞, located at infinity:

$$\lim_{|\vec{r}|\to\infty} |\vec{r}| \left(\frac{\partial p}{\partial |\vec{r}|} + jkp \right) = 0 \tag{3.35}$$

The (3.35) ensures that all acoustic waves propagates freely towards the infinity and that no reflection occurs at this boundary as in a real unbounded fluid domain.

The (3.34) defines an inhomogeneous acoustic problem. The resulting total pressure p may be expressed as the superposition of the homogeneous pressure field p_a and an inhomogeneous pressure field p_b.

$$p = p_a + p_b \tag{3.36}$$

The pressure field p_b represents the free – field pressure due to the source distribution q. An analytical solution for this pressure field can be obtained seeing

the source distribution as a combination of acoustic point sources. The pressure field p_a instead is the solution of the homogeneous Helmoltz equation.

$$\nabla^2 p(x,y,z) + k^2 p(x,y,z) = 0 \tag{3.37}$$

The boundary conditions are derived from the original acoustic problem and the numerical solution procedure is needed only for the homogeneous subproblem. As a result the discussion of the BEM may be confined only to the homogeneous acoustic problems without loss of generality.

The direct boundary formulation can only deal with acoustic problems having a closed boundary. For *combined interior/exterior acoustic problem* having an open boundary an alternative indirect boundary integral formulation has been derived [33].

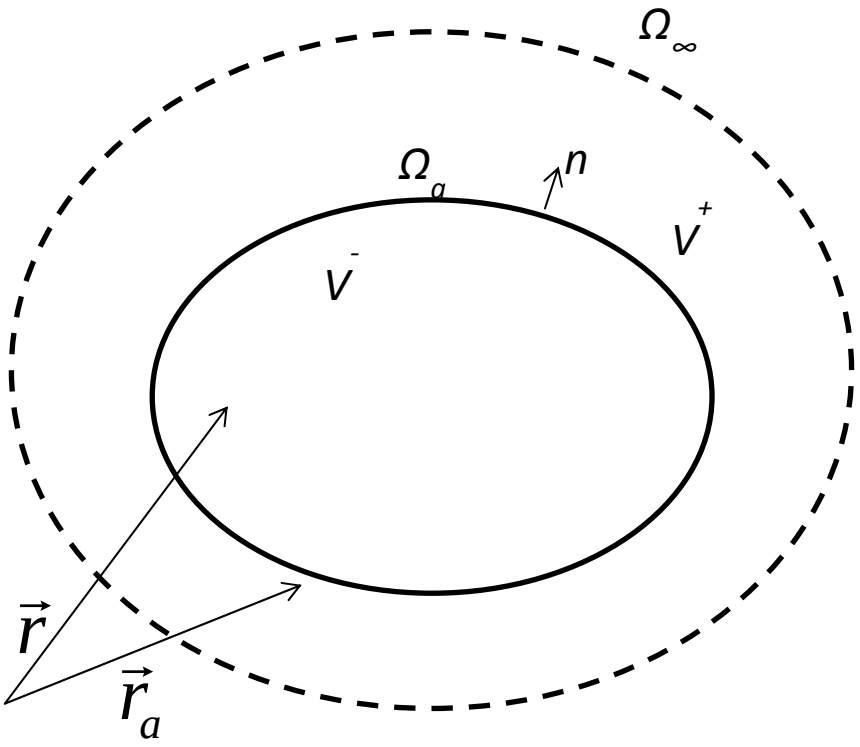

Figure 58 - Problem definition.

Considering at first a position $\vec{r}$ in the interior domain V^- (Figure 58) is it possible to apply the direct integral formulation obtaining:

$$\begin{cases} p(\vec{r}) = -\int\limits_{\Omega_a} \left(p^-(\vec{r}_a) \dfrac{\partial G(\vec{r},\vec{r}_a)}{\partial n} - G(\vec{r},\vec{r}_a) \dfrac{\partial p^-(\vec{r}_a)}{\partial n} \right) d\Omega(\vec{r}_a) \quad \vec{r} \in V^- \\ 0 = \int\limits_{\Omega_a} \left(p^+(\vec{r}_a) \dfrac{\partial G(\vec{r},\vec{r}_a)}{\partial n} - G(\vec{r},\vec{r}_a) \dfrac{\partial p^+(\vec{r}_a)}{\partial n} \right) d\Omega(\vec{r}_a) \quad \vec{r} \in V^- \end{cases} \tag{3.38}$$

where $G(\vec{r},\vec{r}_a)$ is the Green's kernel function. The plus and minus related to the pressure are defined by the normal direction *n* that has a positive orientation into the unbounded fluid domain.

Considering then a position $\vec{r}$ in the exterior domain V^+:

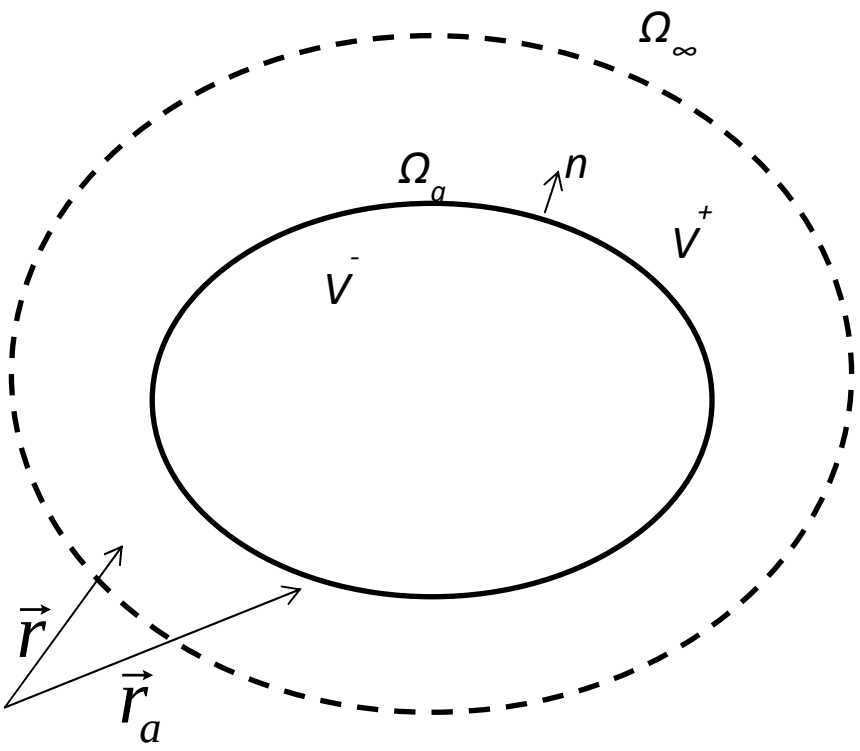

Figure 59 - Problem definiton.

$$\begin{cases} p(\vec{r}) = \int\limits_{\Omega_a} \left(p^+(\vec{r}_a) \dfrac{\partial G(\vec{r},\vec{r}_a)}{\partial n} - G(\vec{r},\vec{r}_a) \dfrac{\partial p^+(\vec{r}_a)}{\partial n} \right) d\Omega(\vec{r}_a) \quad \vec{r} \in V^+ \\ 0 = -\int\limits_{\Omega_a} \left(p^-(\vec{r}_a) \dfrac{\partial G(\vec{r},\vec{r}_a)}{\partial n} - G(\vec{r},\vec{r}_a) \dfrac{\partial p^-(\vec{r}_a)}{\partial n} \right) d\Omega(\vec{r}_a) \quad \vec{r} \in V^+ \end{cases} \tag{3.39}$$

Adding the equations (3.38) or (3.39) a general indirect boundary formulation can be obtained:

$$p(\vec{r}) = \int\limits_{\Omega_a} \left(\mu(\vec{r}_a) \frac{\partial G(\vec{r},\vec{r}_a)}{\partial n} - \sigma(\vec{r}_a) G(\vec{r},\vec{r}_a) \right) d\Omega(\vec{r}_a) \quad \vec{r} \in V \tag{3.40}$$

The integral indirect boundary formulation relates the pressure in any point of the acoustic field to the distribution of a *single layer potential* and a *double layer potential* on the boundary surface Ω_a.

The single layer potential $\sigma(\vec{r}_a)$ is the difference in normal pressure gradient between both sides of the boundary surface Ω_a:

$$\sigma(\vec{r}_a) = \frac{\partial p(\vec{r}_a^{\,+})}{\partial n} - \frac{\partial p(\vec{r}_a^{\,-})}{\partial n} \tag{3.41}$$

This distribution can be regarded as a distribution of monopole sources on the boundary surface.

The double layer potential $\mu(\vec{r}_a)$ is instead defined as the pressure difference between both sides of the boundary surface Ω_a:

$$\mu(\vec{r}_a) = p(\vec{r}_a^{\,+}) - p(\vec{r}_a^{\,-}) \tag{3.42}$$

and represents a distribution of dipole sources on the boundary surface.

The term indirect indicates that the boundary variables, i.e. the monopole and dipole distribution, do not represent any physical quantity of the pressure field. It is possible to show that equation (3.40) is valid also in the case of exterior acoustic problems with open boundary surface.

The boundary conditions to complete the problem definition can be prescribed values of pressure, normal velocity and normal impedance. Under the hypothesis of

thin boundary surface the prescribed normal impedance is considered equal on both side

Similarly to the FEM the boundary surface is discretized in a number of small subsurfaces, Ω_{σ_e} and Ω_{μ_e}, and a number of nodes, respectively n_σ and n_μ, defined at some particular location in each element. Within each element the problem variable, i.e single and double layer potentials, are approximated as expansions in terms of a number of suitable shape functions only defined within the element domain.

$$\begin{aligned} \sigma(\vec{r}_a) \approx \hat{\sigma}(\vec{r}_a) = \sum_{i=1}^{n_\sigma} N_{\sigma_i}(\vec{r}_a)\{a_{\sigma_i}\} \quad \vec{r}_a \in \Omega_{\sigma_e} \\ \mu(\vec{r}_a) \approx \hat{\mu}(\vec{r}_a) = \sum_{i=1}^{n_\mu} N_{\mu_i}(\vec{r}_a)\{a_{\mu_i}\} \quad \vec{r}_a \in \Omega_{\mu_e} \end{aligned} \tag{3.43}$$

Most common BE type are triangular or quadrilateral and the nodes are defined at each corner point: for each boundary variable one degree of freedom is specified per node. Each shape function $N^e_{\sigma_i}$ and $N^e_{\mu_i}$ is designed to have unit value at node *i* and zero at all the others node locations. The contributions a_{σ_i} and a_{μ_i} in the (3.43) represents respectively the approximated single layer potential and double layer potential at the location *i*. Starting from the (3.43) which are locally defined within a single element, it is possible to derive global shape functions N_σ and N_μ, defined respectively on the whole boundary surface

The solution technique for the integral (3.40) relies on a variational formulation that leads to regular integrals and ensures symmetry of the resulting boundary element model. In analogy with the Finite Element Method displacement formulation the solution in terms of singular and double layer potential leads to the stationarity of a suitable functional *J* [33]. Subsequently, the pressure at any position $\vec{r}$ in the acoustic domain, not on the boundary Ω_a is obtained from the indirect integral boundary formulation (3.40), using the surface single and double layer potential results. from the previous step.

3.2. Coupling of structural and acoustic models

The mutual interaction between sound and vibration activates a mechanism in which the structural displacement is excited by sound waves and induces waves in the

surrounding fluid. The numerical model of the problem should be able to handle this phenomenon in order to obtain reliable results. The coupled problem can be tackled connecting the structural numerical model described in paragraph 2.1 and the acoustic model detailed in paragraph3.1.

The transmission of sound through structures has been classified as a combined interior/exterior vibroacoustic problem. This means that an elastic structure, whose both sides are in contact with a fluid, is part of a closed boundary surface. In this case there are two separate acoustic domains: a bounded domain interior to Ω_a and an unbounded one exterior to it. For each of these domains a Helmoltz equation like the (3.37) with its boundary condition has to be formulated. The displacement field of the elastic structure is governed by a dynamic equation like (3.2) where the forcing term becomes a pressure loading term related to the pressure difference between both sides of the structure.

As described in the paragraph2.1the steady state dynamic displacement of the considered plate can be expressed in terms of only nodal variables. Assuming a synusoidal-like excitation, as in case of acoustic excitation, for a generic element *i* the (3.2)can be rewritten as:

$$\left(\mathbf{K} + j\omega\mathbf{C} - \omega^2\mathbf{M}\right)\{a_i\} = \{F_s\} \tag{3.44}$$

the vector $\{F_s\}$ contains the terms in the constrained degrees of freedom, prescribed forces and moments contributions and the contributions from the external pressure load.

The elastic structure is assumed to be entirely comprised in the boundary surface Ω_a. On the common part of the boundary surface the continuity of the normal velocity between the acoustic and structural domain is imposed. In the remaining boundary surface a prescribed normal velocity may be imposed. The discretization of the acoustic domain is generally coarser with respect to the structural one if considering the same maximum frequency. A rule of thumb determines the maximum element length as one tenth of the acoustic wavelength in air corresponding to the maximum frequency of interest:

$$l_a = \frac{c}{10\,f} \tag{3.45}$$

The theory behind the (3.45) is exactly the same of the (3.10). To accurately capture either the structural or the acoustic behavior the element dimension has to be significantly smaller than the characteristic length of the investigated phenomenon.

The nodes in the BE discretization can be divided into two groups: a group n_{a_1} located on the fluid structure coupling interface Ω_s and a group n_{a_2} located on the remaining boundary surface. The previously determined information about the structure dynamic behavior have to be transferred to the acoustic model. In particular, mode shapes have to be projected from the structural to the acoustic mesh.

The force loading of the acoustic pressure on both side of the elastic plate results in an additional normal load. An additional term, discretized according to the (3.43), must be added to the structural FE model (3.44):

$$\left(\mathbf{K} + j\omega\mathbf{C} - \omega^2\mathbf{M}\right)\{a\} + \mathbf{L}_c\left\{\hat{\mu}_1\right\} = \{F_s\} \tag{3.46}$$

the vector $\left\{\hat{\mu}_1\right\}$ contains the pressure degrees of freedom along the coupling interface while the coupling matrix is defined as:

$$\mathbf{L}_c = \sum_{e=1}^{n_e}\left(\int_{\Omega_e}\mathbf{N}^T\left\{n^e\right\}\mathbf{N}_{\mu_1}d\Omega\right) \tag{3.47}$$

where n_e is the number of flat plate elements Ω_e in the structure discretization, $\left\{n^e\right\}$ is a unit vector normal to a plate element. Structural and acoustic normal vectors on the boundary surface are assumed to have the same positive orientation. The pressure degrees of freedom $\left\{\hat{\mu}_2\right\}$ does not appear in the (3.46) since their global shape function are zero on the coupling interface [33].

Solving the coupled problem defined by the (3.46) it is possible to predict the vibroacoustic performances of the considered structure. The structural model provides information on the structural resonant response in terms of modal shapes and related normal displacement relevant for the sound transmission at low frequencies. The solution of the interior acoustic problem defines the additional loading term resulting from the pressure field induced by the sound source while the solution of the exterior acoustic problems defines the external pressure field due to the effective sound transmission through the investigate structure. As a result, such

a model is a powerful numerical tool to evaluate the vibroaocustic performances of different engineering solutions.

4. Sound Transmission Loss prediction for higher frequencies

The evaluation of structural vibroacoustic performances can be summarized with the evaluation of the Sound Transmission Loss (TL) in the frequency range of interest. The graph of the TL towards frequency gives with a quick glance the capability to evaluate the suitability of the proposed solution to the considered practical case.

The main drawback of the coupled numerical approach presented in paragraph 3 is the limited frequency range that can be investigated. The coupled FEM/BEM approach is in fact based on deterministic methods that find their optimal range of applicability in the low frequency range. The meaning of "low" is related to the characteristic length of the investigated problem. Typically, the low frequency range spans a couple of kHz. Element based techniques encounter several problems moving towards high frequencies. The element size should decrease to maintain a sufficient level of model reliability leading to higher computational costs. A bigger model is also more sensitive to numerical errors like the interpolation or pollution one and to uncertainties in structural parameter. The analysis of vibroacoustic performances in the high frequency ranges, e.g. above 4000 Hz, can be pursued applying different numerical modeling techniques like Statistical Energy Analysis. The majority of the TL calculation done with SEA for multilayered structures have been based on equivalent layer modeling of the structure [37]. This simplification, although justified, hides a peculiarity of sandwich structures having soft core. The structure deformations are in this case a combination of symmetric and antisymmetric components due to the spring-like behavior of the porous soft core.

A sandwich structure having two stiff thin skins with a soft, light and shear bearing core can be approximated as a two degrees of freedom mechanical system, a mass-spring-mass system (Figure 60):

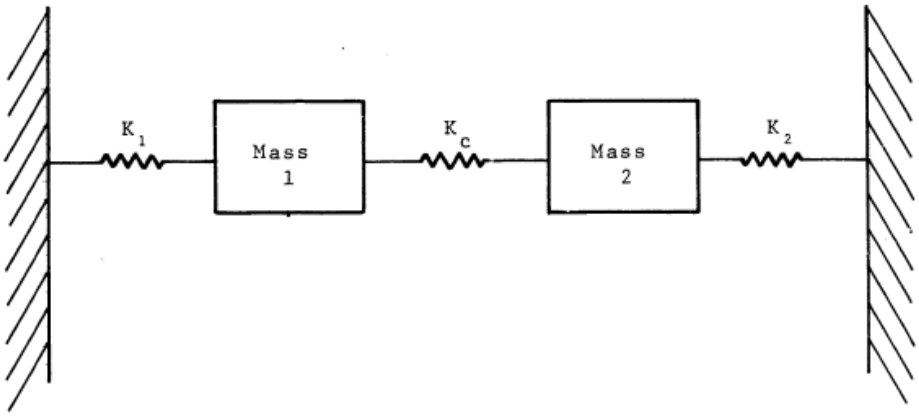

Figure 60 - Mass-spring-mass equivalent system [42].

A system like the one of Figure 60 is characterized by two vibration modes: (i) one with both masses moving in the same direction, (ii) one with masses moving in the opposite directions. A sandwich structure behaves exactly in the same way. It is possible to identify two fundamental modes of vibration: (i) symmetric mode or dilatational mode due to core shear (ii) anti-symmetric mode or flexural mode due to skin bending (Figure 61).

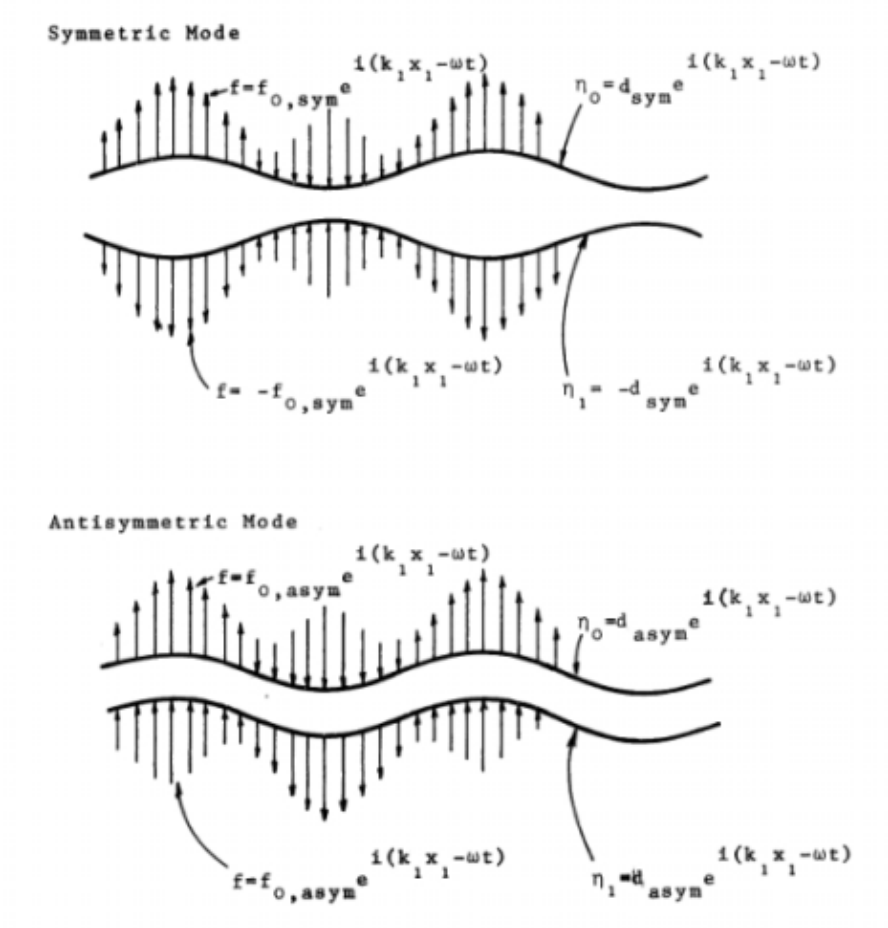

Figure 61- symmetric and anti-symmetric modes [42].

Different studies [43, 10, 38, 42] have pointed out how the panel dynamics and the TL can be expressed in terms of panel impedances taking properly in account the phenomena of symmetric and antisymmetric resonances.

The considered excitation is a downward plane travelling wave incident on the panel from an angle θ with respect to the normal to the plane of the panel, x_3 direction, and the azimuthal angle φ. The latter is defined as the angle made by a plane containing the x_3 axis with respect to the vertical plane defined by the x_3 and x_1 axis. (Figure 62)

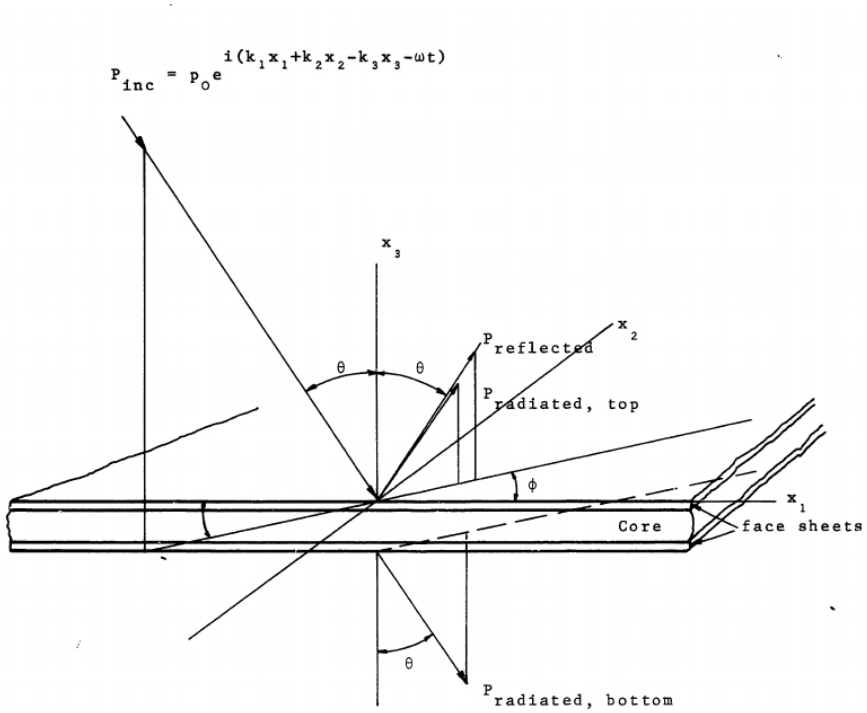

Figure 62 - Problem geometry [42].

The sandwich structure is symmetric, with identical face sheets and homogeneous core material. The incident acoustic plane wave is characterized by the radiant frequency ω and the wavenumbers k_1, k_2, k_3. The wavenumbers are related to the speed of sound as follows:

$$k_1^2 + k_1^2 + k_3^2 = k_0^2 = \left(\frac{\omega}{c_0}\right)^2 \tag{3.48}$$

The wavenumbers are defined as:

$$\begin{aligned} k_1 &= k_0 \sin\vartheta\cos\varphi \\ k_2 &= k_0 \sin\vartheta\sin\varphi \\ k_3 &= k_0 \cos\vartheta \end{aligned} \tag{3.49}$$

In hypothesis of steady state conditions the response to the incident plane wave can be formulated in terms of reflected wave from the top skin and radiated plane wave resulting from the normal displacements of both skins. The TL is usually defined as the ratio of the transmitted to the incident sound power. A different formulation can though be adopted relating the TL to the average transmission coefficient τ :

$$TL_{dB} = 10\log\left(1/\tau\right) \tag{3.50}$$

The transmission coefficient τ is defined as the ratio of the transmitted acoustic intensity I_{trans} the incident acoustic intensity I_{inc}. The transmitted acoustic intensity is a result of the combination of the incident wave transmission through the panel and the normal displacements of the bottom face sheet.

$$\tau\left(\vartheta,\varphi\right) = \frac{\text{Transmitted intensity}}{\text{Incident intensity}} \tag{3.51}$$

Generally speaking, the transmission coefficient is a function of both angles θ and φ. Under the justified hypothesis of in plane isotropy of face sheets and isotropy of the core of the composite panel, τ is independent of the azimuthal angle φ.

The (3.51) can be reformulated in terms of panel impedances:

$$\tau\left(\vartheta\right) = \left| \frac{\frac{\rho_0 c}{\cos\vartheta}\left(Z_{sym} - Z_{asym}\right)}{\left(Z_{asym} + \frac{\rho_0 c}{\cos\vartheta}\right)\left(Z_{sym} + \frac{\rho_0 c}{\cos\vartheta}\right)} \right|^2 \tag{3.52}$$

The symmetric and anti symmetric panel impedances, respectively Z_{sym} and Z_{asym}, are defined as ratio between the corresponding forces per unit area and normal velocities. The latter descend directly from the prescribed normal displacement while the former can be derived from the acoustic pressure disturbances due to the incident sound wave. The acoustic pressure disturbance on the top face sheet is due to either the reflected sound wave or the pressure wave due to the motion of the top face sheet. The acoustic pressure disturbance on the bottom face sheet instead is only due to the motion of the bottom face sheet. The symmetric pressure disturbance is then obtained by the half sum of both disturbances while the anti symmetric one is expressed as the half difference. The global symmetry of the panel makes the symmetric and antisymmetric motions uncoupled and thus the solutions to the two problems may be obtained separately and then linearly superimposed.

The expression for the impedances depends on the material properties of face sheets and core, the frequency and the wavenumber. The whole detailed procedure to determine the panel impedances starting from the description of skins bending and in plane deformation and core shear and dilatational wave propagation can be found in [42].

In many applications the sound waves are not impinging on the structure with a single angle. It is more common to have soundwaves coming from different directions and hitting the surfaces with different orientations angle. The directional distribution of impinging waves is usually unknown and diffuse field model is commonly adopted [44]. The diffuse field model implies plane waves incident from all directions with equal probability and random phase. A suitable transmission coefficient can be evaluated weighting the (3.51) according to the directional distribution of directional intensities and then integrating over angle of incidence. This weighting leads to the following expression for the diffuse field transmission coefficient:

$$\bar{\tau} = \frac{\int_0^{\vartheta_{\lim}} \tau(\vartheta) \cos\vartheta \sin\vartheta d\vartheta}{\int_0^{\vartheta_{\lim}} \cos\vartheta \sin\vartheta d\vartheta} \tag{3.53}$$

The incidence angle is supposed to vary from zero to $\vartheta_{\lim}$ to 78° for coherence with experimental results [44].

The application of the (3.52), (3.53) and (3.51) leads to the numerical evaluation the panel acoustic performances over a wider range of frequencies with respect to FEM/BEM approach, highlighting also the phenomenon of both symmetric and antisymmetric coincidence. Sandwich structures, in fact, exhibit two fundamental modes of vibration and consequently two frequencies that lead to the equality between impinging acoustic and free structural wavelength.

The capability of evaluating the TL on a wide range of frequency allows the exploration of different panel configuration and to tailor structure characteristics to the current application requirements. The expression of the transmission coefficient does not predict the TL oscillations due to the structural modal behavior in the low frequency range. The TL in the frequency range where the modal behavior is relevant can be predicted accurately applying the deterministic techniques described in paragraph 3.

CHAPTER 4

Chapter 4 gives detailed description of the experimental activity that has been carried out to validate the proposed numerical strategy. The adopted techniques for data acquisition and post processing are detailed. The results are presented for either the dynamic or the vibroacoustic behavior identification. Particular attention has been paid to the characterization of the core material behavior and the related parameters.

1. Experimental investigation role in vibroacoustics

Along with numerical modeling, experimental investigation plays a fundamental role in engineering practice. The availability of a number of reliable experimental data allows one to assess the chosen numerical modeling strategy. In fact, two of the most important characteristics of a numerical modeling procedure, i.e. the efficiency and the reliability, can be defined and evaluated only through dedicated experimental activities. In addition, several model parameters which are an input to the problem can often be retrieved through experimental data analysis.

The model detailed in Chapter 3 is developed to predict the structural performances in terms of either the vibration attenuation or sound transmission reduction. A dedicated experimental activity has been designed to accomplish two main tasks: (i)

provide all the required information to develop the numerical model and (ii) check the whole modeling procedure reliability and efficiency.

As a result, the testing campaigns involve three main tracks:

- Identification of the material parameter
- Dynamic behavior characterization of the investigated panel
- Acoustic transmission performances evaluation

An efficient prediction of the structural dynamic behavior is in fact the starting point towards the global vibroacoustic behavior simulation. The FE model developed to extract the vibrational performances of the panel takes as input the problem geometry and the material properties. A correct identification of the material parameters is thus fundamental. In particular, the sandwich panel core is made of a non standard material that requires a specific testing procedure. The properties that identify the foam behavior are frequency dependent. A dedicated experimental campaign has been designed and carried out to obtain reliable material parameter to include in the FE model.

The proposed dynamic model returns the structural behavior in terms of frequency response function and modal parameters. The assessment of the reliability of this modeling step requires then the experimental identification of the structure modal behavior to be able to validate the obtained numerical results. Consequently, the dynamic properties have been obtained through experimental modal analysis. The post processing of the experimental frequency response functions allowed the extraction of natural frequencies and mode shapes of the panel.

Structural modal parameters are the fundamental input to evaluate the acoustic performances through a coupled vibroacoustic model. The global vibroacoustic performance is typically quantified through Sound Transmission Loss (TL) or Sound Insertion Loss (IL)evaluation. Both indexes give a quick overview of the structure vibroacoustic behavior. As well as the TL, the IL index allows the identification of the parameters that mainly influence the acoustic behavior in the different frequency ranges. According to the theory, the low frequency range is dominated by the structural modal behavior. Moving towards higher frequencies instead, it is the mass that drives the acoustic performances. A more detailed explanation has been given in Chapter 2. The experimental identification of TL foresees the fulfillment of specific requirements either on sample size or on the acoustic field in the testing environment. The IL index is instead easier to measure through sound intensity measurements. As a main drawback it carries some information on the testing environment while the TL is a property of the tested object only. Further details are given in the paragraph 4 of the current chapter. Exploiting a specific test

rigdeveloped at KU Leuven, the IL of the investigated panel has been experimentally identified. The availability of IL experimental data allows not onlythe evaluationof the reliability of the coupled model but also of the efficiency of the whole proposed modeling procedure.

Generally speaking, each of the performed experimental campaigns can be subdivided in three fundamental steps:

- Test set up definition
- Data acquisition
- Data post processing and analysis

Each step presents peculiar difficulties and the final adopted solution is always a trade off among the final goal of the experimental activity, hardware availability and time requirement. Several experimental techniques have been developed along years either in the dynamic or in the acoustic framework. In the current chapter, all the three steps involved in the experimental activity are detailed either for dynamic or acoustic behavior investigation starting from the test definition condition to the results interpretation. In particular, a specific paragraph is devoted to the description of the experimental activity that has been carried out to identify the viscoelastic material behavior.

The first part of the chapter focuses on the description of the experimental characterization of the panel materials parameters. Subsequently, the structural dynamic behavior characterization is described. Two sandwich panels have been tested: one of size A2 and one of size A4. Both panels have the same cross section configuration in terms of either materials or layer thickness. The experimental data obtained for the big panel will be used explicitly for dynamic model validation purposes. The data of the small panel instead will be used to check the capability of the proposed numerical technique to predict the behavior of a different structure. Finally, the last paragraph details the experimental campaign for the identification of the structure IL and thus the characterization of the structural vibroacoustic performances.

2. Panel materialscharacterization

An accurate and reliable identification of the material properties is the starting point of the whole vibroacoustic modeling procedure.

The panel under investigation is a three layered sandwich structure with Aluminum skins and polymeric foam core (Figure 63).

Figure 63 - Panel crossection: detail .

The Aluminum of which the skins are made is not pure but an alloy characterized by an elastic modulus equal to 70 GPa and a mass density of 2670 kg/m^3. The acoustic excitation is generally a small oscillation around the ambient pressure value. As a result, the magnitude of the loading acting on the panel is small; thus the deformation of skin material can be considered within the elastic range. The elastic behavior of skin material can then be characterized by simply using the alloy nominal values without any dedicated characterization.

Conversely the core is made of a viscoelastic material, in particular a closed cell polymeric foam (Figure 64). Viscoelastic materials properties are frequency dependent as described in Chapter 2. The material parameters have to be characterized through a dedicated experimental procedure in the whole frequency range of interest.

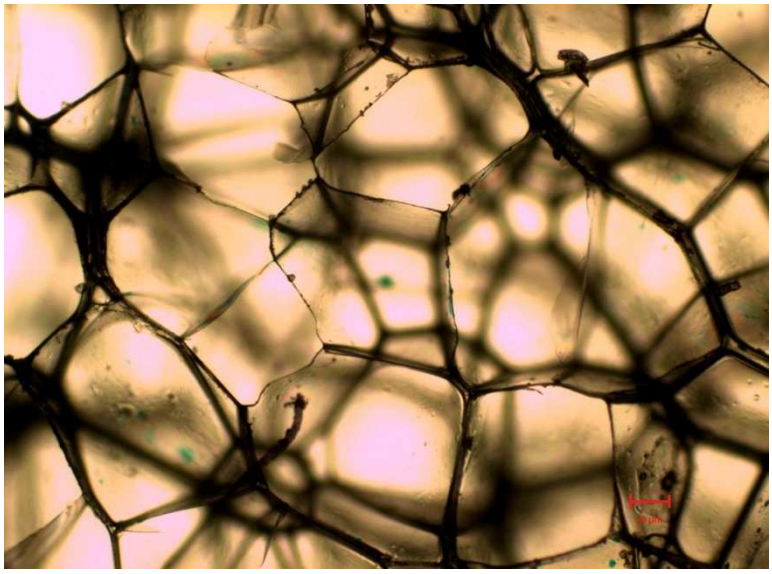

Figure 64 - Foam core: detail

The material data are an input of the developed numerical model that aims to replicate the dynamic response of the investigated panel. The frequency range of interest for the panel FE model spans from 0 Hz to few kHz. The width of the investigated frequency range is determined by the upper frequency limitation typical of modeling deterministic techniques as FE. The foam stress strain relationship has then to be characterized in the frequency range of interest. Given the magnitude of the acoustic excitation, the foam can be considered working. in the linear elastic range, as well as the Aluminum alloy of the skins.

One of the most common methods to characterize the viscoelastic material behavior as a function of frequency is the Dynamo Mechanical Analysis [45]. The basic principle of this experimental technique is represented in Figure 65. A sinusoidal strain is applied to the specimen and the resulting sinusoidal stress is measured. The scale factor between stress and strain represents the Storage Modulus while the phase delay between stress and strain is related to the Loss Modulus. In particular, it represents the phase of the Complex Modulus. The Complex Modulus and its meaning has been defined in Chapter 2.

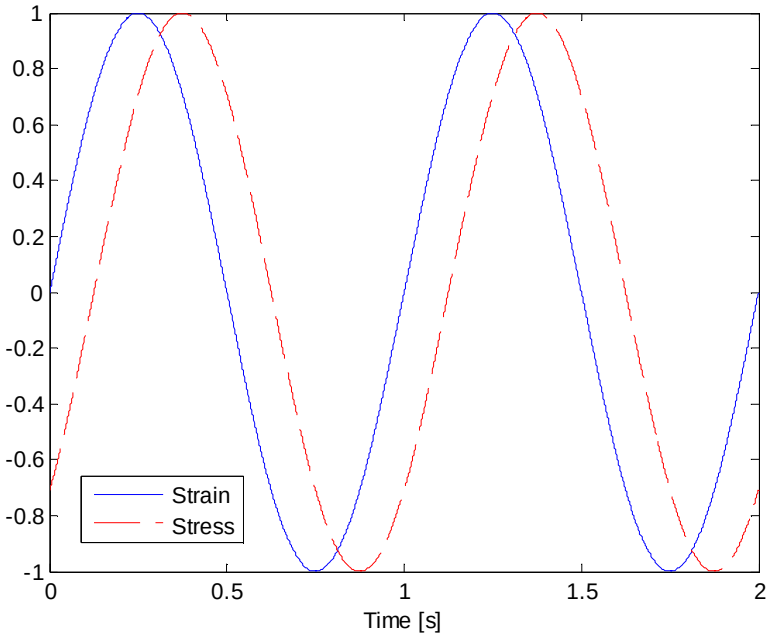

Figure 65 - Qualitative DMA test.

The test instrument that has been considered for the characterization of the foam under investigation is the DMA RSA3 of TA Instruments (Figure 66).

Figure 66 - DMA testing machine.

The test typology that has been considered for the foam is the compression one. A sinusoidal strain is imposed on a cubic specimen of foam. The consequent sinusoidal load is measured with a load cell and the resulting stress is computed. The specimen is in fact under uniaxial load condition, thus the stress can be computed as the ratio of the load to the specimen area. A detail of the specimen clamping is shown in Figure 67

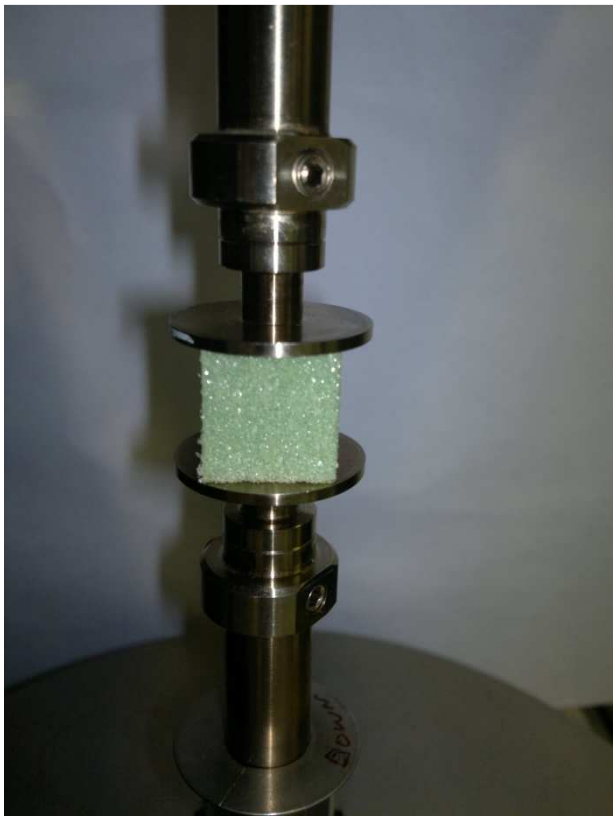

Figure 67- Clamped foam specimen.

A cubic foam specimen has been chosen to avoid bulge effect that may appear with a parallelepiped shaped specimens. The characteristic dimension has been taken exactly equal to the thickness of the foam layer in the sandwich panel.

Preliminary tests have been carried out to evaluate the role of the preload and the degree of anisotropy of the foam [46]. The latter has been quantified carrying out static compression test on a cubic specimen. Three different tests have been performed. In each of them the specimen has been oriented such has the imposed load was directed along one of the three directions depicted in Figure 68. 1 and 2 are the in plane directions while 3 is the direction corresponding to the thickness of the panel.

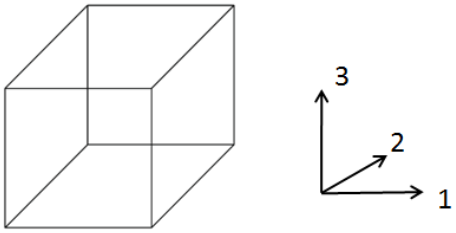

Figure 68 - Foam specimen: directions.

The obtained stress strain curves are displayed in Figure 69. According to the obtained results, the foam can be considered as transversally isotropic. The tests performed applying the load along the directions 1 and 2 gave the same result while the stress strain curve obtained in direction 3 is substantially different.

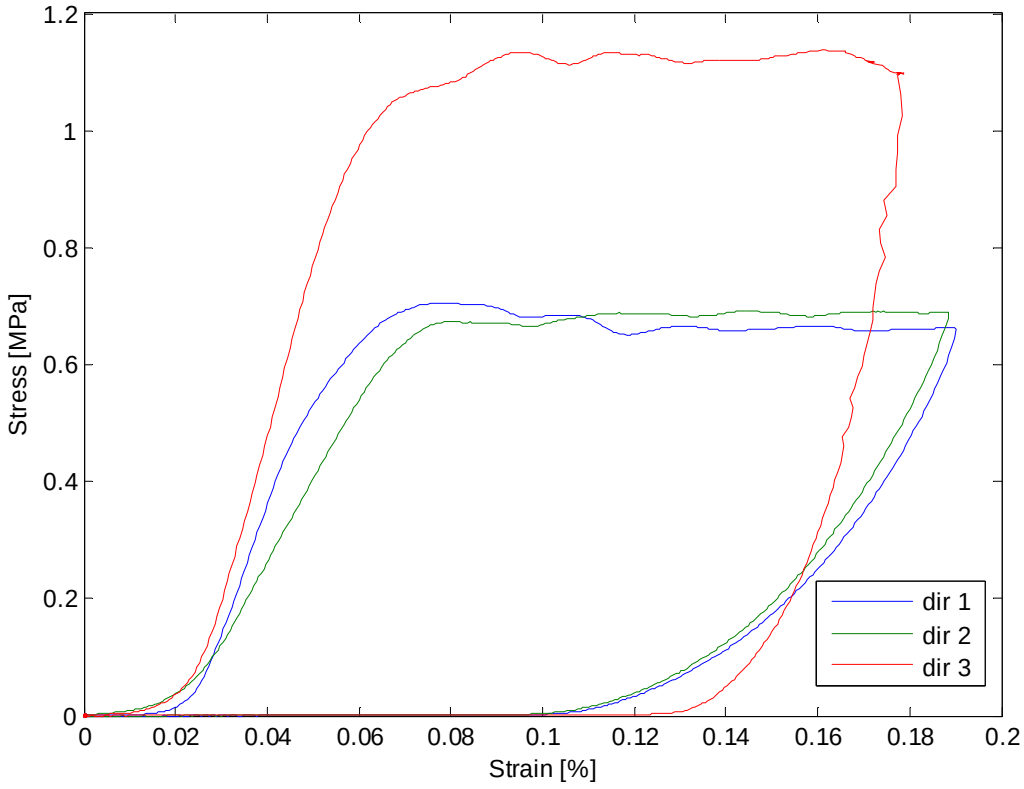

Figure 69 - Stress strain curves foam specimen

A quick and simplified identification of the Elastic Modulus based on the linear interpolation of the initial slope returned the values reported in Table 1. The estimated elastic modulus in direction 3 is around 50 % more than that in directions 1 and 2. This difference may be attributed to the foam manufacturing process.

Direction	Elastic Modulus [MPa]
1	15.8
2	16.4
3	28.8

Table 1 - Estimated elastic moduli.

During the DMA test a preload has to be imposed to the specimen to prevent from its sliding between the clamps the test. A preliminary evaluation of the effect of the preload entity on the foam has been carried out. Quick tests have been done spanning from 0.1 Hz to 10 Hz imposing different preloads. The results are reported in Figure 70. The preload proportionally affects the estimated storage modulus: the higher the preload, the higher the resulting modulus value. To better evaluate the condition under which the foam works constrained between the Aluminum skins, the same test has been done on a panel specimen (skin -foam -skin). The sandwich specimen has been tested with a low preload value. The value has been chosen to ensure a correct test execution and the lowest interfering effect. The blue circles in Figure 70 represent the storage modulus obtained for the panel specimen. As a rough estimation, the foam is preloaded by the Aluminum skins by a load of approximately 20kPa (red solid line in Figure 70). As a result, the mechanical properties on the whole frequency range of interest have been determined imposing a preload of 20kPa on the specimen.

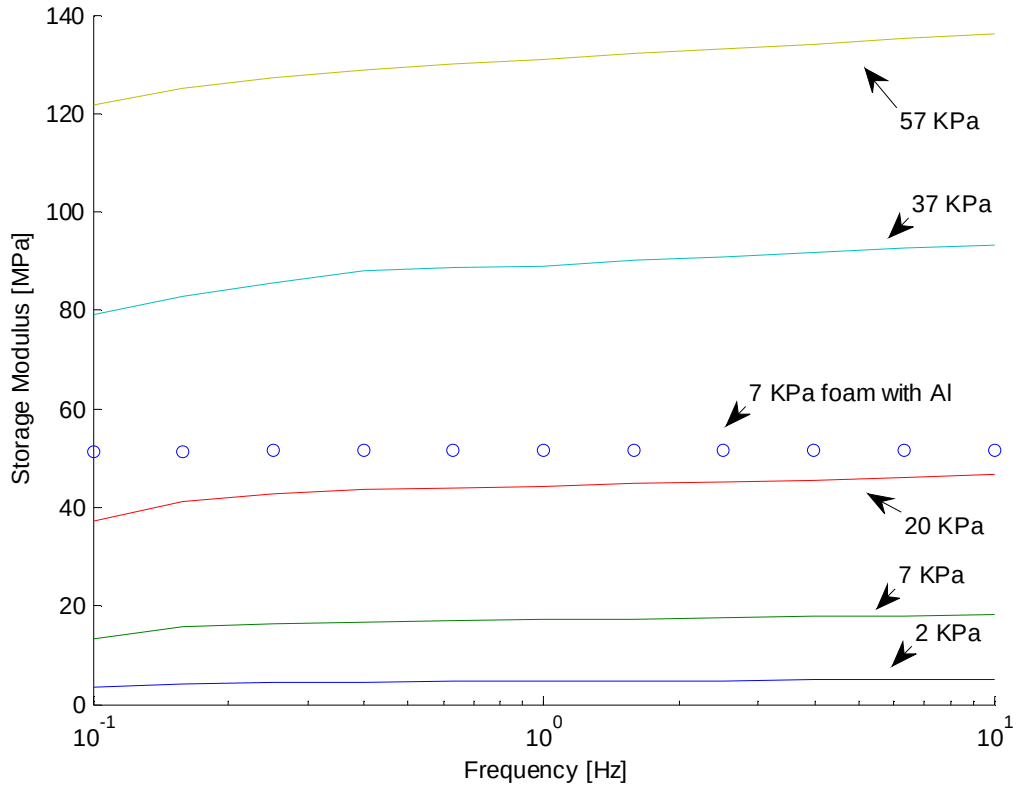

Figure 70 - Preload sensitivity analysis: foam specimen (solid line) and panel specimen (circles).

The foam properties are a fundamental input for the numerical model that aims to predict the structural dynamic response. Given the Complex Modulus typical frequency dependence, it has to be characterized over the whole frequency range of interest. Determination of material properties over a wide range of frequency may be challenging. Each experimental method in fact covers few frequency decades. For certain type of materials it is possible to infer the stress strain behavior over a wide range of frequency from experiments carried out at different temperatures [45]. This class of material is called *thermorheologically simple materials*. An example is the polymeric foam under investigation. For this class of materials a change in temperature is equivalent to a shift in the behavior on the frequency or time axis, following the time-temperature superposition principle. The viscoelasticity of these materials arises from a molecular rearrangement process which occurs under stress. For such materials a change in temperature stretches or shrinks the effective time scale [45]. As a consequence, experiments conducted in the same range of frequency, let's say from 0 Hz to 50 Hz, but at different temperatures result to be

equivalent to experiments conducted over a frequency range that can be extended up to GHz. The behavior of the material is then described by a curve built up by shifting the single curves obtained at different temperatures. This curve is called *master curve* and it is built horizontally shifting the experimental curve for temperatures above or below the curve at a chosen reference temperature until they overlap [45]. Despite an upper frequency limit of the testing machine set around 50 Hz, it has been possible to build the material master curve of the material up to 10kHz (Figure 71).

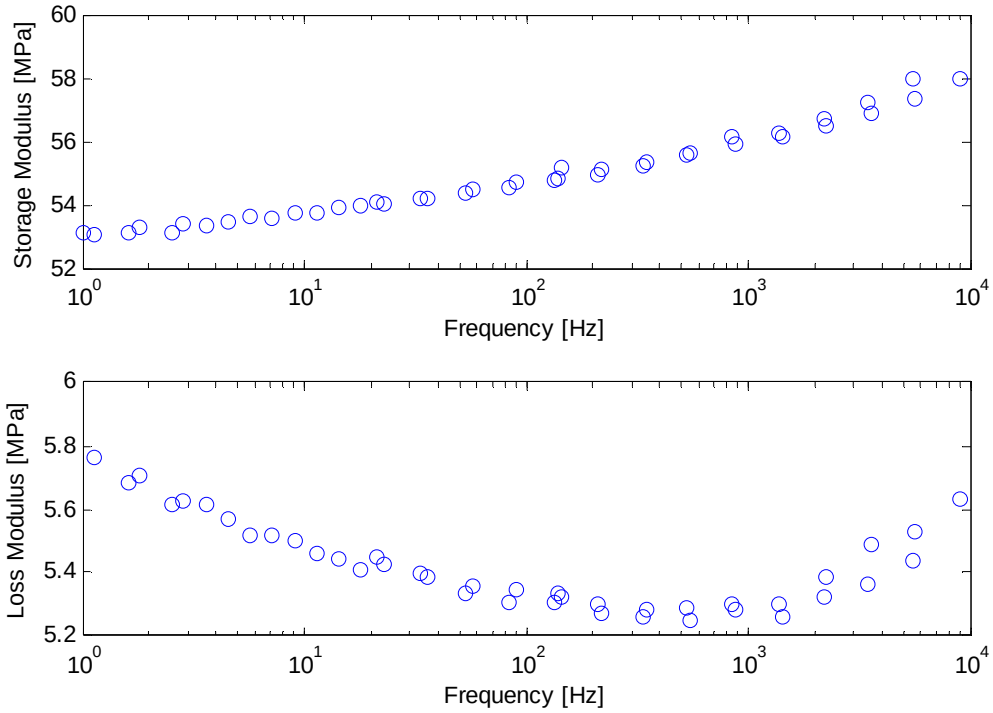

Figure 71 - Foam specimen Master Curve.

The obtained material data are a fundamental input for the structural model. A specific post processing of these data is necessary prior to the material definition in the FE model. As detailed in Chapter 3the most common numerical software requires the definition of the viscoelastic material function as Prony series. This programming choice is mainly due to the improvement of the numerical efficiency given by the use of this kind of series [14]. A minimization procedure between the series mathematical expression and the experimental data led to the evaluation of

the series parameter necessary to numerically define the material behavior. The frequency range has been limited to the one explored with the numerical model. The comparison between the experimental data and the prediction given by the calibrated Prony series is reported in Figure 72. The maximum errors between the experimental data and the numerical estimation are lower than 8% either for the Storage Modulus or for the Loss Modulus as displayed in Figure 73.

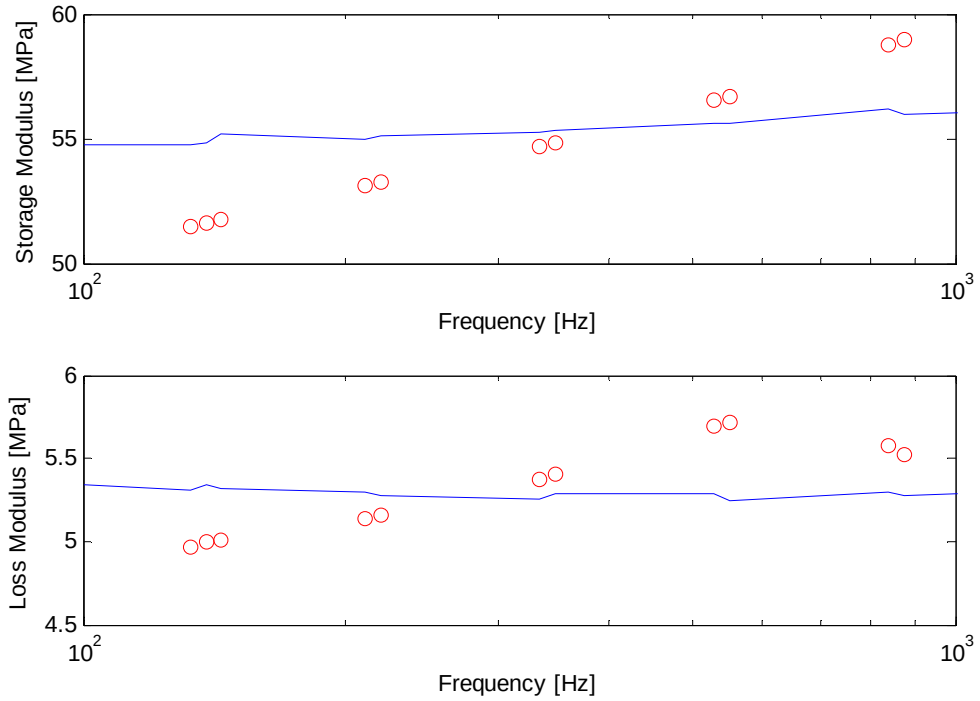

Figure 72 - Foam Material data (blue solid line) vsProny series approximation (red circles).

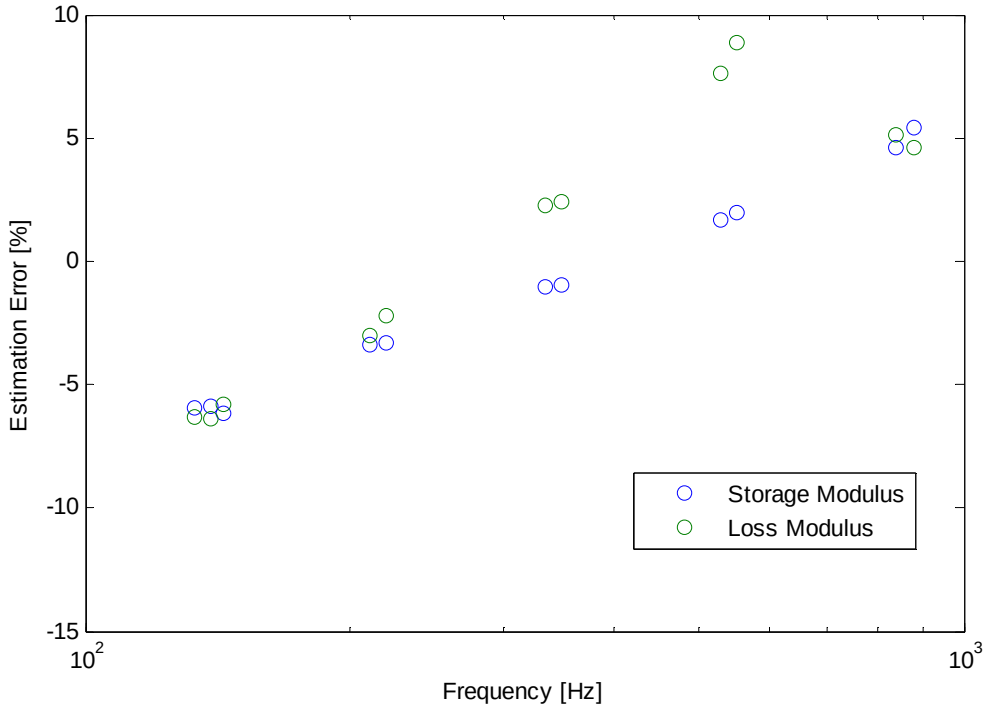

Figure 73 - Estimation Errors.

The definition of the parameters to numerically estimate the material behavior completes the set of input data required to develop the structural dynamic model.The reliability of the latter will be checked through experimental data obtained according to a procedure detailed in the next paragraph.

3. Dynamic identification procedure

The dynamic behavior of a structure can be described in terms of its modal parameters. The natural frequencies along with the associated mode shapes and damping factors define how a structure reacts to the input forces. The problem can be tackled either from a theoretical or from an experimental point of view. The former is the background of the available numerical modeling techniques. Starting from the knowledge of the system boundary conditions, structure geometry and material characteristics it is possible to derive the equation of motion as function of the displacement $\{u(t)\}$ that describes the structure behavior. The mass, damping and

stiffness system distributions are expressed in terms of mass, damping and stiffness matrices:

$$\mathbf{M}\{\ddot{u}(t)\}+\mathbf{R}\{\ddot{u}(t)\}+\mathbf{K}\{u(t)\}=\{f_{ext}\} \quad (4.1)$$

The modal analysis theory shows that the matrices of equation (4.1) are enough to derive the structural modal parameters and that these parameters allows the description of the structure dynamic behavior [47, 48].

The experimental approach instead starts from the measurements of both the input force and the output response on the investigated structure. Usually these measurement sets are transformed into sets of frequency response functions (FRF), i.e. the ratio of the output response to the input force. An accurate postprocessing of the obtained FRFs leads to the determination of the structural modal parameters

3.1. Test case: Sandwich panel with foam core

The investigated structure is a sandwich panel with aluminum skins and polymeric foam core (Figure 74).

Figure 74 - Investigated panel.

Sandwich structures highlight several issues in the experimental identification procedure. In fact the lightweight of these structures makes the testing strategy and setup more challenging. Particular attention should be paid to the selection of sensor type and position to avoid the so called load effect, i.e. the modification of the system modal parameters due to the presence of the instrumentationon the structure. The excitation itself plays an important role. The dynamic response of a mechanically driven structure is composed of a *resonant* and a *forced* response. The latter is given by the steady state response of the structure to the incoming excitation. With linear systems, if the input is a harmonic wave, the structure will vibrate at the same frequency but with an amplitude determined by the structural damping and the possible overlap of the excitation frequency with a resonance. If the excitation frequency is close to a resonant one the resulting vibrational level will be amplified. The resonant response dominates the transient structure behavior. For instance, if

the excitation is a white noise, thus able to transfer to the structure the same input level on a wide range of frequency the structure, will mainly respond according to the superposition of the resonant modes in that frequency range.

3.1.1. Suspended panel modal analysis

The final aim of the structural dynamic characterization is the evaluation of the correlation with the developed FE model in terms of modal parameters. The effective test condition should match the boundary condition of the FE model. Often, the first condition to be investigated is the free free one. In this scenario ideally no connection between the environment and the tested structure exists. This allows the extraction of only the structure dynamic behavior. A FE model able to reply the bare structure dynamic will be theoretically capable to reply the structural behavior in any condition, if these conditions are accurately reproduced.

In practice, the free free boundary condition is replicated hanging the investigated structure with very soft springs that minimize the influence of the suspension system. In the suspension system design two aspects have to be carefully considered: the rigid body resonances and the suspension points. These latter should be nodal point for almost all the investigated mode shapes to avoid any system dynamic modification. The soft suspension system shifts slightly the rigid body resonances to frequencies higher than the theoretical zero. The resulting frequencies have to be way lower than the first structure resonant system. In a nutshell the suspension system has not to interfere with the system dynamics. The free free boundary conditions for the investigated structure have been replied as shown in Figure 75.

Figure 75 - Suspended panel.

Several different methods are available to excite a structure. They basically can be divided into two main categories: contacting and non contacting techniques. The former involves the connection of the exciter to the structure throughout the whole test and the excitation can be transient or continuous. The non contacting techniques include devices that are either out of contact or in contact only for the short time the excitation is given [47]. The major advantage of this latter class of excitation techniques is evident dealing with lightweight structure. The non contact techniques avoid the undesirable mass loading effect to the structure that can significantly modify structural modal parameters. Among the different non contacting techniques one of the most widely applied for its ease of application is the impact hammer testing. The device consists in an impactor, Figure 76, with a set of different tips and heads to modify the level and the frequency content of the excitation.

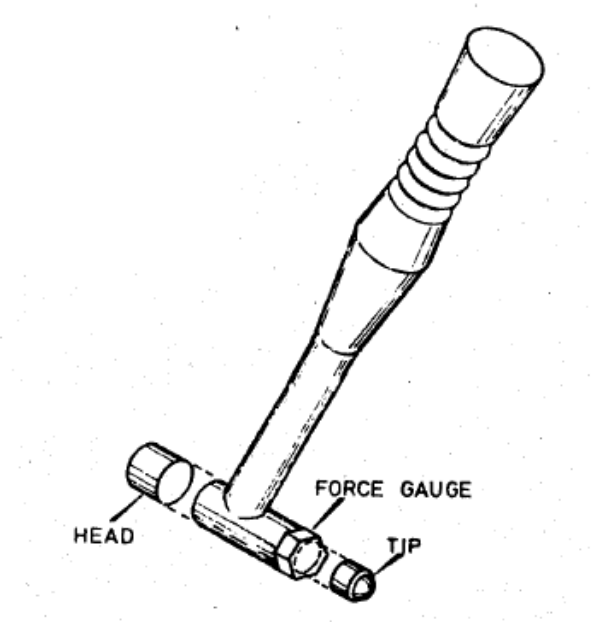

Figure 76 - Impact Hammer [47].

Embedded in the impactor a force gauge measures the magnitude of the force detected by the impactor, typically equal and opposite to the one which is the input of the structure. The magnitude of the excitation is mainly controlled by the impactor mass while the excitation frequency content is controlled by the stiffness of the tip and the mass of impactor head. When the hammer impacts on the structure, this latter undergoes a pulse excitation. The typical time history and frequency spectrum of this kind of excitation is displayed in Figure 77. The useful excitation frequency range is defined as the frequency interval in which the frequency spectrum remains flat. It can be proved that there is an inverse proportionality between the time width of the pulse and the useful frequency range. The narrower the pulse,the wider the excitation frequency content [47].

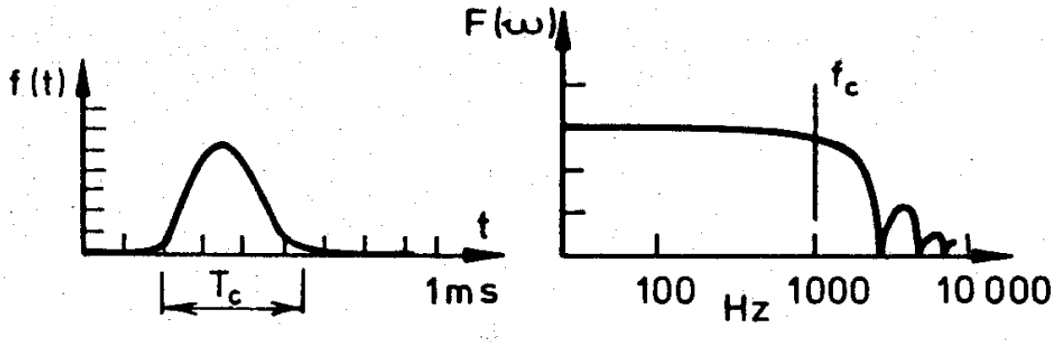

Figure 77 - Typical impact hammer pulse: time history (left) and frequency spectrum (right) [47].

The pulse duration in the time domain is mainly related to the stiffness of the contact between the tip and the surface of the tested object. Generally speaking, the stiffer contact the shorter the impact. In the same way the lighter the impactor the shorter the impact, thus the broader the excited frequency range [47]. Focusing on the investigated panel, the modal analysis has been performed applying the rowing hammer technique. The sensors position has been fixed while the excitation point was moved during the test on the different points defined in Figure 78.The choice of the measuring grid plays a key role in the effectiveness of the experimental campaign. The grid should be dense enough to capture the relevant mode shapes and the sensor position should not be a node for any of the modes of interest. A preliminary FE model can be very helpful in the test design process.

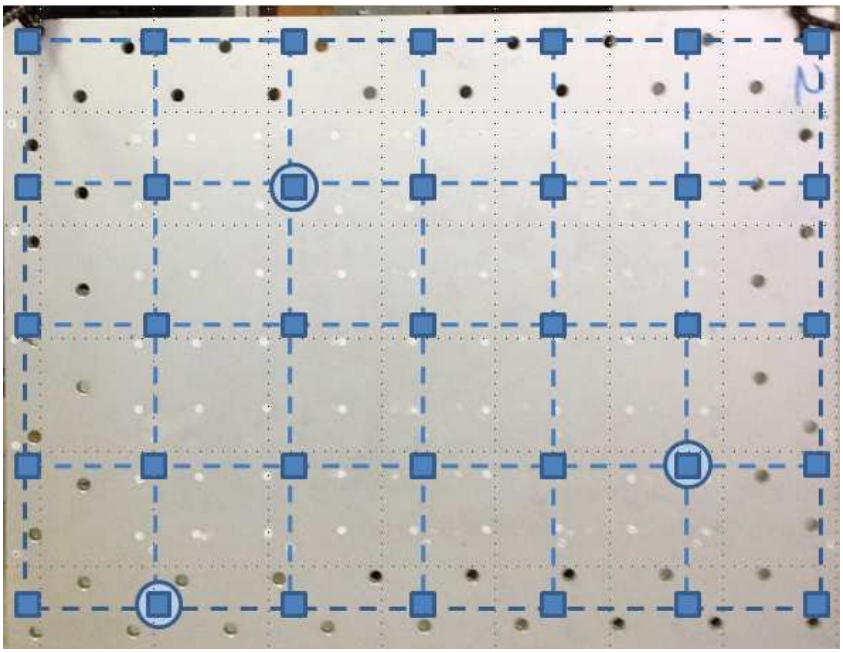

Figure 78 - Suspended panel: measurement grid (Squares: excitation points, Circles accelerometers).

Results and data analysis

In Figure 79 the obtained FRF for a point in the top right quarter of the panel is displayed. The explored frequency range has been limited to 1kHz considering the final goal of the testing campaign. This frequency range is narrower than the one considered for the material properties identification. The aim is to carry out a dedicated experimental activity to obtain reliable data to validate a numerical model. The choice of deterministic methods to simulate the vibroacoustic panel behavior limits the frequency range that can be explored (Chapter 2). The 1kHz range has been chosen as a compromise among computational costs limits and meaningful modal identification for the investigated structure.

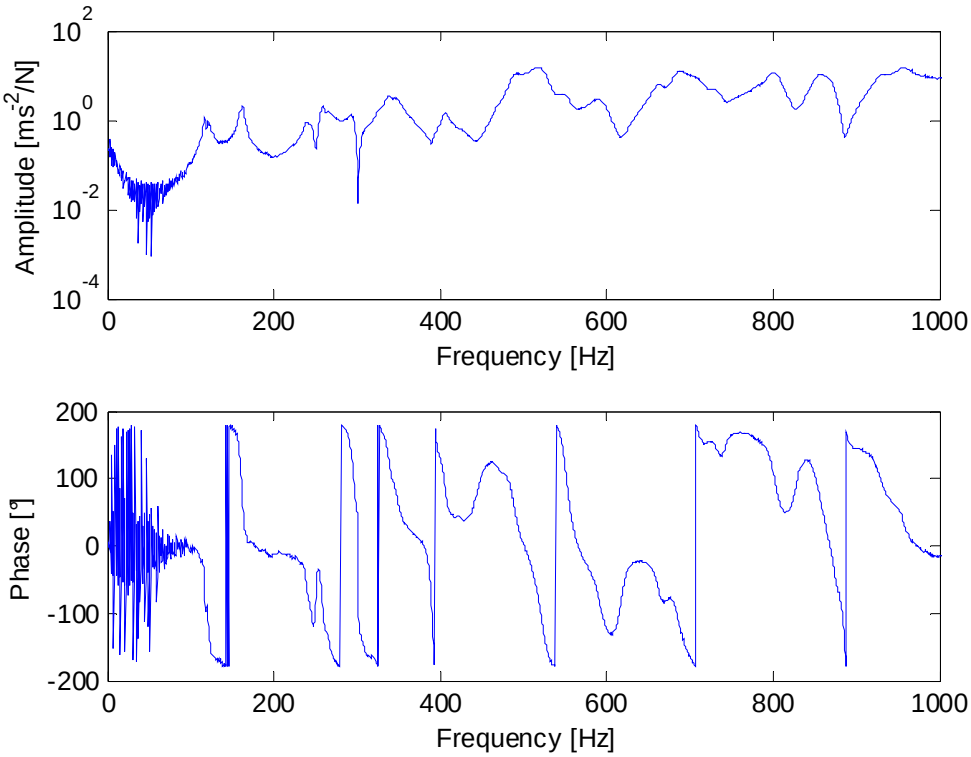

Figure 79 - Frequency Response Function free free boundary conditions.

The extraction of the modal parameters, i.e. natural frequencies, damping ratios and mode shapes, has been performed applying a self developed numerical code that applies the Polyreference Least Squares Complex Frequency Domain Method (p-LSCF). A description of the method can be found in [49].P-LSCF method is a Multiple Input Multiple Output modal parameter identification method that performs a minimization of the difference between the estimated and experimental FRF. The functional to minimize is written in such a way that leads to a non linear expression in terms of the unknown modal parameters.

The basic assumption of the modal analysis is that the response of the analyzed system can be expressed as the sum of responses of its individual modes. This assumption is well satisfied if the damping can be expressed as linear combination of local mass and/or stiffness (Rayleigh damping). A large proportion of real physical system does not conform the Rayleigh idealization. The FRFs of those system exhibit different forms according to the frequency range. In the "low" frequency range, the system response can actually be expressed as the superposition of resonant individual modes. Typically, the "low" frequency range includes the first ten structural modes. In the "high" frequency range it is not possible to identify individual

modes that dominate the system response and the FRF exhibits broader peaks. The peak does not represent anymore the response of a resonant single mode. The broader peaks represent the sum of the responses of all the modes having resonance frequency close to the frequency correspondent to the maximum of the peak [44]. The system under investigation follows exactly this description. Looking at the Amplitude of the FRF of Figure 79, reported in Figure 80, it is possible to distinguish between two macro frequency ranges: a low one up to around500 Hz and a high one that spans from 500 Hz to 1000 Hz. The former is characterized by narrow peaks that indicate the resonant modes contributions. The latter instead exhibits larger less separated peaks.

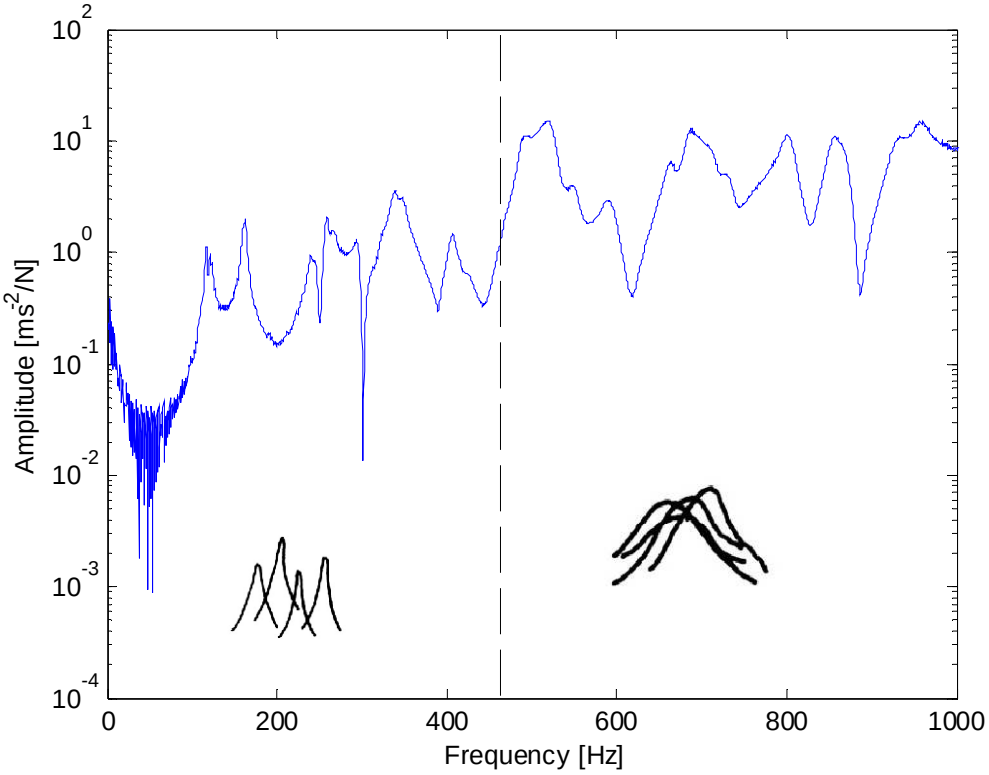

Figure 80 - FRF Amplitude free free conditions.

As a direct consequence of the higher modal density in the "high" frequency range, the extraction of modal parameters has been limited to the "low" frequency range.

In order to have a quick information about the resonant modes in the explored frequency range a simple way is to have a look at the summation of all the measured

FRFs. The different contributions are summed in terms of complex numbers as in the (4.2) [48]:

$$H_{sum} = \sum_i \sum_j \left| \mathrm{Re}\left(H_{ij}\right) \right| + i \sum_i \sum_j \left| \mathrm{Im}\left(H_{ij}\right) \right| \qquad (4.2)$$

In this way all the information carried by the different FRFs are globalised in one curve. The result for the suspended panel of Figure 75 is displayed in Figure 81.

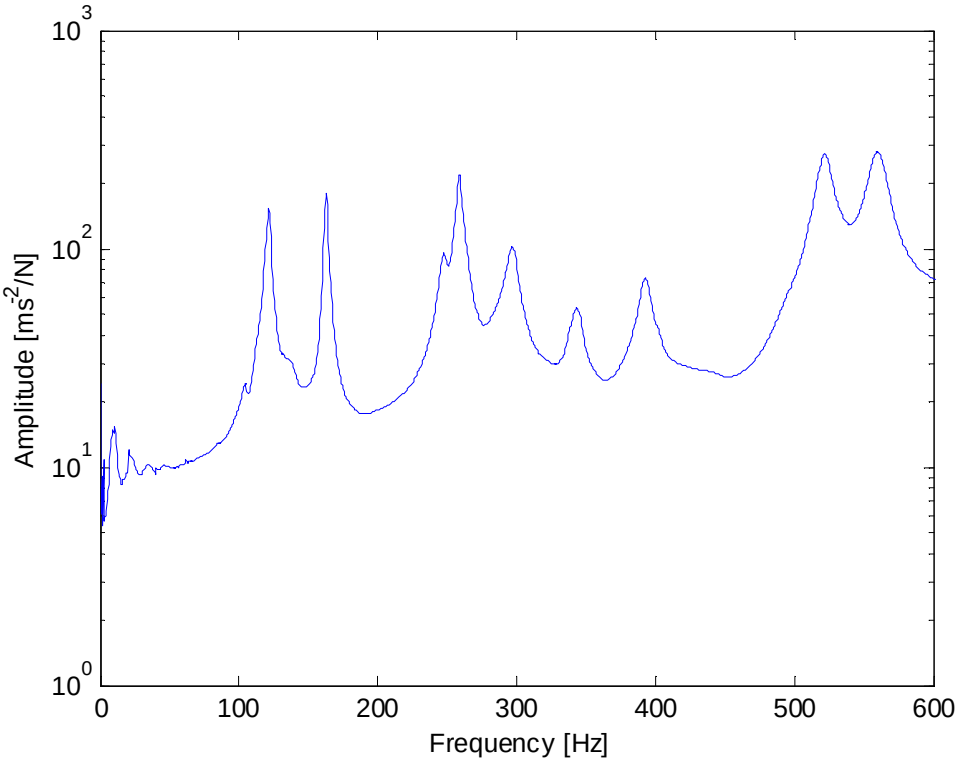

Figure 81 - Sum of FRFs - Amplitude.

The natural frequencies and damping ratios that have been identified with sufficient accuracy in the investigated frequency range are summarized in Table 2. The damping ratios are higher than the typical values of metallic materials (less than 1%) to testify the influence of the viscoelastic layer on the dynamic performances.

Mode #	Natural frequency [Hz]	Damping ratio [%]
1	120.37	2.03%
2	162.8	0.73%
3	245.8	1.83%
4	258.98	1.18%
5	296.7	1.84%
6	341.9	1.55%
7	392.5	1.25%
8	399.5	1.88%
9	492.7	1.79%
10	521.7	1.32%
11	559.1	1.05%
12	595.94	1.72%

Table 2 - Suspended panel: natural frequencies and damping ratios.

The "non Rayleigh" damping that characterizes the investigated structure does not only affect the FRF shape but has a second important consequence related to mode shapes. Each natural frequency is associated to a particular distribution of vibrational amplitude known as mode shape. If the excitation frequency matches exactly a natural frequency the structure will deform exactly according to that vibrational pattern. Mode shapes typically consist in region of vibration of uniform phase separated by nodal lines from cells of vibration characterized by opposite phase. Nodal lines are characterized by zero amplitude of vibrations [44]. Only systems whose damping is distributed proportionally to local mass and stiffness exhibit real modes characterized by points vibrating either in phase or in opposite phase. Any other damping distribution leads to complex modes in which the phase is continuously varying and no pure nodal lines appear [44]. Any region can be considered completely in phase or out of phase with the adjacent one. The phase is position dependent and the mode shape varies throughout a period [44].

The nature of the core material induces a damping that cannot be considered asdistributed in a proportional way. In fact, viscoelastic material typically induces hysteretical damping. In principle hysteresis is nothing but a lag between cause and effect. This can clearly be observed for viscoelastic materials subjected to sinusoidal load (Chapter 2). As a consequence, the damping introduced by the viscoelastic layer cannot be considered as linear combination of local mass density and/or stiffness. This results in the identification of complex mode shapes for the investigated structure.

Anyhow, for the sake of completeness in describing the panel modal behavior, the equivalent real modes have been extracted. The identified mode shapes up to the eleventh mode are reported in Figure 82:

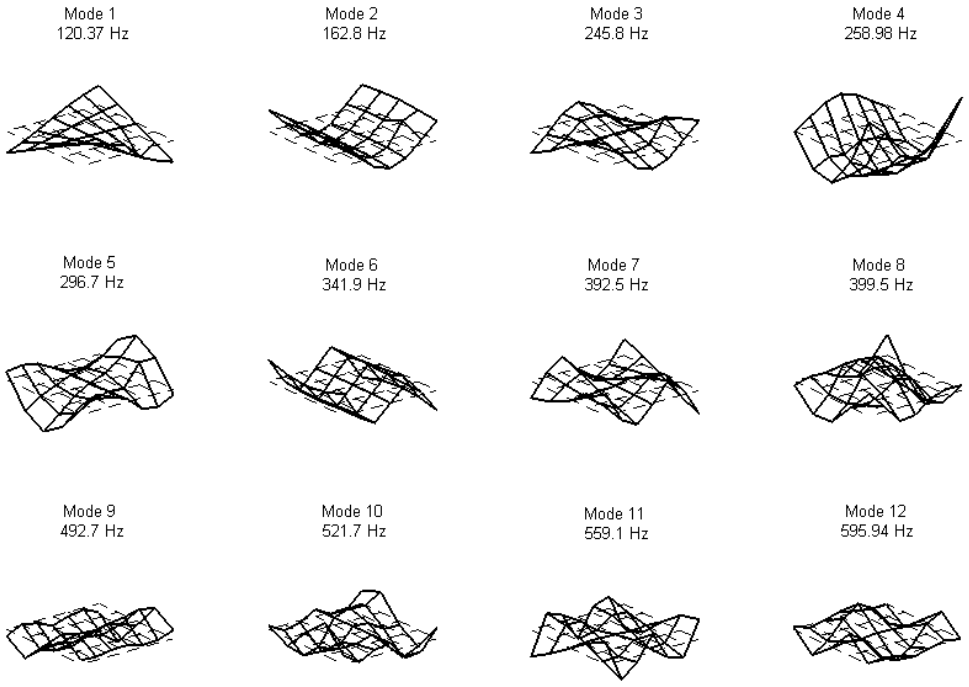

Figure 82 - Mode shapes free free conditions.

3.1.2. Clamped panel modal analysis

Beside the numerical model validation, the experimental activity may be addressed to the characterization of the structure under operating conditions. This means that the experimental set up boundary conditions have to reproduce the structure working conditions. The panel under investigation has to be designed essentially to provide sound and vibration transmission reduction. Irrespectively of the source of the noise and vibration source, it is very likely that the panel will be installed by clamping it along the edges. For this reason, a second experimental modal analysis has been carried out to evaluate the panel response in its possible operational conditions.

The panel has been set between two steel frames and clamped along its edges with a set of bolts.

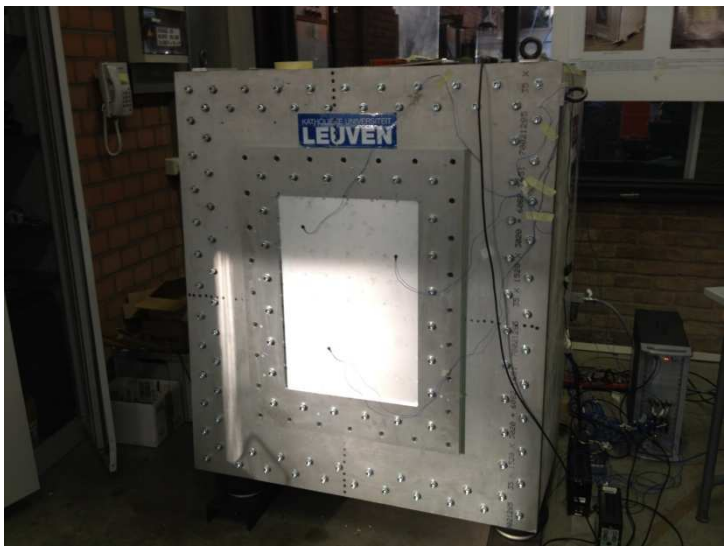

The excitation is given with the impact hammer due to its simplicity and immediacy. As for the case of the suspended panel, the impact has to be narrow enough to ensure the excitation of the whole frequency range of interest.

Concerning the measurement grid, it has to be refined with respect to that defined for the suspended panel. The typical mode shapes of a clamped panel are characterized by an higher number of halfwaves with respect to the homologous mode shapes of a suspended panel. As a result, more measurement points are required to identify with sufficient accuracy the mode shapes of interest. The measurement grid for the clamped panel conditions is displayed in Figure 83. In this

case too the rowing hammer technique is applied. The sensors position is fixed and the excitation point is moved to cover the whole testing area.

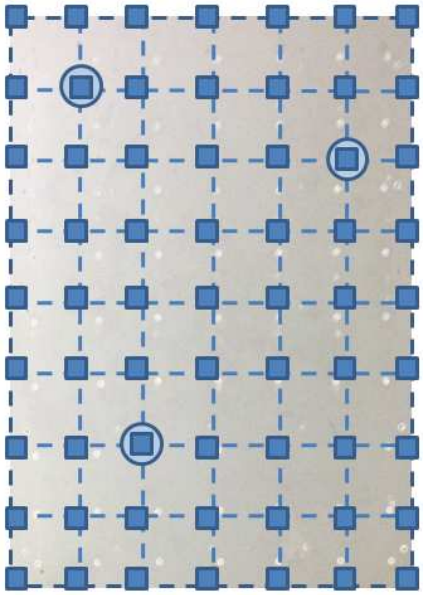

Figure 83 - Clamped conditions : measurement grid (Squares: excitation points - Circles: accelerometers).

Results and data analysis

InFigure 84 an example FRF of the clamped panel is displayed. The global investigated frequency range spans from 0 Hz to 1 kHz in agreement with the experimental campaign carried out on the suspended panel.The frequency region in which it is possible to identify the single resonant modes contribution is limited to around 500 Hz. Above that frequency the modal density and the effect of damping is such any individual mode dominates the structural behavior. As a consequence, the identification of modal parameters has been limited to the 0 Hz - 600 Hz range.

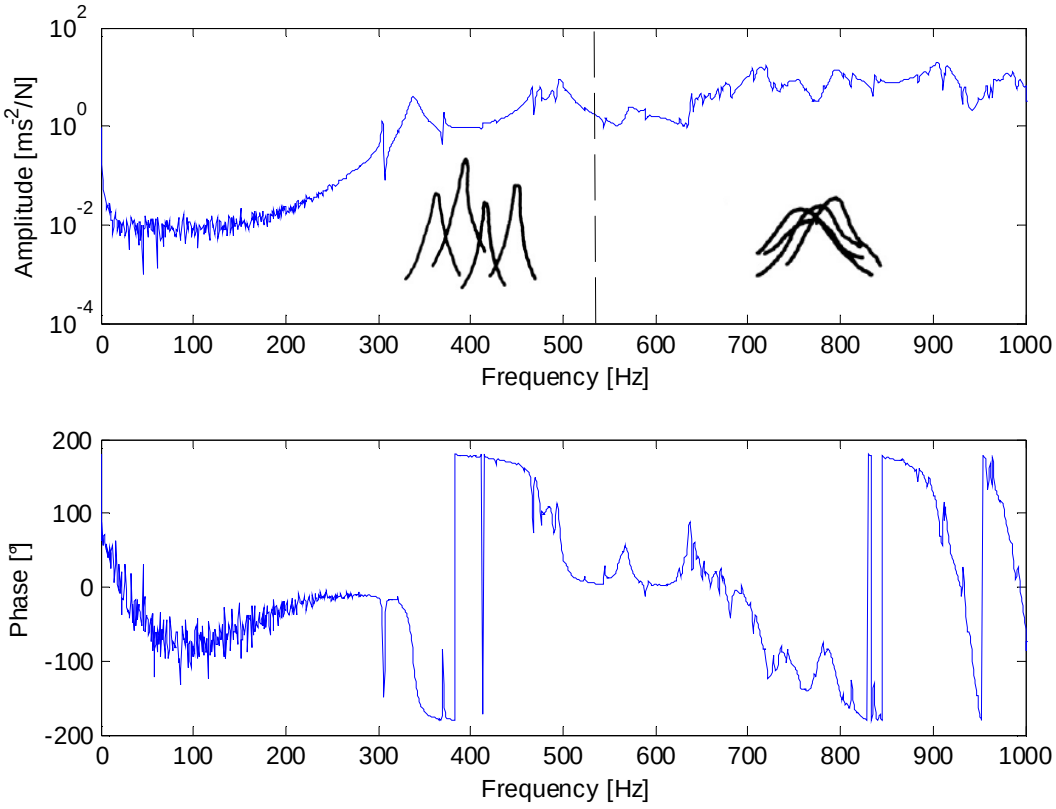

Figure 84 - Clamped Panel: FRF.

The sum of the FRF is calculated according to (4.2) and displayed in Figure 85. The analysis of the FRF sum highlights the fact that the structural behavior can be approximated as sum of single resonant modes only up to around 600 Hz.

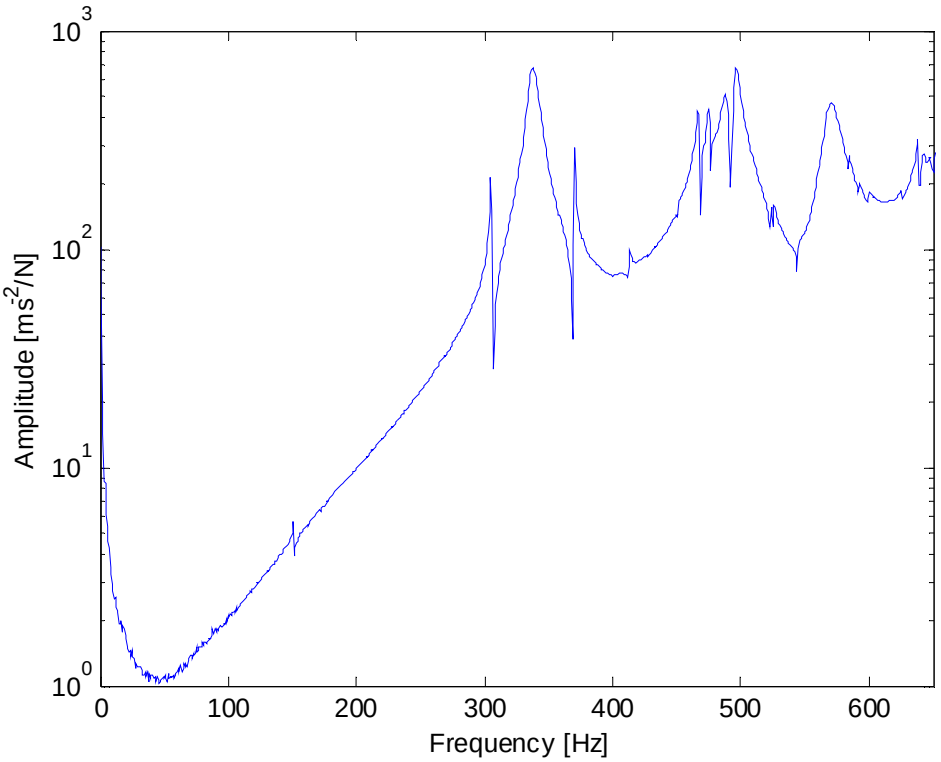

Figure 85 - Clamped panel : FRF sum.

Figure 85 exhibits one of the typical phenomena that occurs in analyzing the clamped structure. Focusing on the first peaks, in the frequency range 200 Hz - 450 Hz (Figure 86), three modes can be expected in that range. The identification of mode shapes for all the three peaks leads to exactly the same structural deformation, although slight asymmetry can be observed comparing the first and third mode shape. The FRF phase, see for instance Figure 84, points out a clear transition in correspondence of the biggest peak, testifying the existence of a structural mode. The phenomenon of "peak splitting" is mainly related to clamping imperfections. It can be demonstrated, that a not uniform distribution of the stiffness results in extra peaks close to the one corresponding to real structural modes[50].

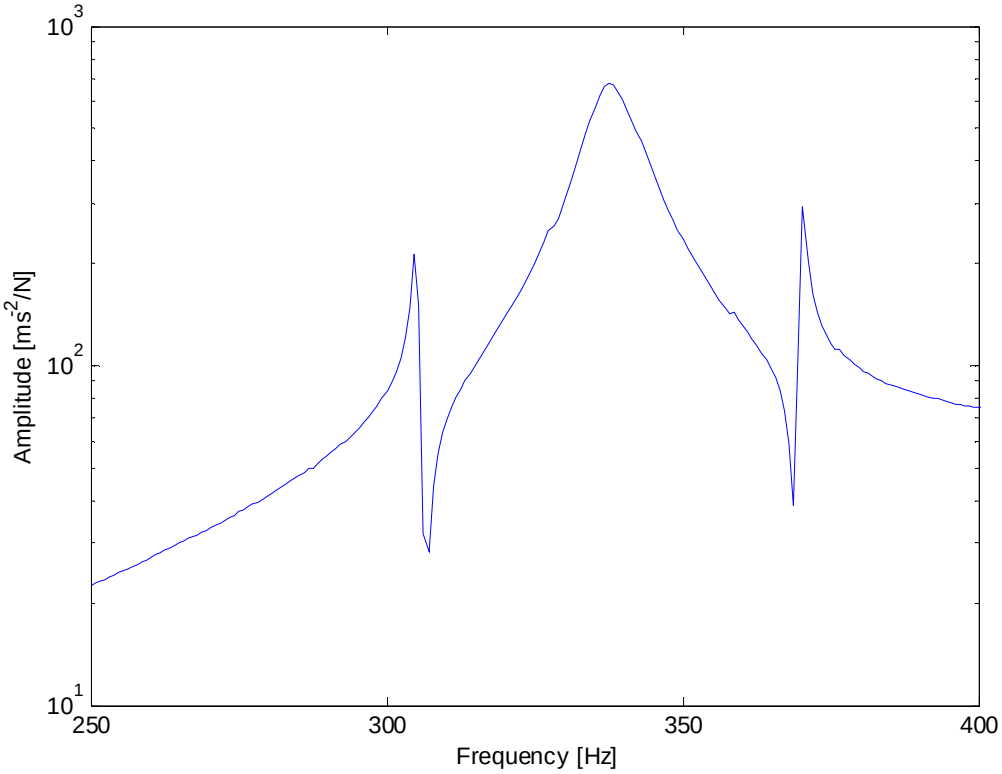

Figure 86 - Clamped panel: FRF sum (zoom on 250 Hz - 400 Hz).

The acquired data have been analyzed with the p-LSCFD method. The natural frequencies and damping ratio that have been identified with sufficient accuracy are reported in Table 3. The damping ratios are higher than 1% to testify the effect of the viscoelastic layer on vibration damping.

Mode #	Frequency [Hz]	Damping ratio %
1	337.56	1.10 %
2	569.81	1.20 %

Table 3 - Clamped panel: frequencies and damping ratios.

As explained in paragraph 3.1.1, the viscoelastic layer leads to a damping distribution that cannot be approximated as a linear combination of local mass density and local stiffness. As a result, the mode shapes of the clamped panel are not real but have an imaginary part that is not negligible. For the sake of

completeness, the equivalent real mode shapes have been calculated and are displayed in Figure 87.

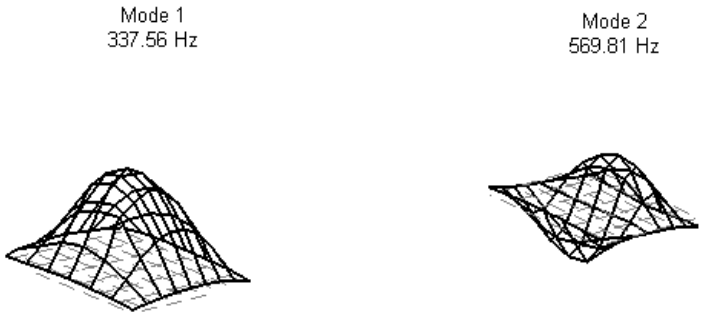

Figure 87 - Clamped panel: Mode shapes.

A dedicated testing campaign has been carried out to evaluate the effect of the boundary conditions. The bolts have been closed with two different but uniform torques, 30 Nm and 50 Nm. The FRFs obtained for a point situated in the low left quarter of the panel are displayed in Figure 88. The non linear behavior induced by the presence of the viscoelastic layer results in a shift of the peaks of the FRF and in a change of the width of the peaks.The difference among the two test conditions influences as well the obtained results.

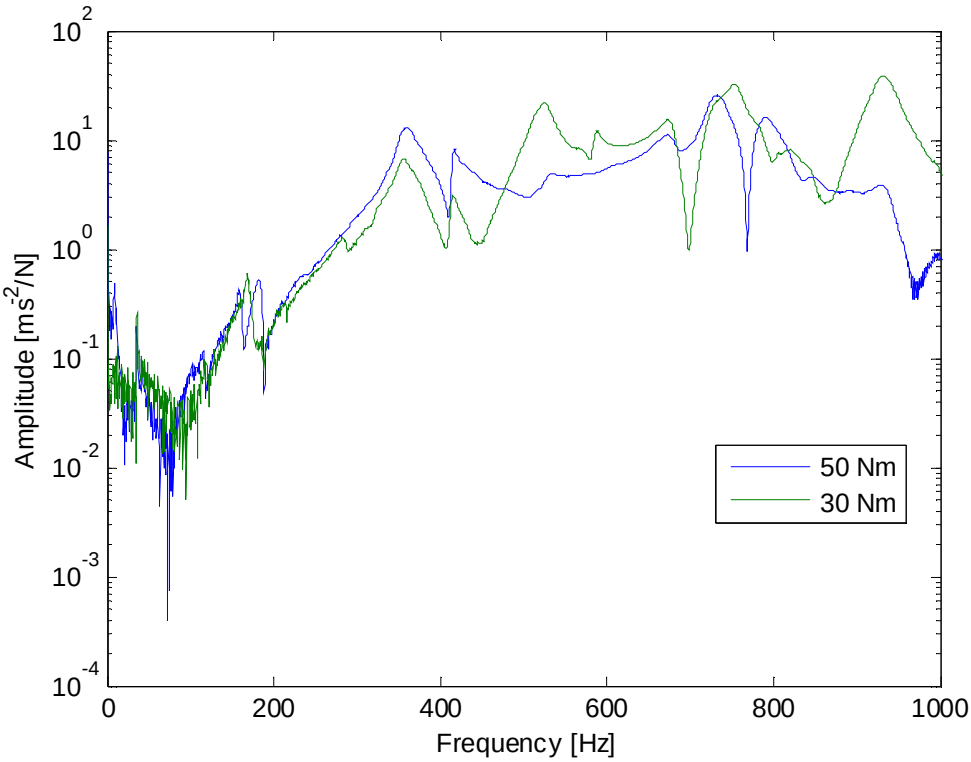

Figure 88 - Clamped panel: comparison between different clamping torques.

The experimental campaign carried out with clamped edges conditions highlighted the high sensitivity of the investigated structure to the boundary conditions. As a result, the better strategy to identify the panel dynamic behavior is the modal testing in free free boundary conditions. In these conditions the interference of the testing setup and the tested structure results to be minimum. As a result the test conditions do not affect the structural behavior and it is possible to accurately extract the dynamic behavior of the investigated panel.

3.1.2.1. Investigation of the adhesive layer dynamic effect

A more detailed analysis of the sandwich panel of Figure 74 reveals the presence of two viscoelastic layer. The structure manufacturing, in fact, implies the insertion of an adhesive layer among the core and the skins to bond together the different panel components. The adhesive layer is made by an epoxy resin that typically exhibits viscoelastic behavior [51]. A dedicated experimental campaign has been carried out

in order to evaluate the influence of this second viscoelastic material on the global panel behavior.

In order to evaluate the effect of the adhesive material on the structural dynamic behavior the test has been performed using simple Aluminum plates and free free boundary conditions. In this way all the possible causes of non linearity have been eliminated, besides the glue layer. The excitation device is the impact hammer and the measurement grid has been designed to capture the first ten modes of the plate, identified on the basis of a simple finite element model. The accelerometer mesh can be seen in Figure 89. The sensors and excitation points are fixed. The latter is situated in the top left corner of the plate rear side.

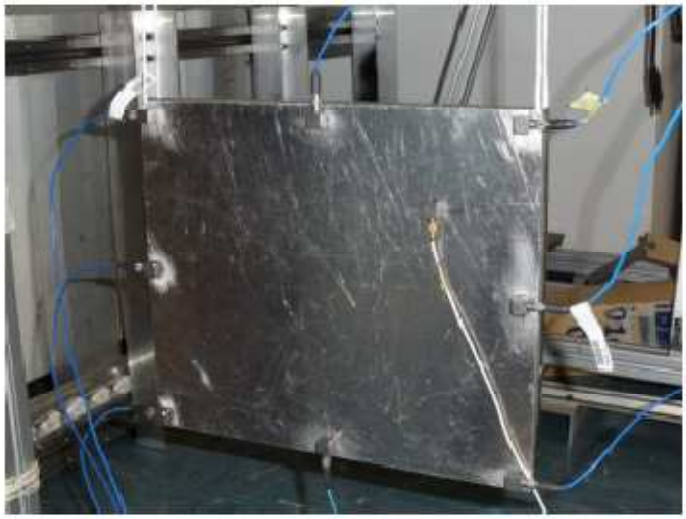

Figure 89 – Adhesive layer dynamic effect evaluation: testing setup.

The test has been performed on two different structures:

- A twelve mm Aluminum plate
- Two six mm Aluminum plate bonded together with a layer of glue provided by the panel manufacturer

The co located FRFs of both investigated structure are displayed in Figure 90. The global function shape is the same in both cases. A slight shift of the natural frequencies can be observed. This has been considered as an effect of the different stiffness of the two structures.

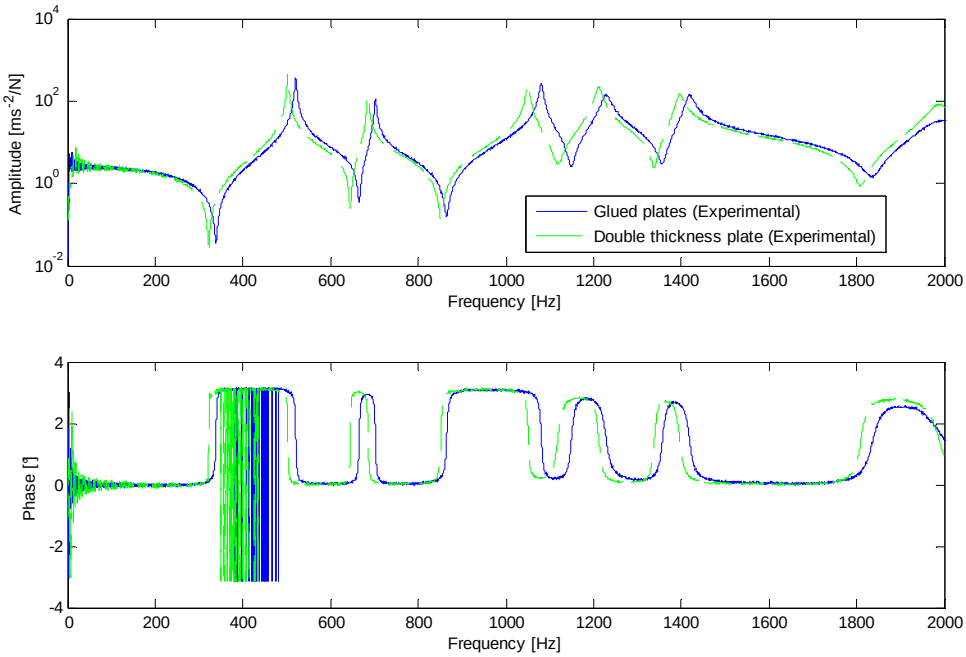

Figure 90 - Comparison among FRF single 12 mm plate - glued plates.

Besides the effect on natural frequencies, the effect on damping ratios has to be carefully investigated. The main consequence of adding a viscoelastic layer to a structure is the enhancement of the structural vibration damping capability. The damping ratios of both structures have been determined applying the p-LSCFD method to the measured FRF data. The values are reported in Table 4and their comparison underlines the absence of additional damping by the adhesive layer. The differences among the values are in the uncertainty range that characterizes the damping estimation.

Mode #	Double Thickness plate damping ratio %	Glued Plates Damping ratio %
1	0.25 %	0.32 %
2	0.23 %	0.26 %
3	0.28 %	0.35 %
4	0.53 %	0.81 %
5	0.56 %	0.62 %

Table 4 - Aluminum plates: damping values comparison.

The presence of a viscoelastic adhesive material has been considered negligible from a dynamic point of view also for the sandwich panel under investigation. This conclusion has been drawn based on the results obtained on the test with Aluminum plates but in particular considering the effective thickness of the glue layer in the sandwich structure. The characteristic dimension of the adhesive layer is way lower than the thickness of core and skins. As a result, the whole damping effect due to viscoelastic material insertion is given by the foam core.

3.2. Test case: Sandwich panel with foam core – A4 size

The experimental campaign described in paragraph 3.1 aims to obtain reliable data to validate the numerical model. The reliability of a numerical model has to be assessed in terms of its predictive capability. The model has to be able to mimic the structural dynamic behavior in a reliable way although the structure has different parameters compared to the one used for the model validation. In this framework a second test case has been investigated. A second experimental campaign has been carried out on a panel having different dimensions with respect to the one chosen for the model validation. Either the skins or the core materials are the same of the panel described in paragraph 3.1 but the dimensions are smaller. In particular the in plane dimensions are 210 mm x 300 mm where the panel of paragraph 3.1 is 860 mm x 660 mm.

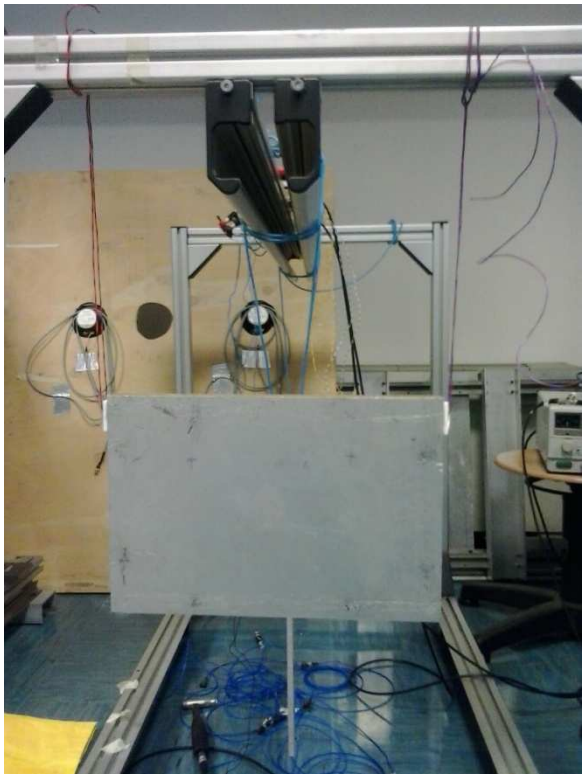

Figure 91 - Small panel.

The small panel has been tested using the impact hammer and considering free free boundary conditions. The excitation and the measurement points remained fixed during the tests. The small sandwich panel has been tested using the same testing setup as the Aluminum plates of paragraph 3.1.2.1. The measurement grid, designed to capture the first ten structural mode shapes, is displayed inFigure 89. The top left corner of the rear side of the panel has been chosen as excitation point.

The lightweight of this small panel with respect to the big one leads to a slight modification of the testing protocol. Among others, the width of the useful frequency range is a key parameter in choosing the impactor. This is particularly important dealing with lightweight structures that exhibits the first natural frequency towards the 1kHz region. The impact frequency spectrumhas to be flat in the whole frequency range of interest to guarantee the excitation of the investigated modes [47]. As mentioned in paragraph 3.1.1, the characteristics of the impactor play an important role in determining the quality of the excitation. Whether used to excite the small panel, the impact hammer commonly used to test medium sized structures leads to a auto power spectrum that can be considered flat for less than 1kHz (Figure 92, left). The input given to the structure is thus almost meaningless above around 600 Hz.

The choice of a smaller impact hammer for testing the "small" panel leads instead to a frequency spectrum that can be considered flat for more than 2kHz.

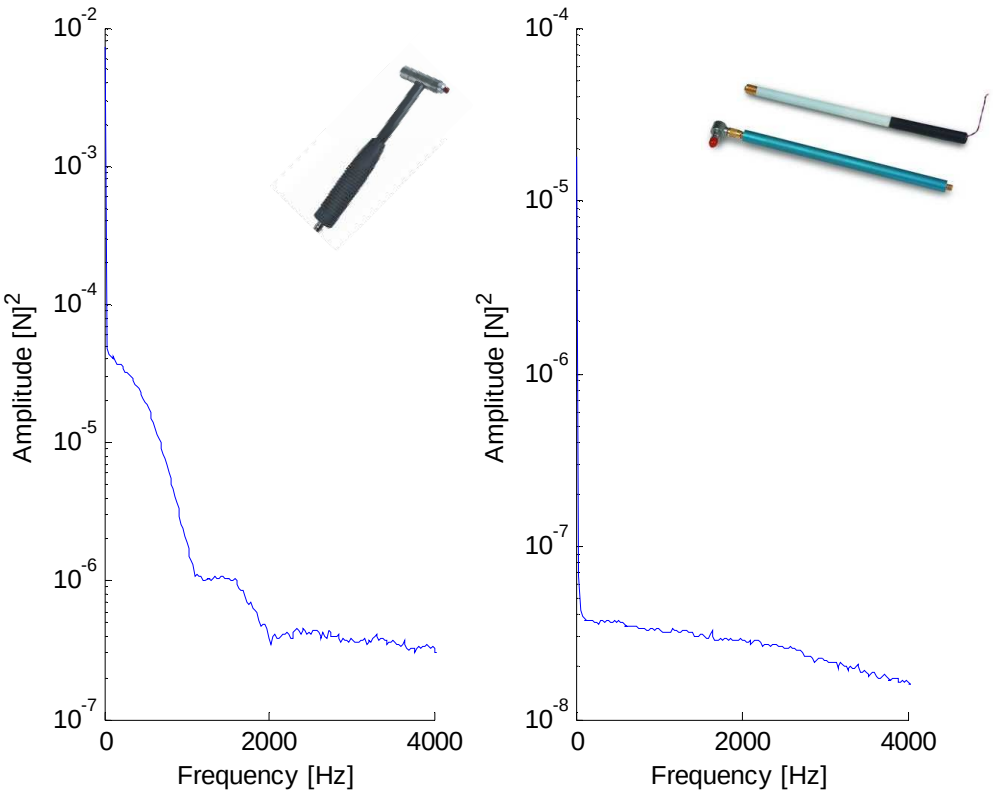

Figure 92 - Comparison between different hammer power spectra.

The co located FRF is reported in Figure 93. The small panel is lighter with respect to the of Figure 75. As a consequence the natural frequencies are shifted towards higher values, thus the investigated frequency range is expanded to 2 kHz. As noticed analyzing the “big” panel, the FRF can be divided in two zones: a “low ” frequency range in which it is possible to identify the contribution of single resonant modes and an “high” frequency range in which the modal density and the damping are such that any mode is predominant on the others. In the case of the small panel the "low" frequency range spans from 0 Hz to 1000 Hz and only two modes can be clearly identified.

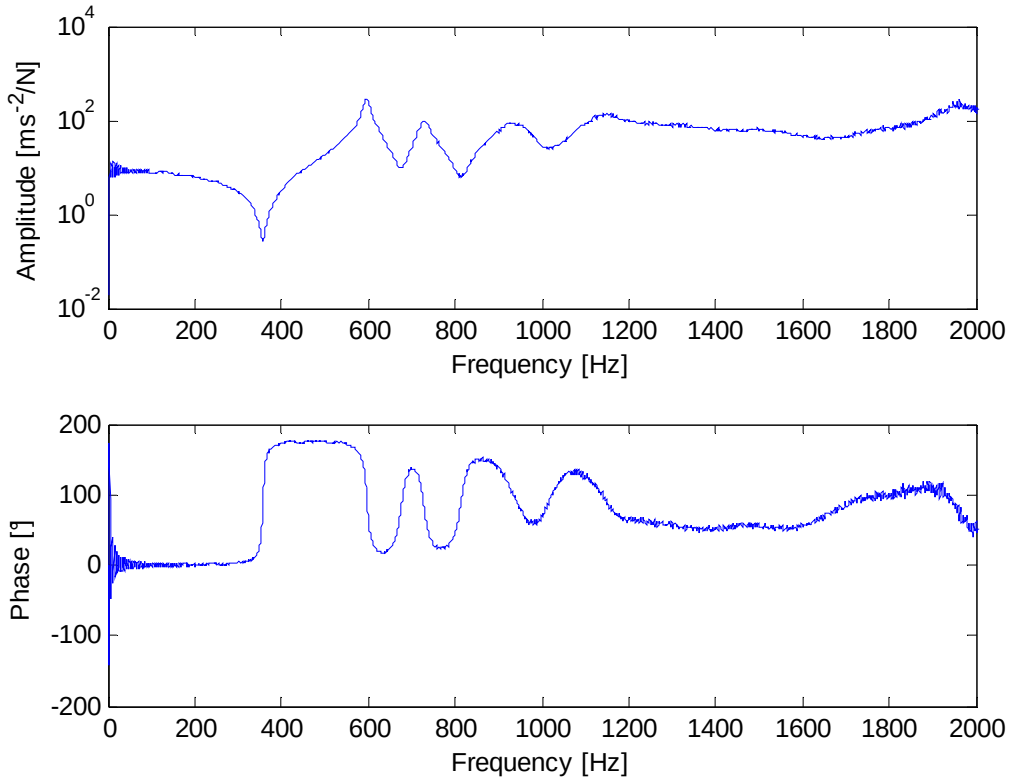

Figure 93 - FRF Sandwich panel small.

The obtained FRF data have been analyzed with the p-LSCFD method. The obtained natural frequencies and damping ratios are reported inTable 5. Although the frequencies are significantly different with respect to the one identified for the big panel (Table 2), the damping ratios are of the same order of magnitude. The values, around 1% or higher, are a consequence of the presence of a viscoelastic layer.

Mode #	Frequency [Hz]	Damping Ratio %
1	596.74	1.16 %
2	727.89	1.71 %

Table 5 - Small panel: natural frequencies and damping ratios.

The mode shapes associated with the frequencies of Table 5are displayed in Figure 94. The viscoelasticity of the core leads to the identification of complex mode shapes as well as in the big panel test case. In Figure 94 the equivalent real modes are displayed.

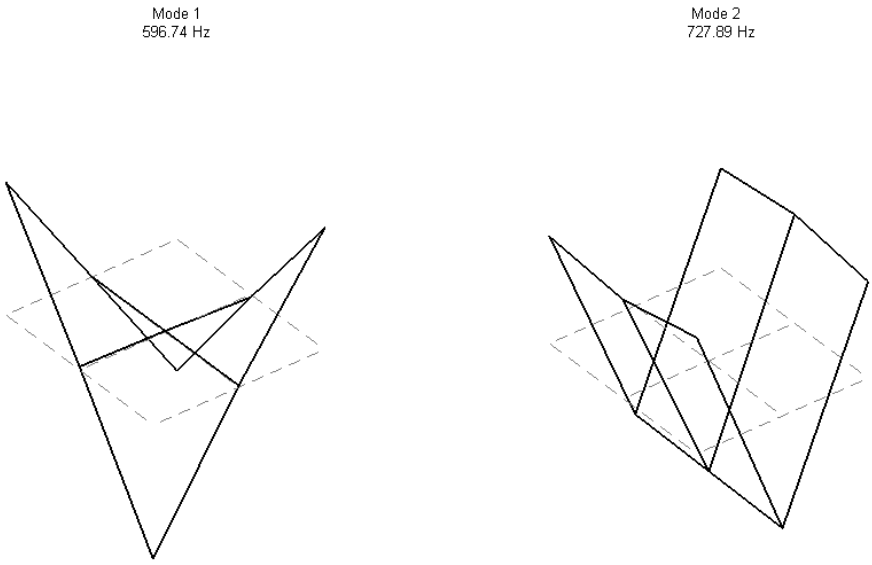

Figure 94 - Small panel: Mode shapes.

The test performed on the big panel showed a significant sensitivity of the panel to the torque applied to the bolts (Figure 88). Given the lightweight and the smaller dimension, the same can be expected for the small panel. A preliminary test has thus been carried out to check the panel reaction to the clamping system. Different torques have been applied to the screws and nuts in a uniform way.

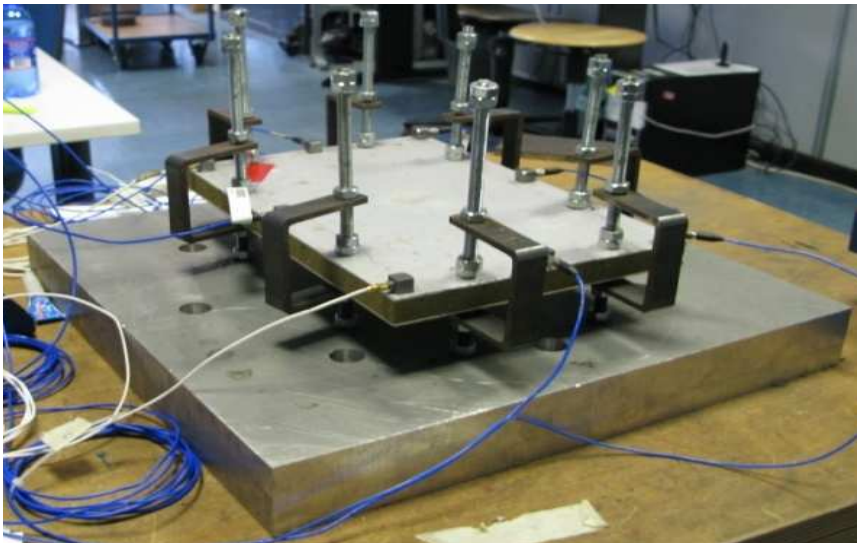

Figure 95 - Small panel: clamped conditions.

In Figure 96 the comparison of the obtained FRFs is displayed. Not only the small panel exhibits sensitivity to the magnitude of the clamping torque but it is barely possible to individuate a frequency range in which the panel response is given by single resonant modes. As a consequence, any mode can be identified with sufficient reliability applying a classical modal analysis theory.

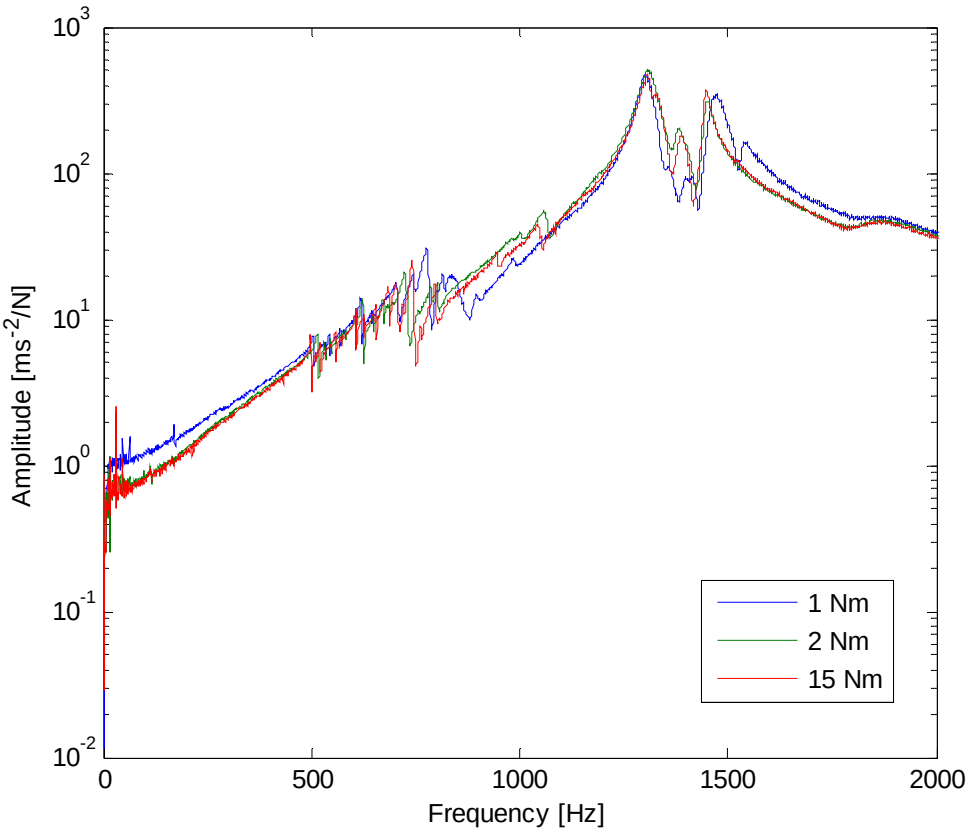

Figure 96 - Small panel: comparison among different torques.

The dynamic of both panels, big and small, is strongly influenced by the viscoelasticity of the core material. As a consequence, an accurate identification of the core material properties, as described in paragraph 2, becomes even more important to lead to a reliable dynamic numerical model. The reliability of the latter is crucial to obtain an accurate prediction of the structure vibroacoustic characteristics. Modal parameters are in fact the main input of the coupled FE-BE model. The accuracy of the vibroacoustic behavior prediction will be checked comparing the numerical results with the experimental data obtained through a dedicated testing campaign that will be detailed in the next paragraph.

4. Vibroacoustic behavior identification

The vibroacoustic numerical model validation is the final aim of the whole experimental activity that has been carried out. The performances of the panel shown in Figure 74 have been investigated either from a dynamic or from a acoustic point of view.

The dynamic behavior has been characterized in terms of modal parameters, such as natural frequencies and mode shapes, and frequency response function. The typical index that is used for the experimental identification of the structural acoustic behaviour in terms of sound transmission performances is the Transmission Loss (TL) described in Chapter 2and defined as the ratio of the incident sound power and the transmitted power (4.3):

$$TL(f) = 10\log\frac{\Pi_{incident}}{\Pi_{transmitted}} \tag{4.3}$$

Measurements standards, as the ASTM E90 [52], define the procedure to evaluate the TL of a structure. The methodology is called “two room method”. Generally speaking, it prescribes the measurement of the space and time averaged sound pressure levels in two adjacent reverberant rooms divided by a partitioning wall that hosts the object under investigation (Figure 97).

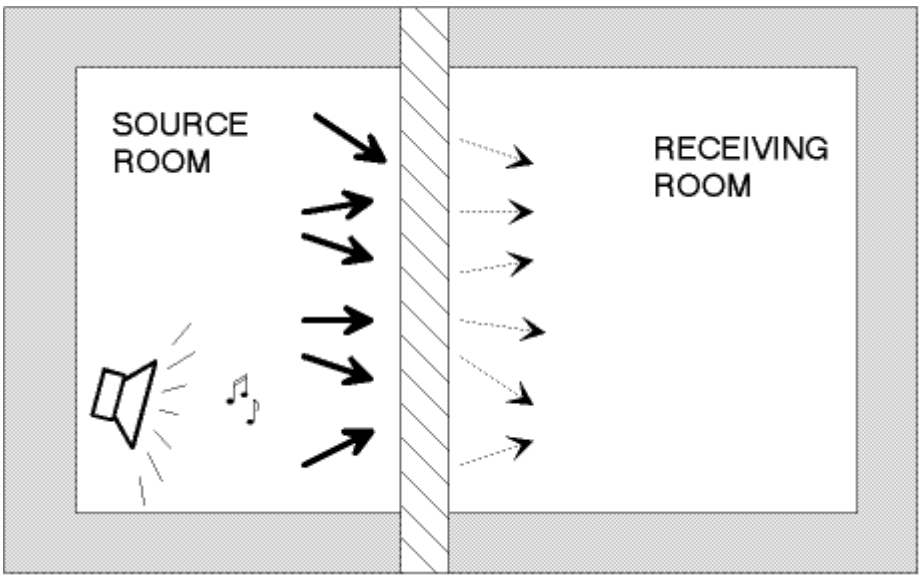

Figure 97 - Two rooms sound TL test rig.

Typical sound TL suites requirevery big volumes resulting to be not easy to implement and they require samples with a minimum dimension of the order of 2.5 m (except for the thickness). Strict requirements are imposed on the sound field characteristics in both rooms. In particular, the configuration with two reverberant rooms requires the presence of a diffuse field, i.e. the acoustic energy is uniformly distributed in the room volume. This condition is reached in an easier way considering a big room volume and highly reflective room surfaces. A different technique has been proposed to partially overcome these last requirements. It can be proved that the direct measurement of the sound intensity on the receiving side provides enough information to calculate the Transmission Loss, provided that the sound field in the source room is diffuse. The condition of diffuse field in the source room is the only requirement for this technique and it is more likely to be satisfied over a wide range of frequency [53].

In many practical cases, a different index to evaluate the sound transmission performances of a structure is considered more significant: the Sound Insertion Loss (IL). The IL defines the change in sound power radiated by a sound source with and without the test object. Mathematically, the IL is defined as the ratio of the sound power without the object and the one with the object:

$$IL(f) = 10\log\frac{\Pi_{open}}{\Pi_{closed}} \tag{4.4}$$

The TL is generally considered a more fundamental index with respect to the IL since this latter depends upon factors not strictly related to the object properties such as the amount of absorption in the receiving space[54]. Anyhow, the analysis of the IL trend towards frequency allows one to identify all the relevant vibroacoustic features as well as the TL curve analysis described in Chapter 2. The evaluation of the sound power, and thus IL, through intensity measurement,releases the constraint of calibrating the absorptivity of the receiving room. Actually not such a room is necessary [54]. Given the future application of the investigated structure, the usage of the IL index instead of the TL one is considered more significant. The final aim is indeed to evaluate the change in terms of acoustic insulation with the proposed solution with respect to the "bare" condition.

The IL index is easy to evaluate experimentally using equation (4.4). Considering an enclosure with an opening, the IL is simply computed comparing the radiated sound power with and without the test object placed at the opening and fully closing the enclosure (Figure 98).

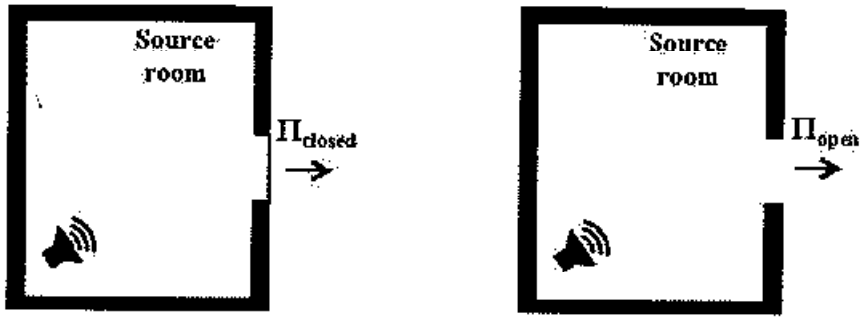

Figure 98 - Sound IL measurement procedure [55].

The panel of Figure 74has been tested using a particular test rig developed by Katholieke Universiteit Leuven. The test rig is a small reinforced concrete cabin, with no parallel walls, designed to give a uniform distribution of acoustic natural frequencies. The facility, displayed in Figure 99, allows to test samples of different sizes thanks to the availability of several mounting frames. Approximately, it is possible to test panels from A1 to A4 standard dimensions. The cabin is equipped with a speaker and microphones that can be placed in several configurations (Figure 99). In addition, the set up is insulated from the ground vibrations by means of air springs. A detailed description of the construction steps and test rig characteristics can be found in [55].

Figure 99 - PMA Sound Box: exterior (left), interior (right).

The testing procedure evaluates the IL starting from intensity measurements. The application of sound intensity measurement to evaluate the transmitted power has been extendedly studied and is demonstrated by Cops and Minten [54, 56]. The transmitted sound intensity distribution is measured using a p-p intensity probe on a

surface parallel to the partition for the both cases of open and closed window (Figure 100).

Figure 100 - Intensity distribution measurement, open and closed window configuration.

The p-p probe is a device in which two nominally identical high quality sound pressure transducers are placed close one to each other in a support designed to minimize the diffraction of the incident sound field. The distance between the two microphones determines the upper frequency limit in the probe application. In particular, the shorter the spacer the higher the frequency limit. A commercial example of sound intensity probe is displayed in Figure 101.

Figure 101 - P-P intensity probe.

A white noise signal has been used for the investigation of the vibroacoustic behavior of the panel. The sound intensity has been recorded at the central point of each square of Figure 83.The analysis of the IL curve towards frequency allows the identification of the regions in which either the modal behavior of the panel or the mass or the coincidence effects dominates the vibroacoustic response. In analogy with the TL curve description detailed Chapter 2, each region is analyzed separatelyhereafter.

Low frequency range - Modal region

In the low frequency range the modal panel behavior dominates the global vibroacoustic response. The spacer between the microphones is 50 mm to limit the measurement range between 20 Hz and 1.25 kHz. The experimental IL is displayed in Figure 102. Two main drops are clearly visible but only the second one is related to the panel behavior. The drop around 150 Hz is mainly due to a resonance of the cavity itself [55]. Instead the drop around 300 Hz is dependent on the modal panel behavior. According to the identified mode shape at 337 Hz, Figure 87, the panel becomes a perfect radiator leading to a poor sound transmission reduction. The other modes below 1kHz are less effective on the panel sound IL.

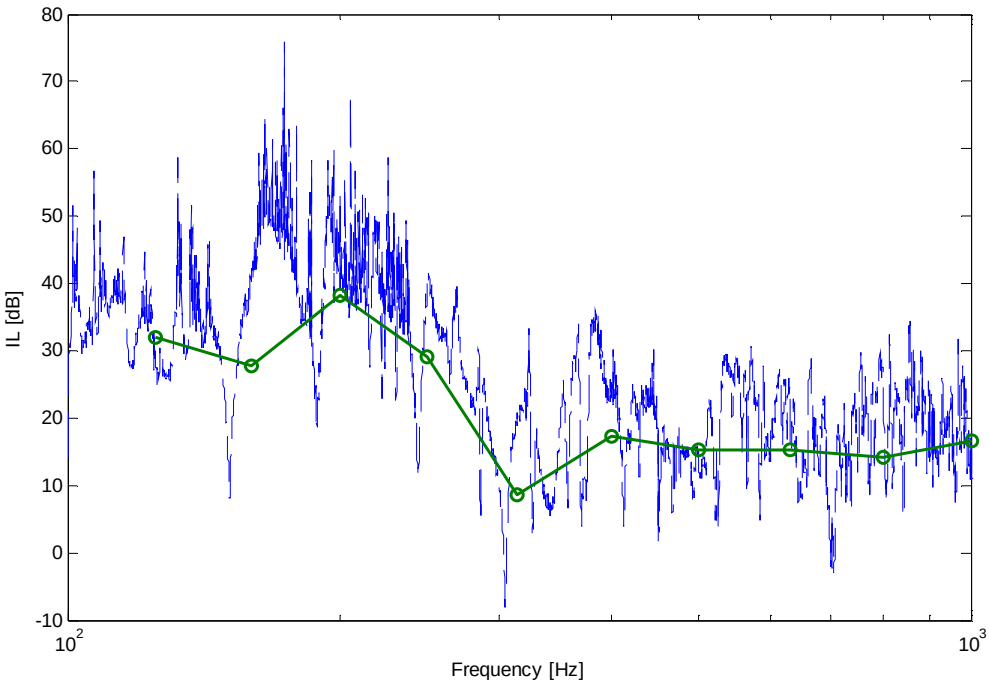

Figure 102 - Experimental IL: narrow band (blue dashed line), third octave band(green solid line).

Figure 103 displays the comparison of sound IL values between the investigated panel and a bare Aluminum panel 3 mm thick (data courtesy of KUL). The thickness of the Aluminum panel is exactly the same as the sandwich panel skins together. The sandwich panel exhibits a greater sound IL below its first natural frequency. After that frequency the addition of a viscoelastic layer doesn't increase the sound transmission reduction performances. This is due to the choice of viscoelastic material. The closed cell foam helps in damping vibrations but it is characterized usually by poor acoustic properties [57, 58].

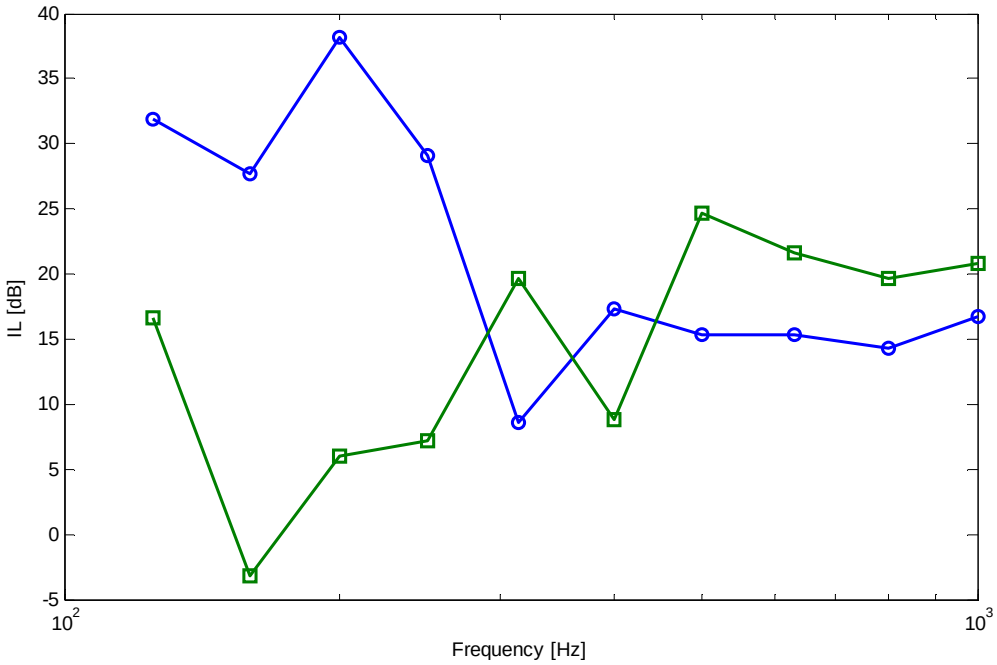

Figure 103 - Sound IL comparison: sandwich panel (blue circles) vs 3 mm Aluminum panel (green squares) (courtesy of KUL).

The pressure map corresponding to the drop in the IL graph is displayed in Figure 104. The measured pressure values confirm the tendency of the panel to radiate sound according to its first mode shape (Figure 87).

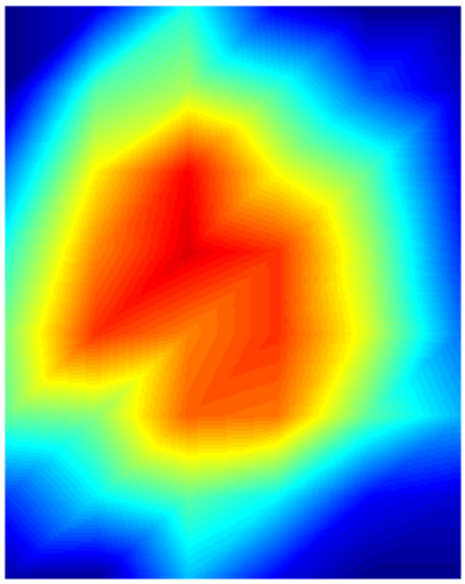

Figure 104 - Pressure map: third octave band centered on 315 Hz.

Mid - high frequency region - Mass control and coincidence effects

The vibroacoustic behavior in the midfrequency range is controlled by the panel mass. The probe set up has been modified inserting a spacer of 8.5 mm to extend the measurement range to 7.1 kHz. The measured sound IL is reported inFigure 105.

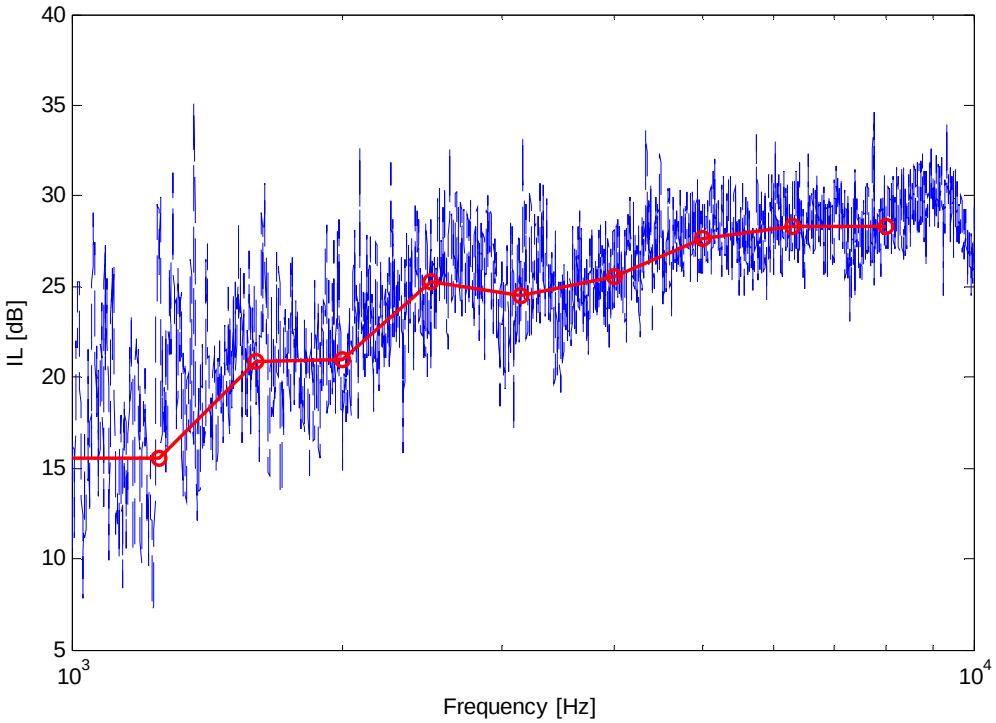

Figure 105 - Sound IL mid - high frequency range: narrow band (blue dashed line), third octave band (red solid line).

The sound IL exhibits the linear trend towards logarithmic frequency scale that is typical of the mass controlled region. The analysis of the narrow band trend of the IL highlights two dips not clearly visible in the third octave trend due to the width of the third octave bands at high frequencies. Figure 106 gives a clearer view of the presence of the dips. The red dashed lines have no relation with the measured data, they are simply visual aids to highlights the change in the sound IL slope that is due to the presence of a dip.

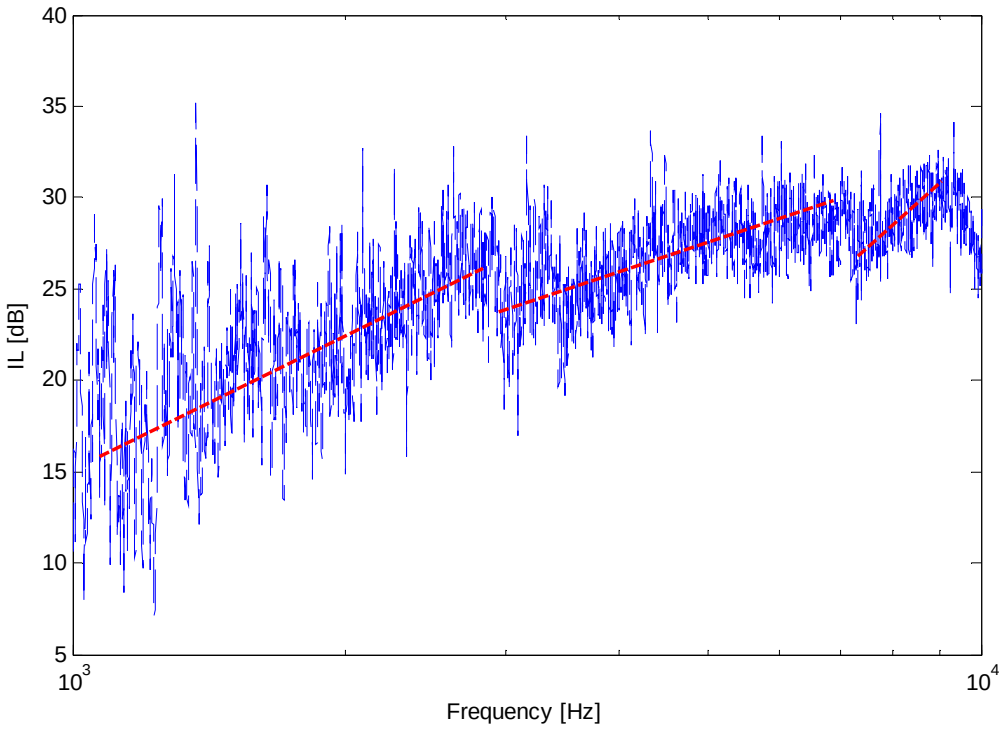

Figure 106 - Sound IL : dips in the mid high frequency range.

The first dip occurs around 3 kHz. This drop in the sound IL trend can be attributed to a coincidence phenomenon. According to equation (2.3), the coincidence for a homogenous 3 mm thick Aluminum panel occurs around 3900 Hz. The analyzed dip is around 3200 Hz. The shift towards lower frequency may be due to the addition of the soft core layer. The foam core increases the stiffness in a way that is proportionally higher than the resulting weight increase. As a result, the coincidence frequency sets at lower values than the one of an Aluminum panel of equal thickness than the panel skins.

The second dip occurs around 7.5 kHz. Considering the type of structure a second coincidence effect can be expected (Chapter 2). The symmetric sandwich motion implies the out of phase displacement of the two face sheets towards the soft core (Figure 107).

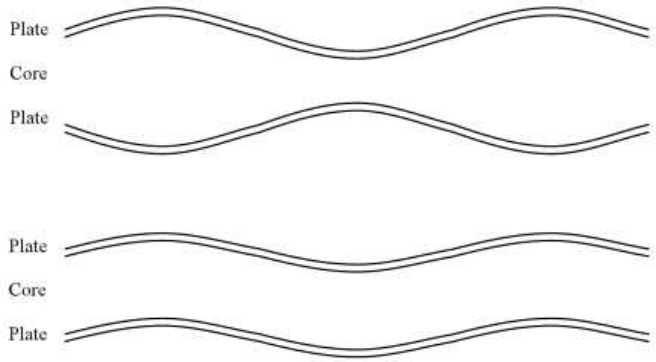

Figure 107 - Symmetric (top) and anti - symmetric (bottom) motion of a sandwich panel[59].

The so called "double wall frequency", proper of the symmetric panel motion, can be estimated roughly through the (4.5):

$$f_{DW} = \frac{1}{2\pi}\sqrt{\frac{E_c}{t_c}\left(\frac{1}{m_{f1}}+\frac{1}{m_{f2}}\right)} \tag{4.5}$$

where E_c and t_c are respectively the Young Modulus and the thickness of the core and m_{f1} and m_{f2} are the surface mass of the face sheets, equal in the investigated panel. The Young Modulus of the core is frequency dependent thus the (4.5) cannot be directly applied. Considering the average value of this parameter, around 63 MPa, and approximation of the double wall frequency is 7060 Hz.

The symmetric motion phenomenon has been investigated through a dedicated experimental campaign. Ten accelerometers have been placed on both sides of the clamped panel of Figure 83 according to the two measurement configurations of Figure 108. The central point acceleration has been measured in both configurations depicted respectively by blue and red squares in Figure 108.

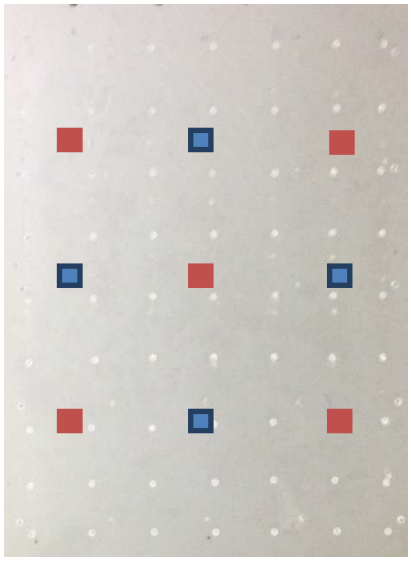

Figure 108 - Double wall motion investigation: measuring grids.

A white noise signal was sent to the speaker to excite the panel. The response of all the accelerometers in both configurations have been recorded and the relative phase has been analyzed. Around 7200 Hz the phase shift of all the accelerometers is approximately 180° corresponding to a symmetric dis placement of the phase shift. This trend has been confirmed analyzing the mode shapes in the identified dip region. The mode shape at 7270 Hz is reported in Figure 109. The arrows highlight how the core behaves as a spring inducing an out of phase movement of the two skins.

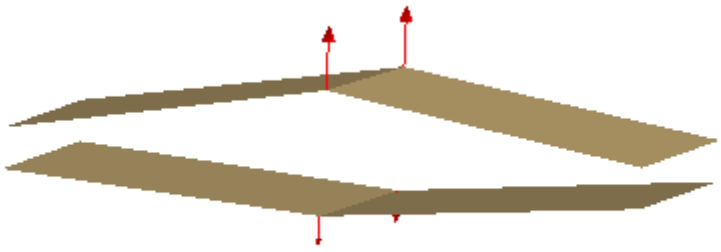

Figure 109 - Double wall mode shape.

The identification of the double wall frequency can be used to retrieve the foam elastic modulus. The inversion of the (4.5) leads to the identification of 67 MPa as

core material Young Modulus. The value isapproximately 15% greater with respect to the one identified through DMA procedure for a frequency of 7000 Hz. The retrieved foam Young modulus will be used for model updating purposes.

The whole experimental campaign led to the availability of a huge amount of data that play a key role in the development of a reliable numerical model. The foam properties characterization is a fundamental input of the model itself while the dynamic and acoustic characterization of the big panel are suitable to assess the model prediction capability. The dynamic tests performed on the small panel instead will be used to verify the model predictive capability.

CHAPTER 5

Chapter 5 focuses on the comparison between the numerical and experimental results. Either the dynamic or the acoustic numerical prediction are validated through the obtained experimental results. Particular attention is paid to the assessment of the dynamic model predictive capability.

1. Numerical and experimental data correlation relevance

Computer Aided Engineering (CAE) methods have become a standard engineering procedure during last years. Dealing with sandwich panels it is possible to combine different material properties to reach the best panel performances. This freedom brings to the fore the need for a reliable modeling tool. The aim of the current dissertation is to develop a model that can predict the vibroacoustic performances of different engineering solutions. To do so a double numerical model has been faced (Chapter 3). The dynamic of the panel has been modeled through a FE approach while the sound transmission performances have been extracted developing a coupled FE-BE model.

A crucial point in the development of numerical models is the model validation. The assessment of the model reliability is in fact fundamental aiming to develop a valuable designing tool. The agreement, within reasonable confidence interval, of the numerical outcome of the model with the corresponding experimental results is a good estimator of the model efficiency. As a result, dedicated experimental tests have been designed to obtain reliable experimental data to use for model validation

purposes. The whole experimental campaign has been extensively described in Chapter 4. The conceptual schema behind this fundamental step is displayed in Figure 110. The comparison among experimental and numerical data often implies a subsequent procedure of model updating, focused on the improvement of the model efficiency.

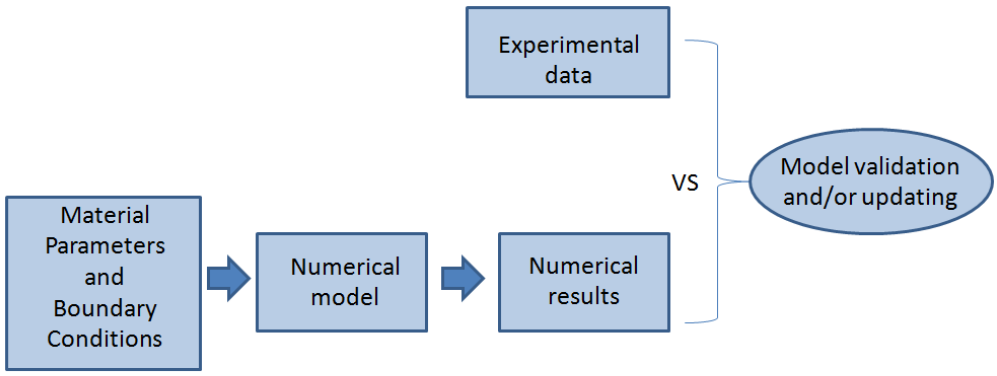

Figure 110 - Experimental and numerical results interaction :Conceptual schema .

The first part of the chapter describes the dynamic model of both tested panels and display the numerical - experimental correlation. Particular attention is drawn on the model predictive capability. Subsequently the vibroacoustic model validation is presented in terms of Insertion Loss comparison.

2. Dynamic model validation

The first step towards the vibroacoustic behavior analysis is the development of a numerical model able to reproduce the modal behavior of the investigated structure. The fundamental outcome of this first step will be the natural frequencies and the associated modal shapes. Due to the modeling choice, this two parameter sets are necessary to reach the aim to evaluate numerically the panel sound transmission performances.

The structural modal parameters are obtained through a FE model of the investigated panel. The panel has been modeled adopting a multilayer approach. The skins and the core have been modeled separately and the three layers have

been connected imposing a tie at the interfaces. The in plane element dimension has been set to 10 mm in order to be able to capture accurately the panel behavior up to at least 5000 Hz according to the (3.10). A screenshot of the adopted model is reported in Figure 111. Free free boundary conditions have been imposed in agreement with the experimental tests described in Chapter 4.

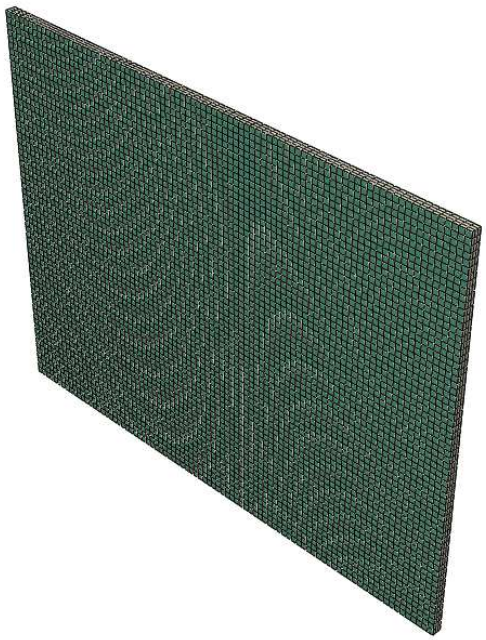

Figure 111 - Finite Element model.

The Aluminum skins have been modeled with shell elements. The material has been considered as linear elastic and the nominal values of that specific alloy have been adopted for density and Young Modulus, respectively 2650 kg/m^3 and 70 GPa. The core has instead been modeled using solid elements. The foam of which the core is made is a viscoelastic material. As a consequence, a Prony series expansion of shear and bulk modulus have been introduced in the numerical model to take in account the viscoelastic effects. As detailed in Chapter 4, a Prony series of suitable order has been fitted on the experimental data to obtain the input model parameter. The adopted FE software requires the definition of the parameters according to the formulas in (5.1). $G^{'}$ and $G^{''}$ are respectively the Storage and the Loss Shear Moduli, as well as $K^{'}$ and $K^{''}$ represent the Storage and Loss Bulk Moduli.

$$G' = G_0\left[1-\sum_{i=1}^{N} g_i\right]+G_0\sum_{i=1}^{N}\frac{g_i\tau_i^2\omega^2}{1+\tau_i^2\omega^2} \qquad K' = K_0\left[1-\sum_{i=1}^{N} k_i\right]+K_0\sum_{i=1}^{N}\frac{k_i\tau_i^2\omega^2}{1+\tau_i^2\omega^2}$$
$$G'' = G_0\sum_{i=1}^{N}\frac{g_i\tau_i\,\omega}{1+\tau_i^2\omega^2} \qquad K'' = K_0\sum_{i=1}^{N}\frac{k_i\tau_i\,\omega}{1+\tau_i^2\omega^2} \tag{5.1}$$

G_0 and K_0 are the instantaneous Shear and Bulk Moduli representative of the material behavior at extremely high frequencies. Bulk and Shear Complex Moduli have been derived from the Complex Modulus experimentally determined through DMA testing (Chapter 4). According to solid mechanics the conversion among these material parameters can be made with the formulas (5.2), where ν is the Poisson Ratio and E the Young modulus:

$$G = \frac{E}{2(1+\nu)} \qquad K = \frac{E}{3(1-2\nu)} \tag{5.2}$$

A first, simple, comparison among experimental and numerical data is the one among natural frequencies. This comparison is of particular relevance since it allows one to assess in a quick glance the correct choice of the material parameter and the appropriate geometric modeling. The data reported in Table 6 show good agreement among experimental and numerical frequencies.

Mode #	Experimental Frequency [Hz]	Numerical Frequency [Hz]	Error [%]
1	120.37	117	2.5
2	162.8	157	3
3	245.8	242	1.2
4	258.98	253	2.3
5	296.7	290	2.03
6	341.9	338	0.88
7	392.5	388	1,02
8	399.5	397	0.5
9	492.7	473	3.8
10	521.7	500	4

Table 6 - Experimental and numerical frequency correlation.

Along with natural frequencies, the correlation among mode shapes is of fundamental relevance from a vibroacoustic point of view. In the low frequency range in fact the panel modal behavior dominates the sound radiation and/or transmission performances. The radiation ratios related to the structural natural frequencies are dependent on the mode shape related to the specific frequency. Consequently, the capability of correctly predicting the structural mode shapes plays a key role aiming to develop an efficient vibroacoustic model. The correlation among numerical and experimental mode shapes can be evaluated through the Modal Assurance Criterion (MAC) index. This index expresses the correlation among numerical and experimental modes. If the MAC between two modes is unity both modes are identical, if the MAC is zero no relation exists between the two mode shapes. The MAC index is typically computed as follows:

$$MAC(i,j) = \frac{\left|\left\{A_{i,num}\right\}^T \left\{A_{j,exp}\right\}\right|^2}{\left(\left\{A_{i,num}\right\}^T \left\{A_{i,num}\right\}\right)\left(\left\{A_{j,exp}\right\}^T \left\{A_{j,exp}\right\}\right)} \tag{5.3}$$

$\left\{A_{i,num}\right\}$ and $\left\{A_{j,exp}\right\}$ are vectors containing the modal constant proper of, respectively, the experimental and numerical mode shapes.

The MAC index has been calculated for the first ten modes of the investigated structure. The result is reported in Figure 112. The correlation is good for the majority of the analyzed modes. This result is a further indication of the efficiency of the modeling strategy, in particular in terms of element kind and dimensions.

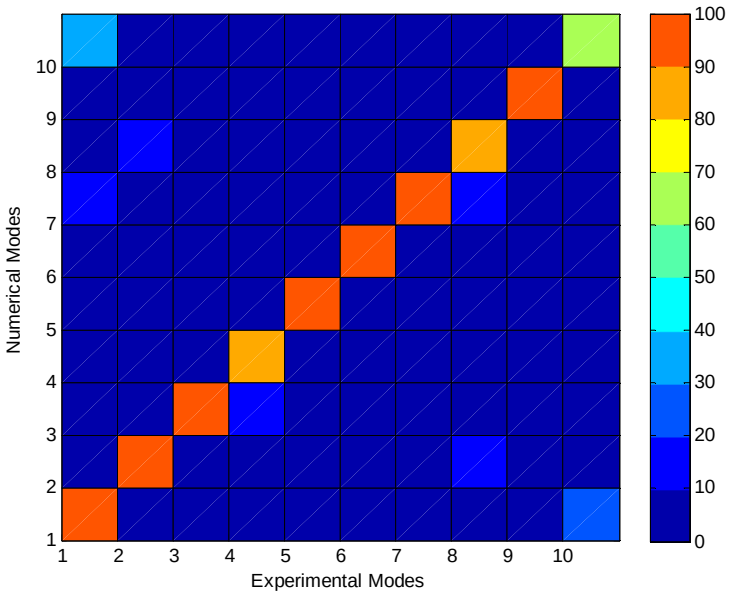

Figure 112 - Modal Assurance Criterion: Suspended Panel.

An additional comparison to evaluate the model reliability is the one in terms of FRF. The experimental and numerical FRFs are compared in Figure 113. The two curves show a reasonable match up to 200 Hz. Moving towards upper frequencies the trend and order of magnitude of the FRFs show still close agreement. However, damping predicted by the numerical model is significantly higher than the experimental one. This can be addressed to a prediction error of the core Loss Modulus through Prony

series. Errors on the Storage Modulus are less likely due to the match among natural frequencies.

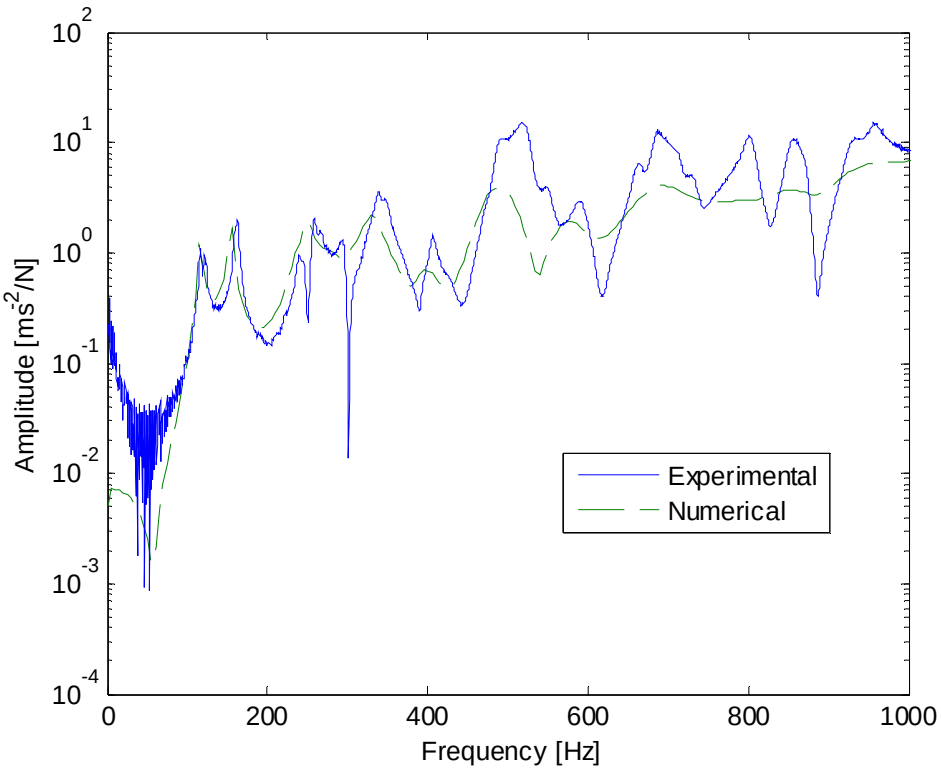

Figure 113 Panel big: FRF numerical-experimental comparison.

The identification of the panel modal parameters, i.e. natural frequencies and mode shapes, leads one step ahead towards the vibroacoustic coupled behavior modeling. Although damping correspondences are to be achieved in dynamic modeling, the effect on the coupled modeling is of less incidence. The structural damping results to be less influent than mode shapes and natural frequencies on the low frequency coupled behavior prediction [44].

2.1. Model predictive capability assessment

The predictive capability is a fundamental requirement for a model meant to be used as diagnostic tool. The procedure of model validation assesses the model reliability on a specific test case. The final aim of the developed mode is to allow the

evaluation of different engineering solution. As a consequence the model has to be able to perform an efficient prediction of the dynamic behavior of structure different from the one used for model validation purposes. In the current dissertation, the model validated on the big panel has been adopted to predict the vibrational behavior of a smaller panel. The model of the small panel considers exactly the same material properties of the model described in paragraph 2. The element type are shells for the skins and solid for the core. The first comparison, in terms of natural frequencies, has been made only on the first two modes (Table 7). This is due to the high damping that flattens the panel FRF and does not allow the extraction of further stable poles. (Chapter 4).

Mode #	Experimental Frequency [Hz]	Numerical Frequency [Hz]	Error [%]
1	596.74	584	2
2	727.89	720	0.96

Table 7 - Small Panel: Natural frequencies comparison.

The errors are lower than 5 % for all the considered modes. The comparison in terms of mode shapes show good agreement as highlighted by the MAC in Figure 114.

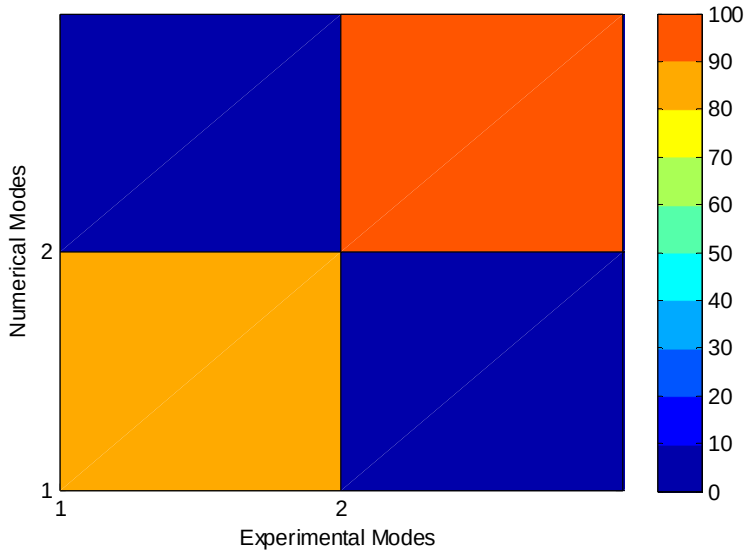

Figure 114 - MAC small panel.

The comparison in terms of FRF is reported in Figure 115. The numerical and experimental data show good agreement as further confirmation of the proposed numerical strategy reliability. In particular, the structure damping capability is well predicted by the numerical model despite the uncertainty on the core material parameters. As for the model of the big panel the numerical FRF exhibits higher damping with respect to the experimental one.

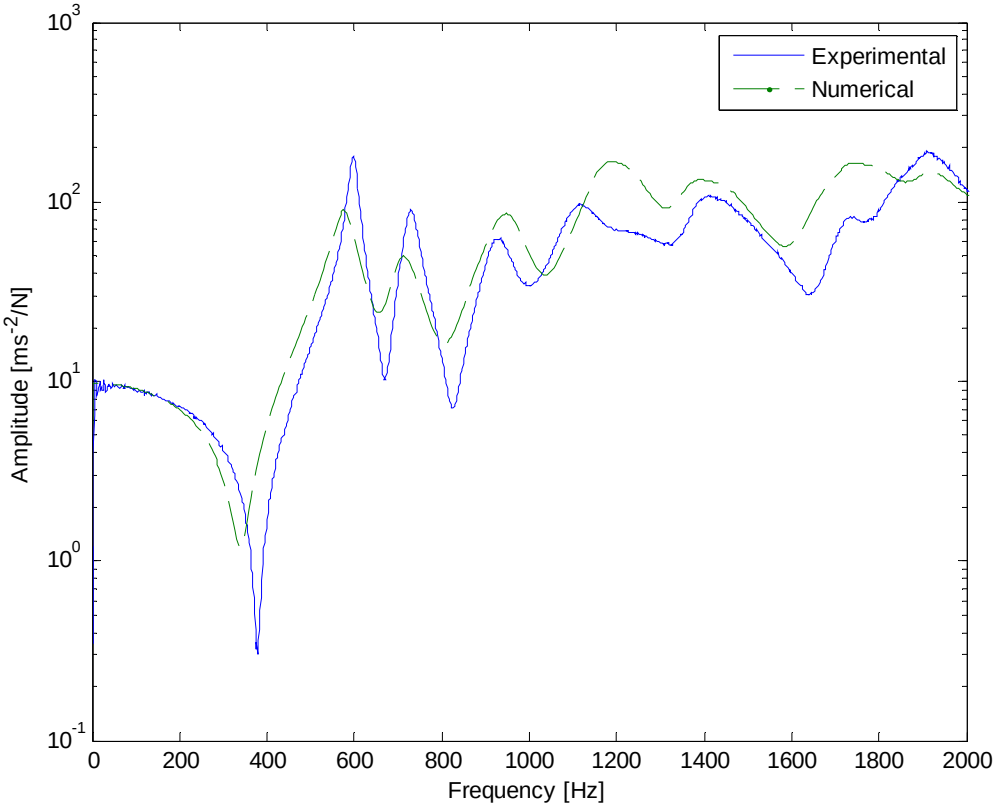

Figure 115 - Numerical - Experimental comparison.

The validation of the dynamic model on two different test cases assesses the dynamic modeling strategy reliability. Both the adopted material model and the modeling choices in terms of element kind and dimension result to be suitable to predict the investigated sandwich panel modal behavior.

3. Vibroacoustic modeling

The aim of the developed numerical - experimental procedure is to predict the global dynamic and vibroacoustic performances of a sandwich structure. While the vibration damping capability has been studied through a FE model, the coupled vibroacoustic problem has been tackled with a coupled FE-BE modeling technique.A typical way to characterize the acoustic structural performances is the Sound Insertion Loss identification (Chapter 4). Given a source emitting sound through an opening, the IL index, quantifies the change in the radiated power due to a structure closing the opening. The sound IL is mathematically expressed as the logarithmic ratio of the radiated power in the two cases ((4.4)). This index is easy to evaluate from an experimental point of view through sound intensity measurements. Anyhow, along with the structural performances information the sound IL carries also some characteristics of the testing rig and testing environment. Whether an experimental campaign is carried out to validate the simulation results, the numerical model has to reproduce both the investigated structure and the testing setup.

The experimental procedure chosen to determine the IL of a structure foresees the coupling of the investigated panel with a small concrete soundbox (Chapter 4). Sound intensity measurements are then performed with and without the structure closing the soundbox opening. A numerical model of the testing rig has been developed and extendedly validated by KUL. This model has been provided to the author and exploited to numerically investigate the acoustic behavior of the investigated panel. The model parameters have been set in order to extract the acoustic power radiated at the opening in both configurations (i) without panel and (ii) with panel (Figure 116). In configuration (ii) the modal parameters, i.e. natural frequencies and mode shapes, of the panel in clamped edge conditions have been imported into the couple model. The panel modal parameters have been extracted from the FE model described in the previous chapter. The FE model boundary conditions have been modified from free free to clamped edges. A acoustic source has been placed in the soundbox top right rear corner (Figure 116). The mesh dimension is set to predict the acoustic power correctly up to 1kHz. Above this frequency the influence of the modal behavior on the acoustic performances is less significant. In addition, the computational cost due to a more refined mesh makes the modeling strategy less efficient.

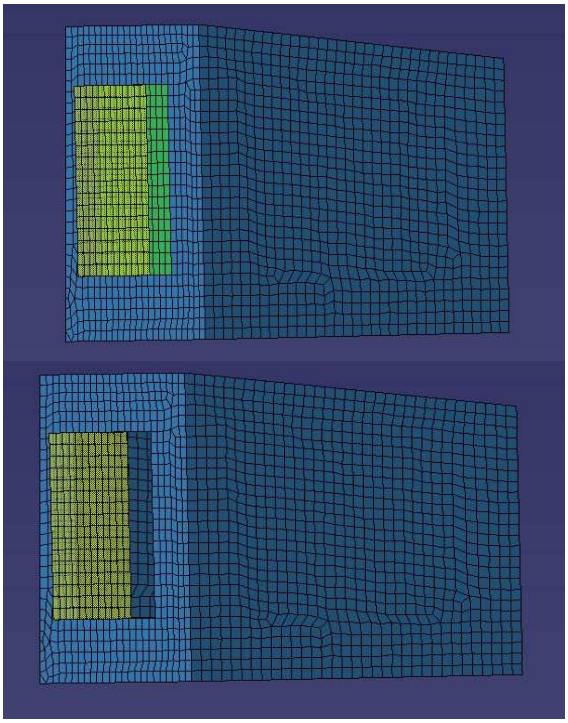

Figure 116 -Coupled vibroacoustic model.

The outputs of the coupled numerical model are the acoustic power with and without panel. A first model validation step has been made comparing the numerical and acoustic power trends toward frequency. Regardless of the difference among numerical and experimental acoustic powers values, the trend results to be the same in both open and closed cavity cases.

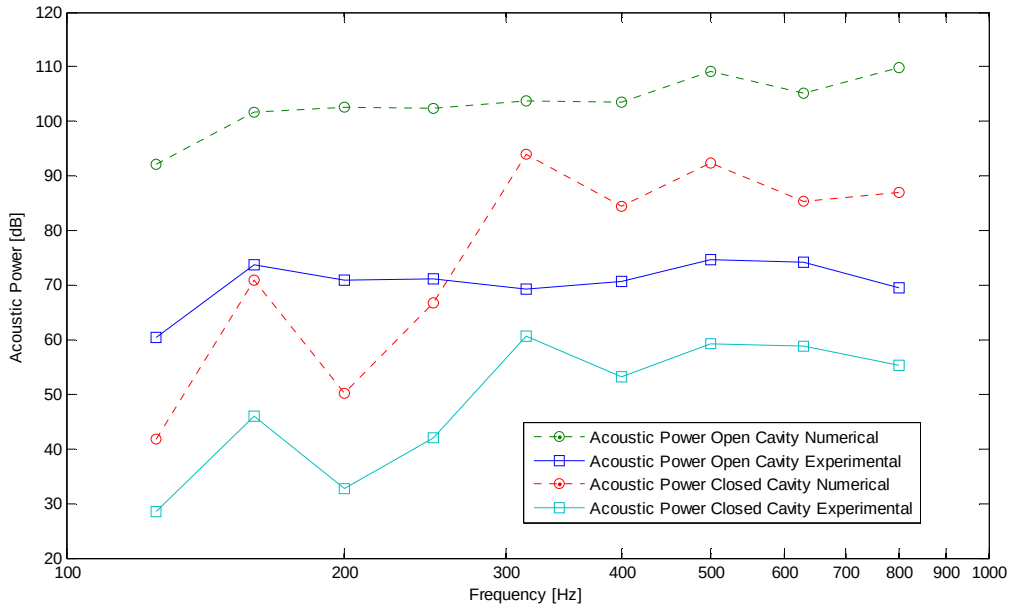

Figure 117 - Comparison among numerical and experimental acoustic powers (third octave band).

The amplitude values difference is due to the choice a unitary sound source in the numerical model. This does not affect the results in terms of Insertion Loss Index. Roughly speaking, the IL evaluates in fact the radiated power through a structure due to a certain sound source power with respect to the sound source power itself. As a result, the only requirement on the equality of the sound source power in the two test conditions: with and without the structure. The numerical /experimental comparison in terms of Sound Insertion Loss in the frequency range up to 1 kHz is reported in Figure 118. The comparison between numerical and experimental IL assess the predictive capability of the whole modeling strategy. As shown in Figure 118, the data agree pretty well in the explored frequency range.

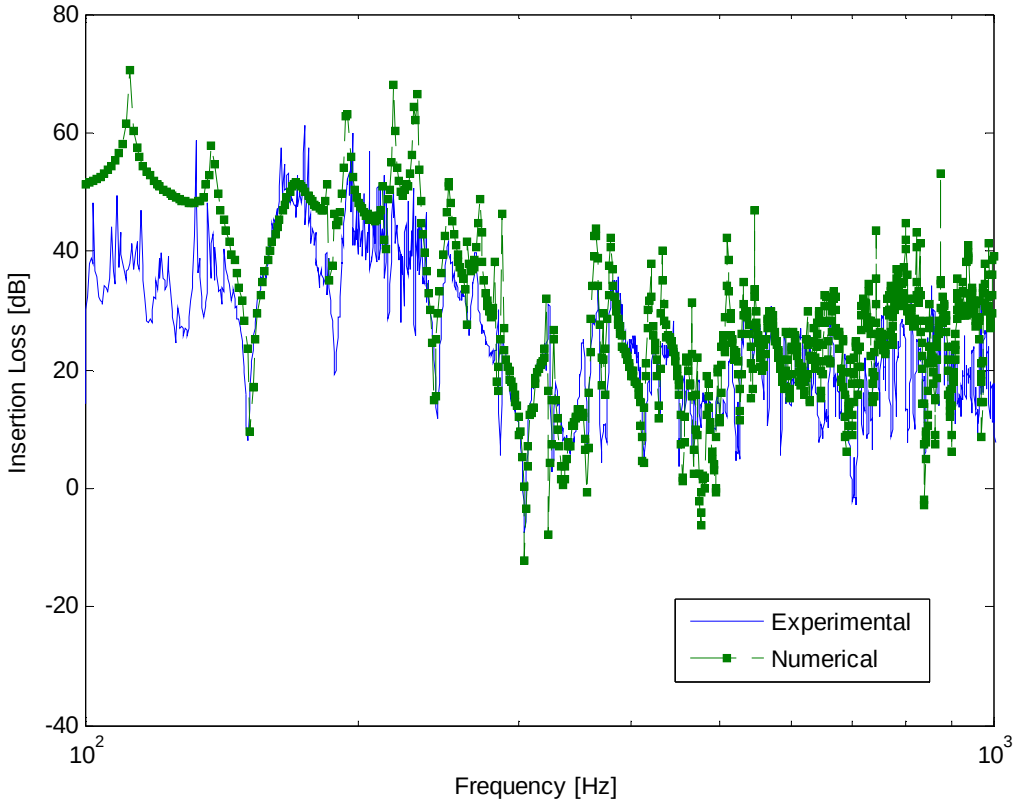

Figure 118 - Sound IL: numerical -experimental comparison.

This last comparison highlights the potentiality of the proposed procedure as powerful designing tool. The reliability of the modal parameters extracted from the dynamic model described in paragraph 2 allows the accurate prediction of the vibroacoustic behavior of the whole structure.

4. Acoustic behavior prediction at higher frequencies

The proposed coupled modeling approach allows the prediction with sufficient accuracy of the sound IL in the low frequency range (Figure 118). Moving towards higher frequencies the computational cost and the uncertainties of the deterministic techniques reduce the reliability of this kind of approach. Several methods are available in literature to evaluate the structural acoustic performances at high frequencies, e.g. SEA (Chapter 2).

The majority of the models done with SEA for multilayered structure are based on equivalent layer modeling. This approximation, although justified, does not highlight a phenomenon typical of sandwich panel with soft core: the double wall resonance. The mode shape associated with this frequency exhibits the out of phase movement of the two skins (Chapter 4).This mode shape is obviously not highlighted by a modeling strategy that considers a single equivalent layer. At the double wall frequency the panel becomes a perfect radiator. Whatever sound performance index is considered, either Sound Insertion Loss or Sound Transmission Loss, the double wall resonance is characterized by a dip in the index trend towards frequency. The experimental investigation carried out on the considered panel highlights the existence of a dilatational mode around 7200 Hz (Chapter 4). It is important to localize the double wall frequency in the design of a structure to optimize the sound transmission reduction.

An impedance based sound TL prediction has been chosen in the current research work to identify the presence of the double wall frequency. The comparison among the experimental IL and the estimated TL is reported in Figure 119. Sound TL and sound IL both quantify the variation of power radiated by a sound source due to the presence of an object. Although they present the same theoretical trend towards frequency (Chapter 2) they cannot be compared in absolute value. The TL value is strictly dependent on the object while the IL is influenced also by the adopted testing procedure. An empirical relation among this two index has been identified resulting in a simple shift of the TL towards lower values [9]. This relation has a validity limited to the specific test case analyzed by the authors. Regardless of the exact value of IL and TL, the comparison displayed in Figure 119 highlights a good prediction of the vibroacoustic performance trend towards the frequency axis.

Regardless the exact value of IL and TL, this comparison is anyhow significant aiming to localize the double wall frequency. The numerical prediction is based on the problem geometry and the experimentally identified material data and it estimates the double wall frequency at 7400 Hz. A coherent value can be obtained through the analytical formula (4.5) using the material parameters identified through DMA analysis.

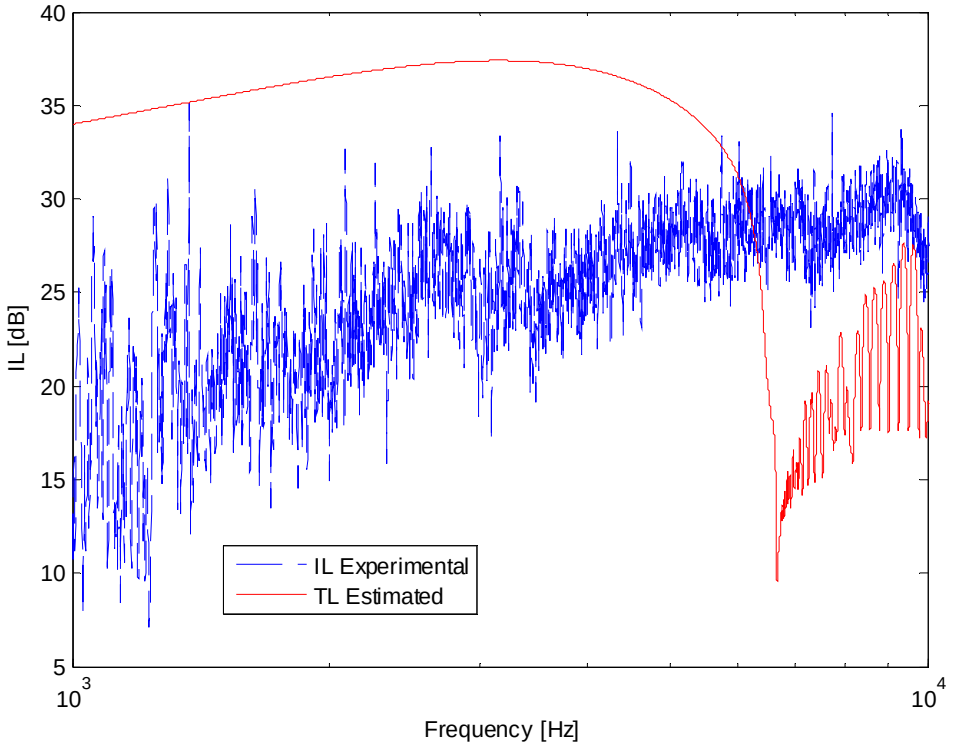

Figure 119- Experimental Sound IL - Estimated Sound TL comparison.

Structures for sound transmission reduction are typically designed to work in the mass law region. The impedance method gives an idea of the optimal working frequency range. This method is characterized by a lower computational cost and allows the prediction of the TL trend on a wider range of frequency with respect to other techniques. In addition, it highlights the existence of symmetric and antisymmetric coincidences (the latter does not exist for the investigated panel [7]). This aspect of the method helps to optimize the final structure design avoiding undesired resonance in the working frequency range.

CHAPTER 6

Chapter 6 sums up the whole research work. The relevance of the dissertation is highlighted recalling its backbone. Conclusions are drawn considering the achieved results. To conclude, some possible further developments are proposed in the field of vibroacoustics.

1. Conclusions

The current dissertation is focused on the development of a combined numerical/experimental procedure to predict vibroacoustic behavior oflightweight structures. Lightweight structures became widespread along the years. Among them,sandwich panels offer a potentially infinite number of engineering solutions. Being characterized by a pretty rich basket of design parameters, sandwich structures can be tailored exactly on a specific requirement. Lightweight structures typically exhibit poor noise and vibration performances. They tend to vibrate easily generating undesired sound. Better performances can be achieved considering sandwich panels with foam core. The porous core, in fact, increases the vibration damping capability of the structure. If optimally tuned, a porous core can improve also sound transmission reduction. Therefore, a reliable vibroacoustic numerical model becomes a powerful designing tool.

The aim of the current research is to develop an integrated numerical/experimental procedure to predict the vibroacoustic performances of a sandwich foam core panel. At the current state of the art, few works are available reporting a methodology that

considers all the relevant aspects for vibroacoustic structural behavior evaluation.In literature, research works are typically focused either in material characterization or in numerical modelling.Conversely, the current research work considers the whole workflow required for a reliable vibroacoustic prediction: material properties characterization, numerical modeling and experimental testing of lightweight structures.The innovative feature of the presented work is the integration of these three main blocks in a structured procedure with particular attention to the model validation through experimental data. A dedicated experimental activity has been designed and carried out to obtain the material parameters required for the numerical model implementation. The panel core is a viscoelastic material that requires a specific identification procedure. At the current state of the art, the nominal values of the material parameters are typically taken as starting point for numerical modeling procedures. Dedicated experimental campaigns are usually neglected. The current research defines insteada general procedure starting from the experimental identification of material parameters to the numerical fitting on a suitable mathematical model. This strategy allows the reduction of the uncertainty on material parameters and leads to a more reliable numerical results

The identified material parameters are the input of the developed modeling strategy. The numerical model foresees a two step schema: a FE model to predict the structural dynamics and a coupled FE-BE model to tackle the vibroacoustic problem. The first modeling step, the FE model, aims to estimate the response of the structure to the incoming excitation. On the other hand the FE model allows the extraction the structural modal parameter, i.e. natural frequencies and mode shapes, that are required for the coupled FE - BE model. The latter gives as output the structure vibroacoustic performances in terms of Insertion Loss trend towards frequency. Vibroacoustic numerical modeling is based on well known numerical techniques like FE and BE. Typically, these kind of problems are addressed developing ad hoc numerical algorithms, especially if they involve viscoelasticity effects. Implementing a specific algorithm requires a deep knowledge of the theory of the selected numerical method. The choice of using commercial software, respectively Abaqus for the FE model and VirtualLab for the coupled model, increases the modeling strategy versatility.

In addition, few works are presented in literature that reports an extended experimental validation of both dynamic and acoustic numerical model. This aspect has instead been considered fundamental in the current dissertation.

Reliability is a fundamental requirement for a numerical procedure used for prediction purposes. The assessment of the numerical procedure reliability is typically made through numerical/experimental correlation.

Concerning the dynamic model, at the current state of art, the validation is typically presented in terms of mode shaped and natural frequencies. A comparison in terms of Frequency Response Function is often neglected, although being of particular significance. In the current thesis the FE dynamic model numerical/experimental correlation has been reported in terms of natural frequency, mode shapes and Frequency Response Function.In addition, two case study have been considered for the validation of the dynamic model.

Dealing with lightweight structures makes more challenging the characterization of the structure dynamic behavior. The structure results to be very sensitive to load effect given by sensors and/or excitation. Considering an impact test technique, the lighter the panel the lighter has to be both sensors and impactor. The choice of the latter has to be careful to ensure a significant excitation in the whole range of frequency of interest. An experimental modal analysis has been carried out on two panels characterized by different in plane extension. The numerical/experimental data agree quite well in terms of natural frequency and mode shapes. The comparison in terms of FRFs shows a numerical FRF characterized by higher damping with respect to the experimental one.

The coupled FE - BE model has been validated comparing numerical and experimental Insertion Loss data. The data agree quite well in the considered range of frequency as confirmation of the reliability of the proposed modeling technique. A second methodology based on the calculation of panel impedances has been applied to identify the panel double wall frequency. The numerical prediction agrees with the experimental identified value.

To conclude, a structured integrated numerical /experimental procedure has been developed to predict the vibroacoustic performances of a sandwich panel with foam core. The workflow includes the design of the experimental campaign required to characterize the viscoelastic core, the development of a numerical model either for structure dynamics or for vibroacoustic interaction and the experimental validation of the proposed numerical technique. The numerical results agree pretty well in terms of structural modal parameters and sound transmission reduction performances

Different aspects can be further investigated. For instance an inverse estimation procedure can be adopted for determining core material parameters through dynamic-acoustic measurements The experimental identification of the double wall frequency with different panel configurations, i.e. adding additional face sheets to increase the mass of the skin, may lead to a better identification of the Young Modulus parameter of the foam that is the core of the investigated panel. Other

possible developments are mainly related to the structure design and tuning in order to optimize the vibroacoustic performances. The use of a numerical optimization performance to analyze the predicted data and investigate the performance trend according to parameters' change will lead to a better performing panel. It may be interesting also to extend of the numerically investigated frequency range to the mid-frequency range, using suitable numerical techniques, to give a more complete acoustic characterization

References

[1] EUROSTAT, Energy, Transport and Environment Indicators - 2010 Edition, 2011.

[2] *UNI 11367.*

[3] F. Fahy and P. Gardonio, Sound and structural vibration, Academic Press, 1985.

[4] L. Beranek, Noise and Vibration Control, Mc Graw Hill, 1971.

[5] G. Kurtze and B. Watters, "New wall design for high transmission loss or high damping," *The Journal of the Acoustical Society of America,* vol. 31, no. 6, 1959.

[6] M. Norton and D. Karczub, Fundamentals of noise and vibration analysis for engineers, Cambridge, 2003.

[7] K. Renji, P. Nair and S. Narayanan, "Critical and coincidence frequencies of flat panels," *Journal of sound and vibration,* vol. 205, no. 1, 1997.

[8] M. Bhattacharya, R. Guy and M. Crocker, "Coincidence effect with sound waves in a finite plate," *Journal of sound and vibration,* vol. 18, no. 2, 1971.

[9] R. Ford, P. Lord and A. Walker, "Sound transmission through sandwich constructions," *Journal of Sound and Vibration,* vol. 5, no. 1, 1967.

[10] C. Dym and M. Lang, "Transmission of sound through sandwich panels," *Journal of acoustical society of America,* vol. 56, no. 5, 1974.

[11] J. Allard and N. Atalla, Propagation of Sound in Porous Media, Wiley, 2009.

[12] S. P. Marques and G. J. Croes, Computational Viscoelasticity, Springer, 2012.

[13] R. Lakes, Viscoelastic Materials.

[14] S. Park and R. Schapery, "Methods of interconversion between linear viscoelastic material functions. Part I.," *International Journal of Solids and Structures,* vol. 36, 1999.

[15] S. Park, "Analytical modeling of viscoelastic dampers for structural and vibrations

control," *International Journal of Solids and Structures,* vol. 38, 2001.

[16] K. Attenborough, "Acoustical Characteristics of porous materials," *Physics Reports,* vol. 82, no. 3, 1982.

[17] F. Pompoli and P. Bonfiglio, "Assorbimento Acustico," 2011.

[18] M. Biot, "Theory of propagation of elastic waves in a fluid-saturated porous media," *Journal of the Acoustical Society of America,* vol. 28, 1956.

[19] L. Beranek and I. Ver, Noise and Vibration Control Engineering: principles and applications, Wiley, 1992.

[20] C. Kosten and J. Janssen, "Acoustic properties of flexible and porous materials," *Acustica,* vol. 7, 1957.

[21] N. Atalla, R. Panneton and P. Debergue, "A mixed displacement-pressure formulation for poroelastic materials," *Journal of Acoustic Society of America,* vol. 104, no. 3, 1998.

[22] S. Pride and J. Berryman, "Connecting theory to experiment in poroelasticity," *Journal of the Mechanics and Physics of Solids,* vol. 46, 1998.

[23] M. Biot, "Generalized theory of acoustic propagation in porous dissipative media," *Journal of the acoustical society of America,* vol. 34, no. 5, 1962.

[24] J. Vilson, The behavior of sandwich materials.

[25] L. Demasi, "Mixed plate theories based on the Generalized Unified Formulation Part III: Advanced mixed high order shear deformation theories," *Composite Structures,* vol. 87, 2009.

[26] H. Altenbach, "Theories for Laminated and sandwich plates, a review," vol. 34, no. 3, 1998.

[27] L. Demasi, "Mixed plate theories based on the Generalized Unified Formulation. Part IV: Zig-zag theories," *Composite Structures,* vol. 87, 2009.

[28] A. Love, "The small free vibrations and deformation of a thin elastic shell," *Philosophical Transactions of the Royal Society of London,* vol. 179, 1888.

[29] O. Zienkiewicz and R. Taylor, The Finite Element Method, Butterworth Heinemann, 2000.

[30] E. Carrera, "Theories and Finite Elements for Multilayered Anisotropic, Composite Plates and Shells," *Archives of Computational Methods in Engineering,* vol. 9, no. 2, 2002.

[31] L. Demasi, "Mixed plate theories based on the Generalized Unified Formulation. Part II: Layerwise theories," *Composite Structures,* vol. 87, 2009.

[32] S. Brischetto, E. Carrera and L. Demasi, "Improved bending analysis of sandwich plates using a zig-zag function," *Composite Structures,* vol. 89, 2009.

[33] KU Leuven, Lecture Notes ISAAC 23, 2012.

[34] C. Brebbia and J. Dominguez, Boundary Elements, an introductory course, Southampton: Computational Mechanics Publication, 1989.

[35] C. Vanmaele, D. Vandepitte and W.Desmet, "An efficient wave based prediction technique for plate bending vibrations," *Computer methods in applied mechanics and engineering,* vol. 196, 2007.

[36] B. Van Genechten, D. Vandepitte and W. Desmet, "A direct hybrid finite element - Wave based modelling technique for efficient coupled vibro-acoustic analysis," *Computer methods in applied mechanics and engineerin,* vol. 200, 2011.

[37] T. Wang, V. Sokolinsky, S. Rajaram and S. Nutt, "Assessment of sandwich models for the prediction of sound transmission loss in unidirectional sandwich panels," *Applied Acoustics,* vol. 66, 2005.

[38] J. Moore and R. Lyon, "Sound transmission loss characteristics of sandwich panel constructions," *Journal of the Acoustical Society of America,* vol. 89, no. 2, 1991.

[39] R. Cook, D. Malkus and M. Plesha, Concept and applications of finite element analysis, Wiley, 1989.

[40] G. Liu and S. Quek, Finite Elements Method A practical course, Butterworth Heinemann, 2003.

[41] Abaqus Theory Manual.

[42] J. Moore, Sound Transmission Loss of three layer composite wall constructions, 1975.

[43] C. Dym, C. Ventres and M. Lang, "Transmision of sound through sandwich panels: a reconsideration," *Journal of Acoustic Society of America,* vol. 59, no. 2, 1976.

[44] F. Fahy, Sound and structural vibration, Academic Press, 1985.

[45] R.Lakes, Viscoelastic Materials, Cambridge, 2009.

[46] V. Tita, J. M. Caliri, R. Angelico and R. Canto, "Experimental analyses of the poly(vinyl chloride) foams' mechanical anisotropic behavior," *Polymer Engineering & Science,* vol. 52, no. 12, 2012.

[47] D. Ewins, Modal Testing: Theory, practice and applications, Research Study Press Ltd., 2000.

[48] W. Heylen, S. Lammers and P. Sas, Modal Analysis Theory and Testing, KU Leuven, 2007.

[49] B. Peeters, H. Van der Auweraer, P. Guillaume and J. Leuridan, "The PolyMAX frequency domain method: a new standard for modal parameter estimation?," vol. 11, no. 3-4, 2004.

[50] G. Bassi and L. Frascino, Indagine sperimentale e numerica sulla caduta di tensione nelle strutture in cemento armato precompresso ai fini del monitoraggio strutturale, MsC Thesis, 2010.

[51] P. Theocaris, "Viscoelastic properties of epoxy resins derived from creep and relaxation tests at different temperatures," *Rheologica Acta,* vol. 2, no. 2, 1962.

[52] ASTM, *Standard Test Method for Laboratory Measurement of Airborne Sound Transmission Loss of Building Partitions and Elements.*

[53] R. Halliwell and A. Warnock, "Sound transmission loss: comparison of conventional techniques with sound intensity technique," *Journal of Acoustic Society of America,* vol. 77, no. 6, 1985.

[54] F. Fahy, Sound Intensity, E & FN Spon, 1995.

[55] M. Vivolo, Vibro-acoustic characterization of lightweight panels by using a small cabin., PhD Thesis, 2013.

[56] A. Cops and M. Minten, "Comparative study between the sound intensity method and the conventional two room method to calculate the sound transmission loss of wall constructions," *Noise control engineering journal,* vol. 22, no. 3, 1984.

[57] C. Cameron, P. Wennhage, P. Goransson and S. Rahmqvist, "Structural acoustic design of a multi functional sandwich panel in an automotive context," *Journal of Sandwich Structures and Materials,* vol. 12, 2010.

[58] M. Ashby and L. Tianjian, "Metallic foams. A survey.," *Science in China,* vol. 46, no. 6, 2003.

[59] C. Hopkins, Sound Insulation, Butterworth - Heinemann, 2007.

List of Symbols

A surface area

$\{A\}$ Modal constant vector

$\{a\}$ nodal variables vector

$\{a^b\}$ nodal variable vector plate bending condition

$\{a^p\}$ nodal variable vector plane stress condition

α eigenvalue

c speed of sound

$\mathbf{C}$ damping matrix

D bending stiffness

$\mathbf{D}$ elasticity matrix

$\mathbf{D}^b$ elasticity matrix plate bending condition

$\mathbf{D}^p$ elasticity matrix plane stress condition

δ phase shift between imposed strain and resulting stress in DMA testing

E_∞ long term or equilibrium elastic modulus

E_c core Young modulus

E'' loss modulus

$E(t)$ relaxation modulus

E' storage modulus

E_i, τ_i coefficient of Prony Series for Elastic Modulus

ε strain

η viscosity

f frequency

f_{cr} critical frequency

f_{DW} double wall frequency

$\{f_b\}$ vector of boundary terms

$\left\{f_{ext}^{b}\right\}$ vector of external forces and boundary terms plate bending condition

$\left\{f_{ext}^{p}\right\}$ vector of external forces and boundary terms plane stress condition

$\{F_s\}$ vector of external forces and boundary conditions of the coupled model

$\{\phi\}$ eigenvector

φ Azimuthal angle

G shear modulus

G_0 shear instantaneous modulus

G'' loss shear modulus

G' storage shear modulus

g_i, τ_i Coefficient of Prony series for Shear modulus

$G(\vec{r},\vec{r}_a)$ Green's kernel function

$g(x, y, z)$ time harmonic external source

γ shear deformation

Γ boundary FE model

h plate thickness

H Frequency Response Function

i imaginary unit

$\{I\}$ internal force vector

$\{I(t)\}$ sound intensity vector

J functional

$J(t)$ creep compliance

k wavenumber

K Bulk modulus, spring parameter in rheological models

K_0 Bulk instantaneous modulus

K' storage Bulk modulus

K'' loss Bulk modulus

k_i, τ_i coefficient of Prony series for Bulk modulus

$\mathbf{K}$ stiffnes matrix

$\mathbf{K}^b$ stiffness matrix plate bending condition

$\mathbf{K}^p$ stiffness matrix plane stress condition

l in plane FE dimension

l_a acoustic mesh element dimension

$\mathbf{L}$ matrix of differential operators to relate strain and displacement for plate bending condition

$\mathbf{L_c}$ coupling matrix FE-BE model

λ wavelength

M moment

$\tilde{M}$ prescribed moment

$\mathbf{M}$ mass matrix

$\mu(\vec{r})$ double layer potential

$\mathbf{N}$ FE shape functions

N BE shape function

$\{n^e\}$ unit vector normal to a plate element

$\{P\}$ external force vector

ν Poisson's ratio

ω radiant frequency

Ω boundary surface BE model

p pressure

Π sound power, total potential energy

q external load

$\vec{r}$ position vector

R dashpot parameter in rheological models

$\{R^{ext}\}$ external forces resultant vector

ρ material density

ρ_s mass per unit area

$\tilde{S}$ prescribed shear

$\mathbf{S}$ matrix of differential operators to relate strain and displacement for plane stress condition

σ stress, radiation ratio

$\sigma(\vec{r})$ single layer potential

t time

t_c thickness of the core

τ shear stress, transmission coefficient

$\overline{\tau}$ diffuse field transmission coefficient

ϑ incidence angle

θ rotation of lines normal to the plate midsurface

$\{\theta\}$ rotation vector

$\{u\}$ displacement vector

$\{v(t)\}$ instantanous particle velocity

$\langle v^2 \rangle$ r.m.s. velocity

V volume

$\{\overline{w}\}$ discretized displacement fields

Z_{asym} anti symmetric panel impedance

Z_{sym} symmetric panel impedance

$\{u, v, w\}$ displacement in x, y, and z direction respectively

∇ gradient operator

Acronyms

BEM Boundary Element Method

CLT Classical Lamination Theory

ESL Equivalent Solid Layer

ESLM Equivalent solid layer model

FDA Finite Difference Analysis

FE FInite Elements

FEM Finite Elements Method

FRF Frequency Response Function

FSDT First order shear deformation theories

HOT Higher order theory

IL Insertion Loss

LW LayerWise

LWM LayerWise Models

MAC Modal assurance criterion

r.m.s. Root mean square

SEA Statistical Energy Analysis

TDO Third octave band

TL Transmission Loss

TMM Transfer Matrix Method

List of figures

Figure 1 GHG emissions reduction Kyoto Protocol base-year /2011 (source: European Environment Agency). 2
Figure 2 - Energy consumption in residential homes (source: European Commission). 3
Figure 3 - Schematic example of composite materials. 4
Figure 4 - Schematic example of sandwich panel. 4
Figure 5 - Acoustic problem. 5
Figure 6 - Sound insulation strategy - example. 6
Figure 7 - Example of sound wave induced by structural vibration. 10
Figure 8 - Incident, absorbed, reflected and transmitted sound. 11
Figure 9 - Conceptual schema. 12
Figure 10 - Deformation patterns of different type of waves in flat plates and bars. . 15
Figure 11- Sound radiation by an infinite plate [6]. 17
Figure 12- Dispersion curves [3]. 18
Figure 13 - Fundamental mode of vibration of a layered panel having compressible core: (i) Flexural and (ii) Dilatational [9]. 19
Figure 14 - Sandwich panel: stainless steel skins, polymeric foam core. 20
Figure 15 - Qualitative comparison among different material behavior. 21
Figure 16 - Qualitative strain and stress trend during a relaxation test [12]. 22
Figure 17 - Qualitative strain and stress trend during a creep test [12]. 23
Figure 18–Qualitative strain and stress trend during dynamo mechanical test. 24
Figure 19 - Basic elements for rheological models. 26
Figure 20 - Maxwell model. 27
Figure 21 – Creep compliance and relaxation modulus for Maxwell model. 29
Figure 22 - Kelvin Voigt Model. 30
Figure 23 - Creep Compliance and Relaxation Modulus for Kelvin Voigt model. 31
Figure 24 - Zener or SLS model. 32
Figure 25 - Creep compliance and Relaxation modulus for SLS model. 34
Figure 26 Bi - logarithmic plot of Shear creep compliance and Relaxation Modulus of PMMA at 110 ℃. 35
Figure 27 - Porous material as assembly of parallel tubes. 37
Figure 28- Porous material set between two elastic shells. 39
Figure 29 - Sound Intensity, schematic interpretation. 41
Figure 30 - Typical TL trend of a bounded homogeneous single panel. 42
Figure 31 - Interregion cancellation and edge effect [3]. 44
Figure 32 - Continuum discretized with FE. 45
Figure 33 - Sketch of a multilayered structure [25]. 46

Figure 34 - Displacement field: FSDT vs HOT [31]. 48
Figure 35 - LWM displacement field [31]. 49
Figure 36 - ZZF and ESL approach combination [32]. 50
Figure 37 - (a) acoustic cavity (b) finite elements mesh [3]. 52
Figure 38 - FE model with artificial boundary. 53
Figure 39 - Surface discretized with linear BE [34]. 54
Figure 40 - Coupled FE BE model [3]. 56
Figure 41 - Coupled FE FE model [3]. 56
Figure 42 - Plane wave impinging on a multilayered domain [11]. 59
Figure 43 - Conceptual connection among modeling techniques. 62
Figure 44 - Continuum divided into a set of elements [29]. 64
Figure 45 - Triangular element [40]. 66
Figure 46 - FE discretization: element in plane dimension. 68
Figure 47 - Bending and in plane (membrane) deformations [29]. 70
Figure 48- Plate subjected to transverse action resulting in bending deformation [40]. 71
Figure 49 - Variables definition [39]. 72
Figure 50 Relation among strains in x and y directions and displacements. 73
Figure 51 Relation among shear strain and displacements. 74
Figure 52 - Thick plate element after loading [39]. 74
Figure 53 - Boundary tractions [29]. 77
Figure 54 - An element in plane stress [29]. 78
Figure 55 - Displacement definition for a solid thetraedrical element [40]. 80
Figure 56 - Generalized Standard Linear Solid (GSLS) model. 82
Figure 57 - Schematic representation of fluid domains for a combined interior/exterior problem. 85
Figure 58 - Problem definition. 86
Figure 59 - Problem definiton. 87
Figure 60 - Mass-spring-mass equivalent system [42]. 93
Figure 61- symmetric and anti-symmetric modes [42]. 94
Figure 62 - Problem geometry [42]. 95
Figure 63 - Panel crossection: detail 102
Figure 64 - Foam core: detail 103
Figure 65 - Qualitative DMA test. 104
Figure 66 - DMA testing machine. 104
Figure 67- Clamped foam specimen. 105
Figure 68 - Foam specimen: directions. 106
Figure 69 - Stress strain curves foam specimen. 106
Figure 70 - Preload sensitivity analysis: foam specimen (solid line) and panel specimen (circles). 108

Figure 71 - Foam specimen Master Curve. 109
Figure 72 - Foam Material data (blue solid line) vsProny series approximation (red circles). 110
Figure 73 - Estimation Errors. 111
Figure 74 - Investigated panel. 112
Figure 75 - Suspended panel. 114
Figure 76 - Impact Hammer [47]. 115
Figure 77 - Typical impact hammer pulse: time history (left) and frequency spectrum (right) [47]. 116
Figure 78 - Suspended panel: measurement grid (Squares: excitation points, Circles accelerometers). 117
Figure 79 - Frequency Response Function free free boundary conditions. 118
Figure 80 - FRF Amplitude free free conditions. 119
Figure 81 - Sum of FRFs - Amplitude. 120
Figure 82 - Mode shapes free free conditions. 122
Figure 83 - Clamped conditions : measurement grid (Squares: excitation points - Circles: accelerometers). 124
Figure 84 - Clamped Panel: FRF. 125
Figure 85 - Clamped panel : FRF sum. 126
Figure 86 - Clamped panel: FRF sum (zoom on 250 Hz - 400 Hz). 127
Figure 87 - Clamped panel: Mode shapes. 128
Figure 88 - Clamped panel: comparison between different clamping torques. 129
Figure 89 – Adhesive layer dynamic effect evaluation: testing setup. 130
Figure 90 - Comparison among FRF single 12 mm plate - glued plates. 131
Figure 91 - Small panel. 133
Figure 92 - Comparison between different hammer power spectra. 134
Figure 93 - FRF Sandwich panel small. 135
Figure 94 - Small panel: Mode shapes. 136
Figure 95 - Small panel: clamped conditions. 136
Figure 96 - Small panel: comparison among different torques. 137
Figure 97 - Two rooms sound TL test rig. 138
Figure 98 - Sound IL measurement procedure [55]. 140
Figure 99 - PMA Sound Box: exterior (left), interior (right). 140
Figure 100 - Intensity distribution measurement, open and closed window configuration. 141
Figure 101 - P-P intensity probe. 141
Figure 102 - Experimental IL: narrow band (blue dashed line), third octave band(green solid line). 143
Figure 103 - Sound IL comparison: sandwich panel (blue circles) vs 3 mm Aluminum panel (green squares) (courtesy of KUL). 144

Figure 104 - Pressure map: third octave band centered on 315 Hz. 145
Figure 105 - Sound IL mid - high frequency range: narrow band (blue dashed line), third octave band (red solid line). 146
Figure 106 - Sound IL : dips in the mid high frequency range. 147
Figure 107 - Symmetric (top) and anti - symmetric (bottom) motion of a sandwich panel[59]. 148
Figure 108 - Double wall motion investigation: measuring grids. 149
Figure 109 - Double wall mode shape. 149
Figure 110 - Experimental and numerical results interaction :Conceptual schema 152
Figure 111 - Finite Element model. 153
Figure 112 - Modal Assurance Criterion: Suspended Panel. 156
Figure 113 Panel big: FRF numerical-experimental comparison. 157
Figure 114 - MAC small panel. 158
Figure 115 - Numerical - Experimental comparison. 159
Figure 116 -Coupled vibroacoustic model. 161
Figure 117 - Comparison among numerical and experimental acoustic powers (third octave band). 162
Figure 118 - Sound IL: numerical -experimental comparison. 163
Figure 119- Experimental Sound IL - Estimated Sound TL comparison. 165

List of Tables

Table 1 - Estimated elastic moduli..... 107
Table 2 - Suspended panel: natural frequencies and damping ratios. 121
Table 3 - Clamped panel: frequencies and damping ratios..... 127
Table 4 - Aluminum plates: damping values comparison..... 132
Table 5 - Small panel: natural frequencies and damping ratios. 135
Table 6 - Experimental and numerical frequency correlation. 155
Table 7 - Small Panel: Natural frequencies comparison. 158